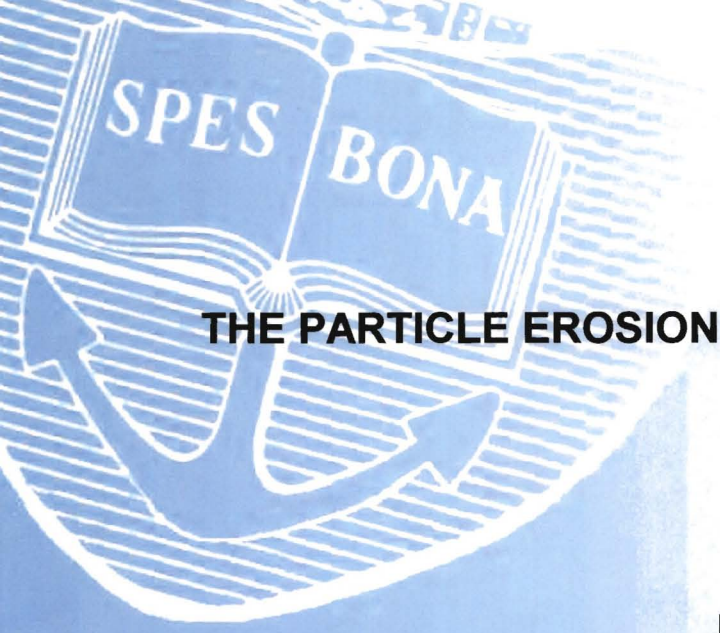

THE PARTICLE EROSION OF STEEL BY MAGNETITE

By

Sean E. Fewell

A thesis submitted to the Faculty of Engineering of the University of Cape Town
in fulfillment of the requirements for the degree of Master of Science in Engineering

Centre for Materials Engineering
Department of Mechanical Engineering
University of Cape Town
November 2002

ABSTRACT

This work addresses the problem of erosion of steel heat exchanger coils in a petroleum producing plant by magnetite catalyst particles entrained in the flowing gas stream.

Particle erosion of commercial reactor coil tube steel has been performed in a laboratory gas-blast erosion apparatus as a function of magnetite erodent impingement angle from 10° to 90°, velocities from 30 ms^{-1} to 90 ms^{-1}, mass fluxes from 1.9 $kg.m^{-2}s^{-1}$ to 32.9 $kgm^{-2}s^{-1}$ and size ranges from < 38 μm to 180 μm.

It has been shown that the maximum erosive wear rate occurs at impingement angles between 30° and 40° and that the mechanisms contributing to material loss are typically those found in ductile erosion: namely cutting and micro-ploughing. Interestingly, increasing the testing time or quantity of erodent impacting the steel when testing at low impingement angles, led to the development of elongated wear scars which were similar to those found on the steam coil tubes in practice. Such characteristic patterns suggest that during normal reactor operation, streaming of the flowing gas and catalyst occurs leading to enhanced attack in particular areas. Design suggestions have been advanced: using baffles attached to the steel tubes in practice, to reduce streaming and the associated accelerated attack.

The size of the magnetite particles was found to influence the wear rate; a reduction in particle size from 180 μm to < 38 μm led to an increase of approximately 27% in the wear rate. This increase was believed to be due to the increased angularity of the particles with a decrease in size. The loss of the very fine particles during repeated testing using nominally the same erodent also led to a slight decrease in wear rates. It is suggested that filtering these fine particles out of the system would be beneficial in practice.

A change in mass flux, within the limits shown above, did not appear to alter the wear rate substantially. Furthermore, testing carried out using spent catalyst removed from the reactor, which had a somewhat different composition and more rounded morphology, caused lower erosion rates compared to those obtained with milled (fresh) catalyst. However, a change in velocity was found to have the greatest influence on erosive wear, giving rise to an exponential

increase as the velocity increased from 25 $m.s^{-1}$ to 90 $m.s^{-1}$ with a velocity exponent close to a value of 2.

ACKNOWLEDGEMENTS

I would like to thank **everyone** who played a part in this project, but particularly the following:

Professor Colin Allen for his encouragement, approachability and excellent advice.

Mr Glen Newins and Dr Mira Topic for technical support and advice, Mr James Petersen for photographic work and Mrs Lisa Duminy for proofreading the final document.

The staff and research students at the Centre for Materials Engineering for contributing towards making my time spent there memorable; in particular Mr Craig Pike for, amongst other things, help with the SEM.

Mr Mike Holland and Ms Fikile Mahlangu of PetroSA for supplying materials and information related to the project.

PetroSA and the South African Foundation for Research and Development (NRF) for financial support.

My family, without whose support and love this project would have been an impossible undertaking.

CONTENTS

CHAPTER ONE

INTRODUCTION

The Petroleum Oil and Gas Corporation of South Africa (Pty) Limited (PetroSA) is a state-owned gas-to-liquids petrochemical producer formerly known as Mossgas (Pty) Limited. It operates a gas-to-liquids plant at Mossel Bay, 400 km southeast of Cape Town on the South African Southern Cape coast. The onshore plant went into full production in January 1993, and since then has contributed significantly to the South African economy. PetroSA employs over 1000 people, with over 7000 jobs associated with the company. PetroSA produces approximately 7% of South Africa's total transportation fuel requirements, and saves the country two billion rand per annum in foreign exchange as a result of crude oil import replacements, equivalent to 45 000 barrels a day.

An offshore production platform 85 km south of Mossel Bay supplies methane rich natural gas and condensate by pipeline to the onshore plant for conversion into a range of transportation fuels and associated products.

The conversion of this natural gas to petroleum products is carried out in a synthol reactor, which is in essence a circulating fluidised bed (CFB) unit in which an iron-based catalyst is entrained in a fast moving gas stream. The catalyst used in the process is produced by melting together haematite, millscale and various promoters (alkaline earth metals that aid the reaction), which is crushed altogether such that between 93% and 99% is less than 176 μm in size, with an average of 32 μm. Fluctuations in size are inherent in the process. Online analysis of the catalyst composition is reported in table 1-1.

The synthol reactor, which is 42 m in height, is illustrated in figure 1-1. The gas enters the reactor at the bottom, and a controlled amount of catalyst is fed into this stream. The conversion of the gas to higher hydrocarbons is accompanied by exothermic reactions and three banks of heat exchangers in line are employed to remove this heat. These heat exchangers are 7.5 m in height and are constructed from low alloy steel tubes through which 'water' at a pressure of 4600 kPa is circulated, to maintain the tubes at 260°C. The steel of the steam coil tubes conforms to DIN 1.6580, which is a 1.8 – 2.2% Cr/Ni steel in the normalised condition

(see section 3.1.1 for composition). BS 4360 GR 43A is used for the tube supports and guides (see figure 1-1b). More detailed drawings of the synthol reactor and internal steam coil tubes are included in Appendix I.

Train	Total Iron	Free Carbon	Total Carbon	Wax	Bulk Density
1	60 – 63	16 – 22	19 – 30	0.3 – 6	2.1 – 2.6
2	58 – 63	16 – 21	18 – 30	0.7 – 4.3	2.2 – 2.5
3	59 – 64	13 – 26	17 – 31	2.5 – 2.8	2.2 – 2.5

Table 1-1 Online analysis of catalyst composition from each of the three synthol trains. Value ranges are in percentages, and are recorded over a three-month monitoring period.

The catalyst and gas disengage in the wide settling hopper (left of figure 1-1a) above the standpipe. The gas leaves the hopper via cyclones that remove the entrained finer catalyst particles and return them to the settling hopper. Catalyst is replaced on-line. There is thus always a measure of fresh and "old" catalyst circulating through the reactor. Catalyst that is removed from the reactor is discarded in a landfill and is referred to as spent catalyst.

The entrained catalyst moving relative to the reactor components, causes erosive wear within the reactor. The banks of heat exchangers, figure 1(b), display the most severe erosion, as shown in figure 1-2. The first (lowest) two banks experience the most wear, with the third bank experiencing minimal erosive damage. The velocity of the gas stream decreases with increasing height, as it flows through the reactor. The most severe erosion is observed as long, deep furrows (gouges) in the surface of the steam coil tubes, on the lower 1.5 m and starting 150 – 500 mm from the tube elbow (figure 1-2d).

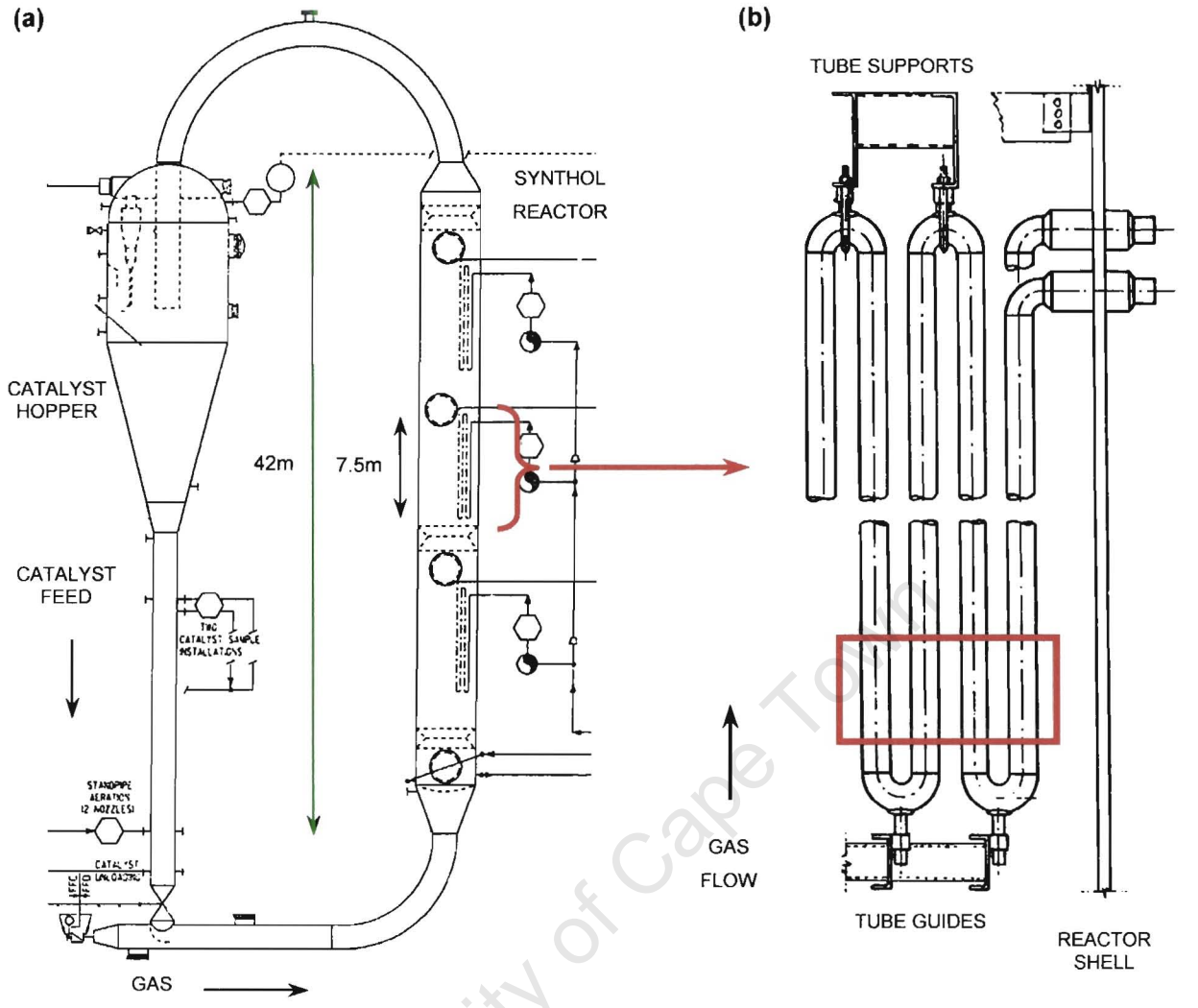

Figure 1-1 (a) Schematic of the synthol reactor. The catalyst hopper and standpipe are on the left. **(b)** Schematic of a portion of one of the three banks of heat exchanger tubes (steam coil tubes). Region of maximum erosion, characterised by long, deep gouges (see figure 1-2d), is indicated by the rectangle.

As a consequence of this erosive wear damage, many steam coil tubes have to be replaced at every plant shutdown. Replacement of these tubes is a tedious and time-consuming job, especially when the eroded tubes are in the middle of the bundle (see Appendix I, figure A-3 for a cross-section of the reactor showing the layout of a bank of steam coil tubes). For every day that a reactor is not in service, losses mount in the millions of rands. Besides the enormous loss of revenue, safety is the major concern. The consequences of a failure of one of the pressurised steam coils, leading to a sudden failure of the reactor, could be catastrophic.

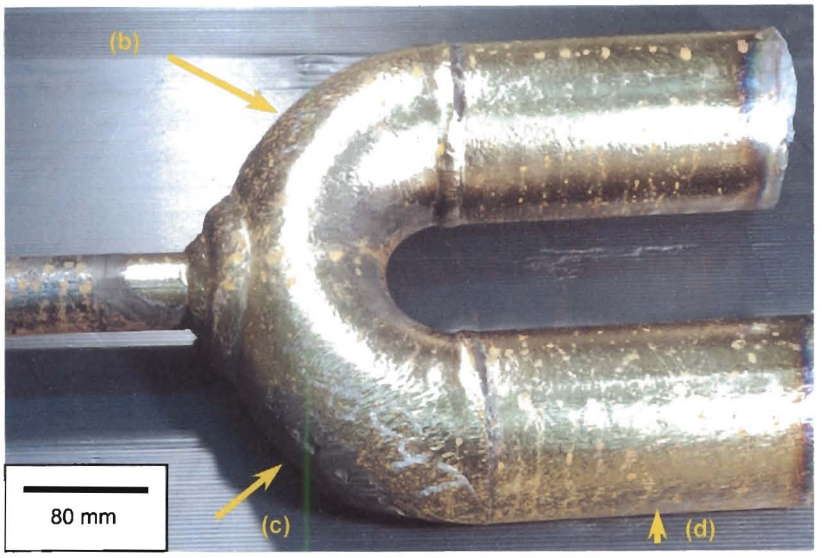

(a) Lower elbow of a heat exchanger tube (steam coil tube).

Arrows indicate the orientations of images (b) – (d).

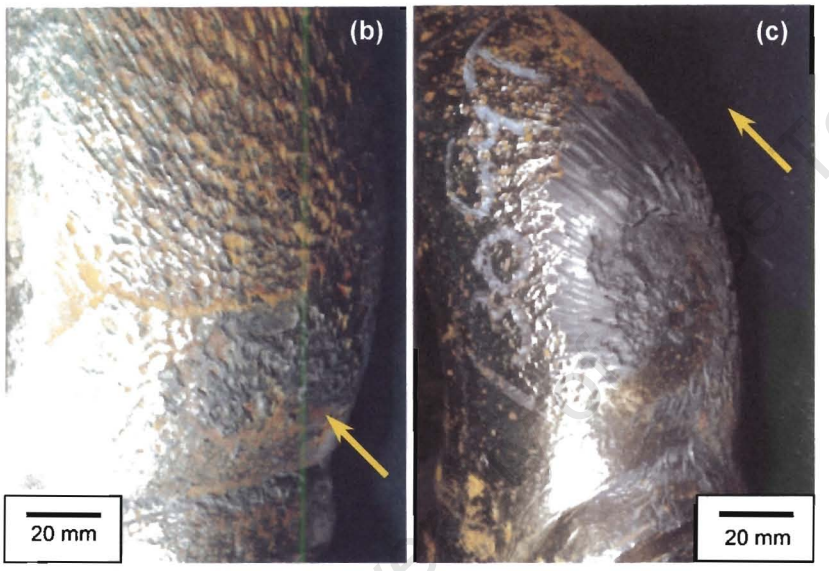

(b) Erosion of the tube end.
(c) Catalyst accumulation on the tube end.

Arrows indicate the direction of the gas flow.

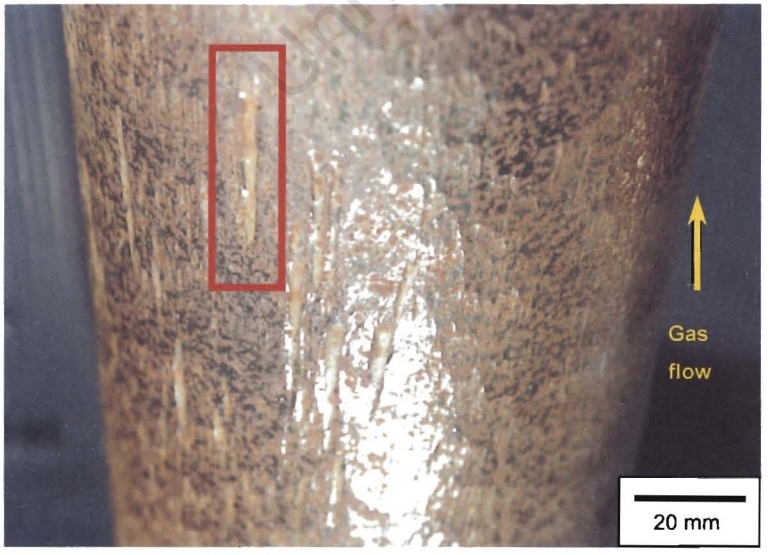

(d) Long, deep gouges in tube wall, highlighted by the red box.

Figure 1-2 Wear damage of the lower end of a heat exchanger tube (steam coil tube) removed from service. Arrows in (a) indicate the orientations of subsequent images.

PROJECT AIM

While much research has been done to understand erosive wear, it is a phenomenon that is very sensitive to the system and associated variables. No work has been reported using magnetite as an erodent. This study is an attempt to redress the balance by investigating the solid particle erosion of low alloy steel by magnetite particles, with the overall aim of reducing erosive wear damage in the synthol reactors.

RESEARCH OBJECTIVES

- To identify and evaluate the process variables in the synthol reactor that are relevant to the erosion process.
- To evaluate erosive wear rates of reactor steel by catalyst in a laboratory apparatus.
- To investigate the mechanisms of erosive wear.
- To quantify the effects of operational parameters on the wear process.
- To investigate the effect of surface treatment of the steel on the wear process.
- To make recommendations to limit the effects of erosion in the synthol reactors.

CHAPTER TWO

LITERATURE REVIEW

2.1. INTRODUCTION TO SOLID PARTICLE EROSION

Solid particle erosion can be defined as a tribological phenomenon which occurs due to the relative motion of a fluid stream, in which solid particles are entrained, and a solid surface[1,2]. In this work erosion by solid particles in a gas stream impacting on a ductile material is considered.

Erosion by solid particles is caused by the impingement of these particles on a solid surface, thereby damaging the surface. The specific damage is related to the properties of both the erodent particles and the target material. There are also a number of system variables such as velocity of the particles due to their acceleration by the gas stream, mass flux of particles and specific impact angle that play a major role in determining the extent of erosion.

Generally, a distinction is made between erosion of ductile and brittle materials. The distinction is sometimes made in terms of the dependence on impact angle. Ductile materials have a maximum erosion rate at oblique angles of impact, while brittle materials display a maximum at normal incidence.

Brittle erosion is characterised by cracking of the target leading to loss of material as chips which are knocked from the surface. Thus, the resistance of the material to cracking under the influence of impacting erodent particles is a major consideration.

Erosion of ductile materials involves considerable plastic flow. Material is removed from ductile targets either directly by cutting or micromachining, or through the formation of flakes or platelets that are removed after a number of impacts. Cutting generally displaces some material as shear lips or ridges. These highly strained layers extruded by the impacting particles, are susceptible to removal by subsequent impacting particles. The platelet

mechanism of ductile erosion is widely accepted. Platelet formation is related to ductility, while cutting models predict an inverse dependence of erosion rate with hardness[2].

Erodent factors such as shape and friability are very important. Friability is a measure of how effectively the particle transfers its kinetic energy to the target. If the particle breaks apart, or chips on impact, much of its energy is dispersed. Thus the erosion rate is lowered.

An angular particle, with sharp edges and corners is very effective in localising the transfer of energy to the target, by virtue of the smaller area of contact. These protrusions can more effectively cut into the target, producing gouges in the surface. Smoother, more spherical particles will tend to plough into the surface, forming lips that are highly work hardened and easily removed by subsequent particles at the trailing edge of the wear scar. The rake angle of a particular protrusion in contact with the surface will determine the efficiency of the cutting process. This is defined as the angle between the perpendicular to the target surface and the leading edge of the impacting particle.

Erosion is quantified by defining the erosion rate, E_R, as the volume of material removed per unit mass of impacting erodent, or as a function of time (under known loading conditions). Volume is preferred over mass loss because it allows comparison between materials of different densities.

2.2. SYSTEM VARIABLES AFFECTING EROSIVE WEAR

The primary force of eroding particles impacting on a material's surface is represented by their kinetic energy, KE, expressed in its most basic form by:

$$KE = \frac{1}{2}mV^2$$

where: m = mass of the particle

V = impact velocity of particle.

A portion of this kinetic energy is transmitted to and absorbed by the target material upon impact. Other segments of the energy are taken up in such events as rotation of the particle,

breaking off of portions of the particle and rebounding of the particle from the target surface[3]. If this energy is low enough (low velocity, small mass) for the material to absorb it elastically, no damage will result.

Several factors relating to the target material and erodent particles affect the portion of kinetic energy absorbed by the target material, and will be discussed in subsequent sections. These factors are affected by the impingement angle (α), particle morphology and the velocity.

2.2.1. VELOCITY AND THE NATURE OF GAS FLOW

Velocity is perhaps the most critical variable to be considered in solid particle erosion. It has been noted that below 10 – 20 $m.s^{-1}$, erosion becomes insignificant for metals[4]. Changes in velocity can eclipse the effects of changes in other variables such as impact angle, target material and erodent angularity. The dependence of erosion rate, E_R, on velocity is widely accepted[2,4-8] as being a power law of the form:

$$E_R = kV^n$$

where: k = material constant
V = impact velocity of the particle
n = velocity exponent

The velocity exponent is generally in the range of 2 – 2.5 for metals and 2.5 – 3 for ceramics, although an early review by Preece and MacMillan[9] reports *n* as 2 – 3.4 for metallic materials and 2 – 6.5 for brittle materials. In a study of erosion of 1Cr½Mo (low carbon, high strength, low alloy) boiler tube steel, Suckling[10] found that at room temperature, *n* was 1.90 for fly ash, 2.12 for silica and 2.16 for silicon carbide particles. The velocity exponent decreased slightly up to 450°C.

The velocity exponent can be calculated from experimental results using the following equation:

$$\frac{E_1}{E_2} = \left(\frac{V_1}{V_2}\right)^n$$

where: E_1 = erosion rate at velocity V_1

E_2 = erosion rate at velocity V_2

The velocity exponent can also be determined from the logarithmic plots of erosion versus velocity[11]. Erosion tests performed at elevated temperatures reveal a lower velocity exponent than at room temperature. Levy et al. calculated n = 1.23 at 800°C for a 310SS alloy impacted by 240 μm silicon carbide particles at 20° and 10 g.min^{-1} particle loading, which was half the values measured in room temperature testing of the same alloy[12]. This was typical of the trend observed for the range of commercial, ferritic and austenitic steels tested.

Lindsey and Marder[6] found that n is independent of both target material and erosion mechanism, for Fe–0.6%C alloy and 70–30 brass, and is governed by test conditions, including particle characteristics and erosion test apparatus. In contrast, Tabakoff[11] found that n is dependent on the temperature, impact angle, particle characteristics and target properties for AM355 steel impacted by fly ash and silica. Lindsey and Marder[6] found that a change in erosion rate of one and a half orders of magnitude was brought about by changing the velocity from 20 m.s^{-1} to 64 m.s^{-1} for an Fe–0.6%C binary alloy, water quenched and tempered, impacted by alumina particles. Testing at these velocities also had a dramatic effect on incubation time. At 20 m.s^{-1} the incubation time was approximately 30 minutes, but at 64 m.s^{-1} the incubation time was nearly zero[6].

Incubation describes part of the initial transient behaviour of an erosion system before steady-state erosion is observed, and is related to particle velocity. Rao and Buckley[13] identified four general stages in the solid particle erosion process:

i. Incubation period, the time span or mass of erodent particles for which there is little or no weight loss. In a few cases there is a slight weight gain due to embedment or adhesion of particles[14].

ii. Acceleration period, the time span in which the weight loss rate increases rapidly.

iii. Deceleration period, the time span representing rapidly decreasing weight loss rate.

iv. Steady-state period, the time span in which the weight loss rate becomes constant and continuous for a long time.

When a gas stream approaches the surface of the material target, its velocity decreases and stagnation ultimately occurs on the surface. Kagimoto et al. showed that particles in the gas stream are decelerated and strike the surface with velocities lower than those of the gas stream[7], as shown in figure 2-1. They recommend that velocity measurements be taken as close to the surface of the target as possible, in order to report the true impact velocity.

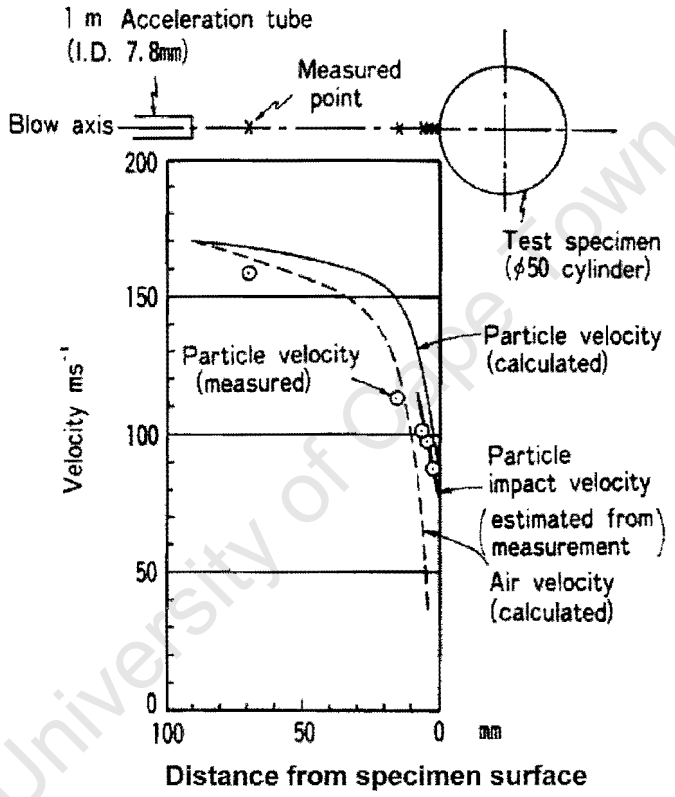

Figure 2-1 Decrease in velocity as particles approach specimen surface, for 3.7 μm alumina particles. (After Kagimoto et al. 1987[7])

The particle stream spreads out after exiting the acceleration tube during laboratory testing, with a bell-shaped distribution of velocity normal to the particle stream, as shown in figure 2-2. The number of particles present in the low velocity region of the gas stream follows the same profile. Thus, while the velocity decreases with distance from the erodent stream centre-line (blow axis), the number of particles available to damage the target also decreases.

The different velocities (and hence different erosion rates) cause a hole or crater to be formed in the target surface which changes the local impingement angle and rebound characteristics of the erodent particles (see section 2.7.3, Wear Scar Geometry). According to Lindsey and Marder this situation should be avoided because a steady-state erosion rate that is constant across the sample surface will not be obtained[6]. In spite of this observation, erosion tests reported in this work show (an overall) steady-state erosion rate despite the dimensions of the specimen being larger than the wear scar and relatively deep craters being formed.

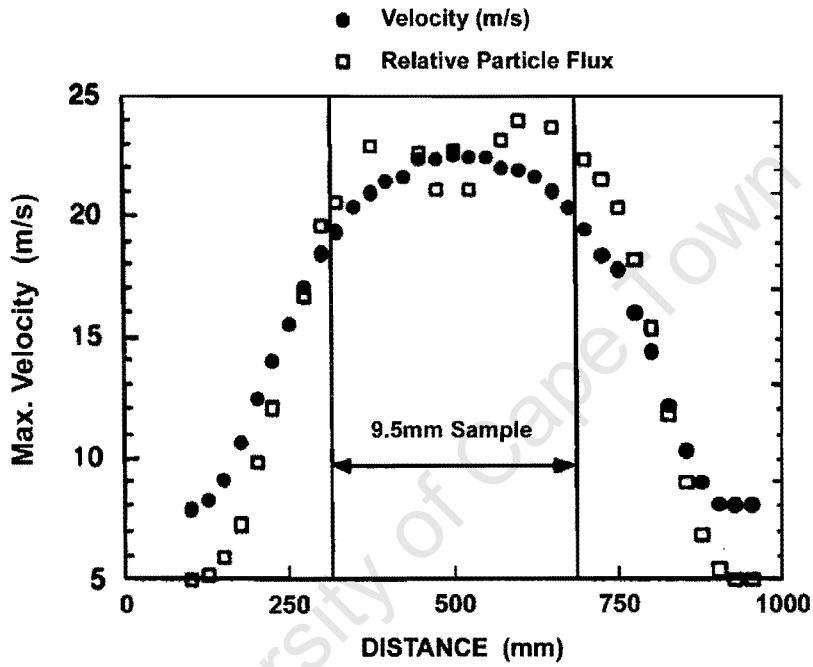

Figure 2-2 Particle velocity and relative particle flux variation across the erodent stream, for 355-425 μm alumina passing through a 1.5 m acceleration tube 15 mm in diameter. (After Lindsey & Marder 1999[6])

2.2.2. IMPACT ANGLE

The effect of impact angle on erosion is well established[2,4,5,9,15,16,17]. Ductile materials generally display maximum erosion rates at low angles, generally 15° - 30°, depending on the erosive system, while brittle materials experience maximum erosion near normal incidence, as illustrated in figure 2-3. Finnie et al.[18] and Branch[19] have shown that the volume removed from a ductile metal at normal impact is 30% – 40% of that removed at 20° impingement. The metals tested were 1100-0 aluminium with 80-mesh silicon carbide, high purity gold with 120-

mesh silicon carbide; and cadmium, iron, magnesium and tantalum with 60-mesh silicon carbide particles. This behaviour is similar for a wide range of ductile metals. The shape and position of the peak for ductile erosion is dependent on the erosive system, but the trends portrayed in figure 2-3 are widely recognised.

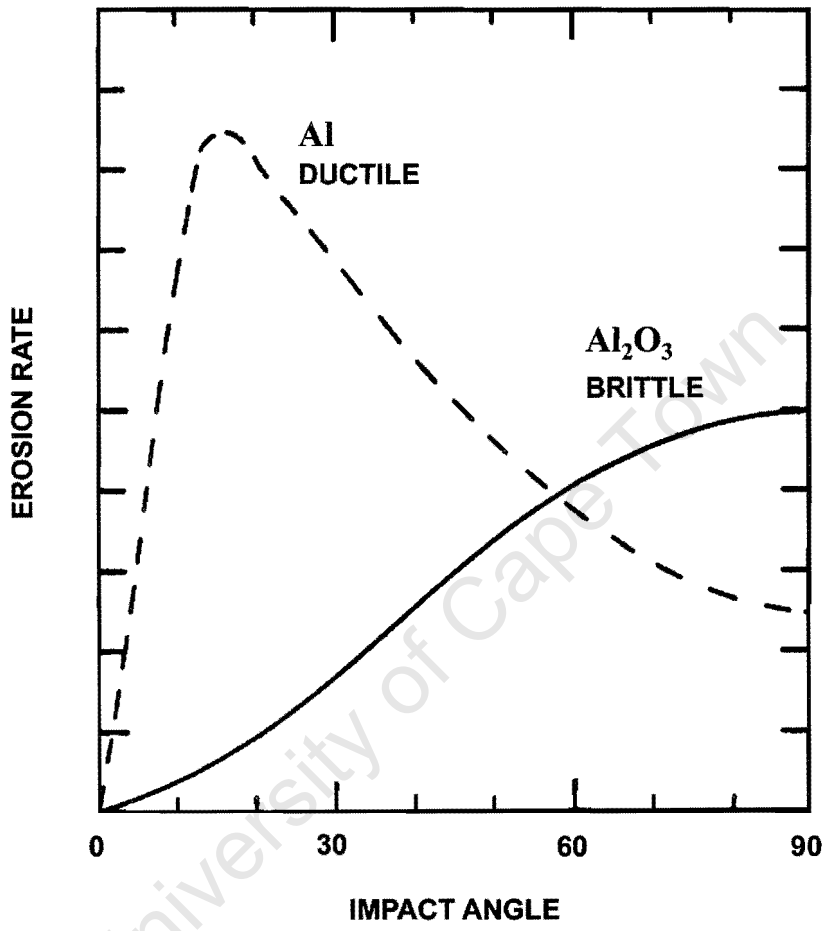

Figure 2-3 Variation of erosion rate with nominal impact angle for aluminium and alumina eroded by silicon carbide grit at 152 $m.s^{-1}$, typical of ductile and brittle materials. (After Hutchings 1979[17])

The impact angle curve is flattened as material ductility increases, because ductile materials are able to distribute the kinetic energy of impacting particles in a less angle-dependent manner[16].

McCabe et al.[8] found that for plain carbon steels (AISI-SAE 1078, AISI-SAE 10105) eroded by alumina particles, the maximum erosion rate was at 40°. Work performed by Yee et al.[20] showed maximum erosion at 35° for BG303 steel impacted by fly ash particles 42 – 66 μm in diameter at 130 $m.s^{-1}$ and 750°C. This result is illustrated in figure 2-4, together with the curve

for type 304 stainless steel impacted by 38.4 μm fly ash particles with an impact velocity of 150 $m.s^{-1}$ at 649°C.

The shape of the curve is explained by Levy[3] in terms of plastic deformation of the material. At low angles, material displaced by eroding particles is piled up immediately adjacent to the impact crater. This raised material is vulnerable to removal by subsequent particle impacts. At angles closer to normal incidence, the more widespread plastic deformation caused by the particles absorbs the kinetic energy without piling up material in such a vulnerable manner.

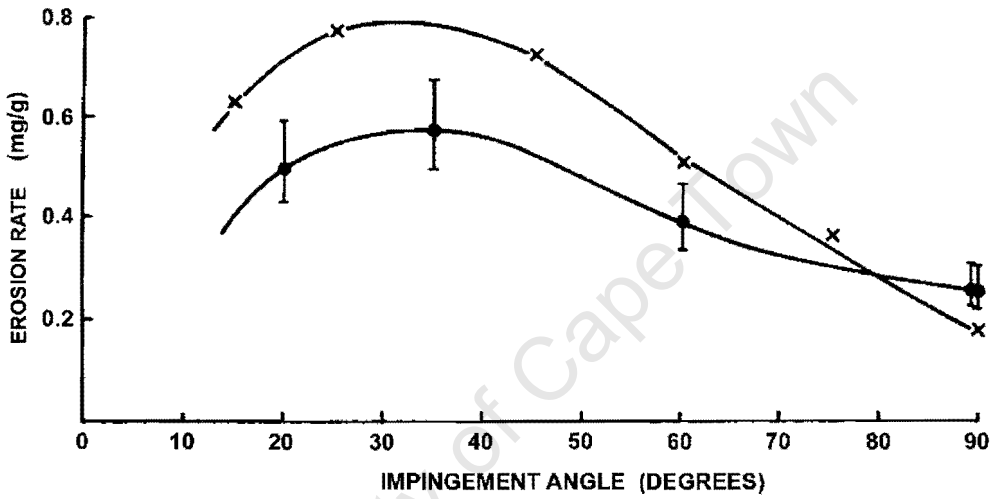

Figure 2-4 Dependence of erosion rate on impact angle for BG303 and type 304 steel targets impacted by fly ash particles. (After Yee et al. 1983[20])

Tabakoff[11] found that for AM355 (a precipitation-hardening semi-austenitic stainless steel) tested with fly ash and silica, the shape of the impact angle curve is independent of particle velocity, the temperature, or the type of impacting particles, with a maximum erosion at 25°. Cousens and Hutchings[21] found that the shape of the curve is dependent on the shape of the impacting particles for a 0.06%C mild steel, with maximum erosion at normal incidence for spherical glass beads and at 25° for crushed glass and angular silicon carbide particles. Naim and Bahadur[22] found that extensive coldwork had a negligible effect on the shape of the curve, when using 3 mm steel balls impacting α brass targets.

Conventional theories describing erosion mechanisms of ductile metals by angular abrasive particles, attribute erosion at oblique (glancing) angles to cutting processes, with gouging wear (ploughing, platelet formation) predominating at normal and near-normal angles of impact[18,21].

2.2.3. MASS FLUX OF ERODENT

Erosion rate decreases exponentially with increasing flux. This is because rebounding particles interfere with incident particles, which shield the surface, resulting in less damage.

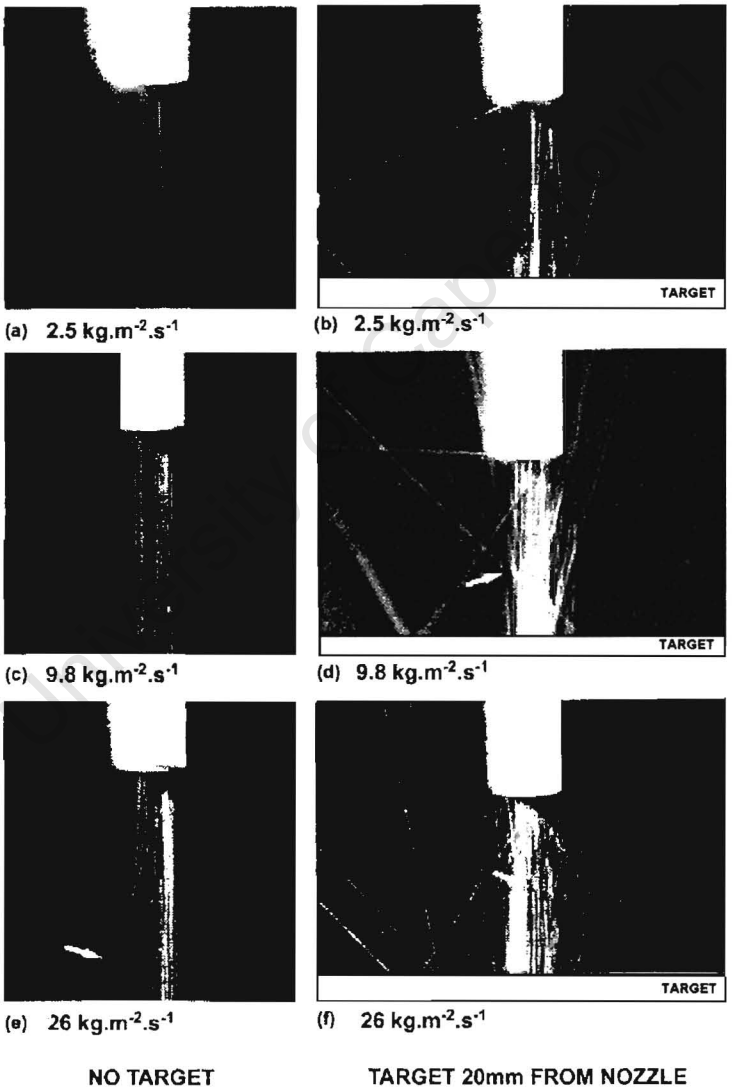

Figure 2-5 Interaction of spherical particles for different particle fluxes. Photographs on the left have no target in place, while those on the right have a flat steel target 20 mm from the nozzle end, orientated normal to the particle stream. (After Shipway & Hutchings 1994[23])

Shipway and Hutchings[23] used long-exposure photographs of the trajectories of 650 – 750 μm lead glass spheres passing through a nozzle of 4.72 mm inside diameter and 308 mm long to show how particles interact with each other when striking a target at normal incidence. Three mass fluxes, namely 2.5 $kg.m^{-2}.s^{-1}$, 9.8 $kg.m^{-2}.s^{-1}$ and 26 $kg.m^{-2}.s^{-1}$, were used for the photographs in figure 2-5, showing increasing interference with increasing mass flux.

Tabakoff[11] showed that erosion rate decreased with increasing particle concentration above 0.25 $mg.cm^{-3}$, for an AM355 steel impacted by petroleum product particles at 30°. Negligible influence on erosion rate was observed up to 0.014 $mg.cm^{-3}$. For 106 – 125 μm silica particles striking a 1Cr½Mo steel, Suckling[10] found similar erosion rates at different temperatures for fluxes of 0.17 $kg.m^{-2}.s^{-1}$ and 2.1 $kg.m^{-2}.s^{-1}$. The latter value was identified as a critical mass flux with attendant transition in erosion rate, above which the erosion rate decreased.

2.3. ERODENT VARIABLES AFFECTING EROSION

The shape of a particle and its mass determine the effectiveness of the particle in concentrating its destructive energy[3]. The erosivity of an erodent particle is a function of how efficiently it transfers its kinetic energy to the target surface. Thus, it is a measure of the angularity (shape), density (mass), size and friability of the particles; and of whether the particles cut into the surface or tumble across it.

2.3.1. SHAPE

Erosion rate is strongly dependent on erodent particle shape[21,24,25]. A sharp angled protrusion from a large particle can be considerably more destructive than a spherical particle of the same mass, or an angular particle of much smaller mass[26]. It has been shown that erosion rate can be up to an order of magnitude higher for angular particles compared to spherical particles[24,25].

The rake angle is defined as the angle between the perpendicular to the target surface and the leading edge of the impacting particle. Figure 2-6 shows how the same non-spherical particle can impact a surface at a range of rake angles. The rake of a particle's protrusion determines its cutting efficiency, especially at lower impact angles[3]. Winter and Hutchings[27] and Gane and

Murray[28] studied the effect of rake angle in ploughing and microcutting. They concluded that microcutting was favoured by positive or small values of negative rake angles while ploughing occurred with large negative rake angles. Non-spherical (angular) particles may cause cutting or ploughing, depending on the orientation to the surface. Highly angular particles are expected to rarely cause ploughing. O'Flynn et al.[29] proposed that a critical rake angle exists above which cutting occurs. High ductility or work hardening rate is expected to give rise to high critical angles (i.e. much reduced occurrence of cutting) leading to low wear rates.

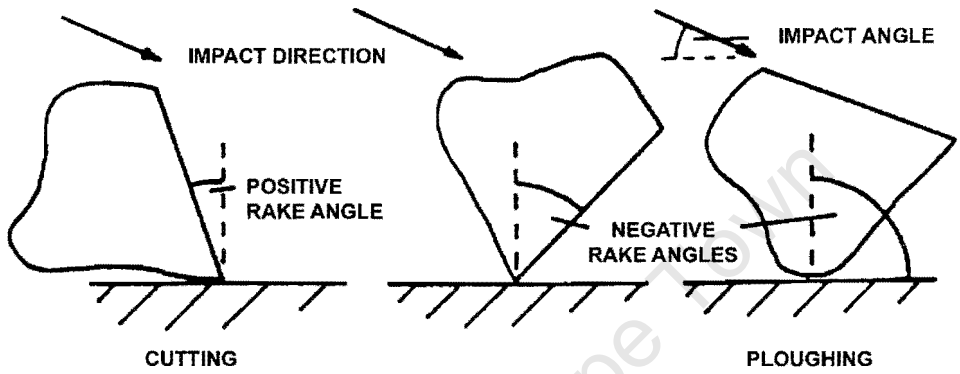

Figure 2-6 Non-spherical particles may strike a target surface at a range of rake angles, dependent on the orientation to the surface. (After Winter & Hutchings 1974[27])

Cousens and Hutchings[21] observed that changing particle shape can change the impact angle which results in maximum erosion. Maximum erosion was found at 25° for angular grit, but maximum erosion was found at normal incidence for spherical particles. Different mechanisms of material removal are observed for angular particles and for spherical particles[18,21,25]. Angular particles remove material by cutting and gouging, while spherical particles remove platelets of material. The appearance of the eroded surfaces indicates the reason for the difference. The angular steel grit caused much sharper craters to form, which resulted in a more efficient production of extruded platelets. The spherical steel shot developed more shallow, rounded craters that did not produce platelets as efficiently[30]. Erosion behaviour can be analysed by considering the effect of rake angle in ploughing and microcutting as observed in erosion. It is the changing contribution from ploughing (for spherical particles) and cutting (angular particles) with changes in shape and size of particles that accounts for the variation in erosion rates[31].

The rake angle experienced by the target material depends on the shape of particle and, in the case of angular particles, on the orientation to the target surface at the point of impact. Spherical particles will always impact the target surface with a large negative rake angle resulting in ploughing being the only plausible mode of deformation. On the other hand, an angular particle may impinge with either positive or negative rake angles. Thus, angular particles are expected to produce both microcutting and ploughing, dependent on the orientation to the surface. Furthermore, the rounder the particle, the greater will be the likelihood of ploughing (due to larger included angle at polyhedral corners – see figure 2-6) in comparison to microcutting[31].

It is not possible to measure the angle of every corner of every particle. Particle angularity can be measured by calculating the width-to-length (W/L) and square of the perimeter-to-area (P^2/A) ratios, which is reasonable for polyhedral-shaped particles.

Local concentration of force is an important factor in erosion. Angular particles concentrate this force more effectively than rounded particles. The local stress is necessarily greater for a more angular particle, because the force, which is similar for similar-sized particles, is applied over a much-reduced area.

Deposition or embedment of impacting erodent particles is also dependent on particle shape[4]. Embedment of angular particles has been observed, while this has not been observed for spherical particles. When particles embed in the surface of a metal, the embedded tip often breaks off and remains in the surface. Rao and Buckley[13] studied this behaviour by reviewing relevant published data and found that, when embedment took place, the steady-state erosion rate was little changed. They also found that the incubation and acceleration periods for angular particles were short compared to those obtained with spherical particles.

Tumbling has been shown to affect the erosion rate[3]. The amount of tumbling across the target surface depends on the particle's faceting. A particle tumbling across the target surface transfers less energy to the target causing less wear damage.

2.3.2. SIZE

According to a study by Goodwin et al.[32], particles lose their erosion effectiveness below about 100 μm in diameter. Above a size of 100 μm, size has little or no effect on erosion rate. Bahadur and Badruddin[31] postulate that extremely fine particles may not result in any erosion because their impact is limited to producing elastic deformation in the target surface. A minimum particle size must therefore exist, depending on particle density, impact velocity and target properties, above which erosion will be observed.

Schematic view	Particle diameter [μm]	Impact velocity [$m.s^{-1}$]	Kinetic energy [J]	Particle feed rates [s^{-1}]
Velocity / Particle size	23.5	131.9	2.4 x 10	2×10^{9}
	34.1	75.4	2.4 x 10	2×10^{9}
	42.5	54.2	2.4×10^{-7}	2×10^{9}

Table 2-1 Simultaneous variation of particle size and velocity necessary to maintain constant kinetic energy. (After Kagimoto et al. 1987[7])

Erosion rate increases with increasing particle size, for a given particle velocity[11,31,33]. This is known as the size effect in solid particle erosion. Kagimoto et al.[7] agree that small particles have a lower impact velocity than larger particles, but they claim that if the particle velocity is the same, the erosion rate is the same. They explain the effect of particle size by variations in impact velocity, i.e. by relating erosion rate to kinetic energy. Table 2-1 shows how larger particles with a lower velocity can have the same kinetic energy as smaller particles with a higher velocity.

For a given free stream velocity, the velocity of erodent particles is dependent on the particle size. Kagimoto et al. found that for particles under 20 μm, impact velocity increases as particle size increases. In the range 20-40 μm, impact velocity is constant; and for particles over 40 μm, impact velocity decreases with increasing particle size (figure 2-7). Particles larger than 100 μm, which are less susceptible to air flow, had lower velocities than those in the range 20-40 μm. This was ascribed to the lack of acceleration in the 1 m acceleration tube used in their erosion testing[7].

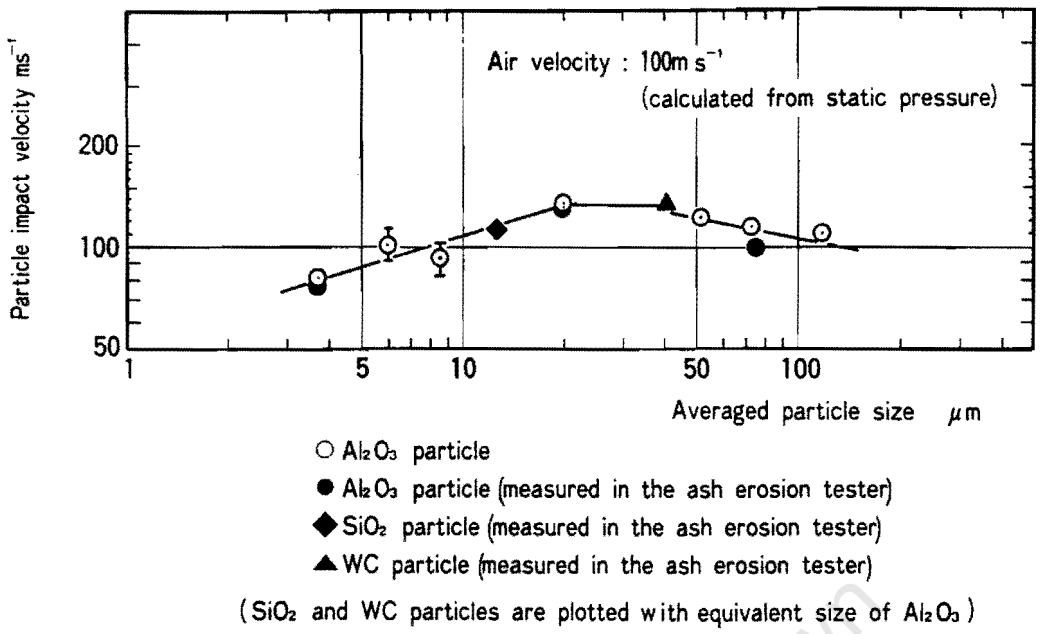

Figure 2-7 Impact velocities for various particle sizes. (After Kagimoto et al. 1987[7])

Sparks and Hutchings[34] used the one-dimensional flow model developed by Ninham and Hutchings[35] for calculating particle velocities in a gas-blast erosion test rig, to predict the velocities of spherical particles of various sizes. Figure 2-8 shows the theoretical velocities predicted for 137 μm particles, with a density of 2.60 $g.cm^{-3}$ and free stream velocity of 270 $m.s^{-1}$. The predicted values shown in figure 2-8 agreed well with measured velocities of silica particles, but overestimated the velocity of glass spheres. The trend was thus supported by both theory and testing.

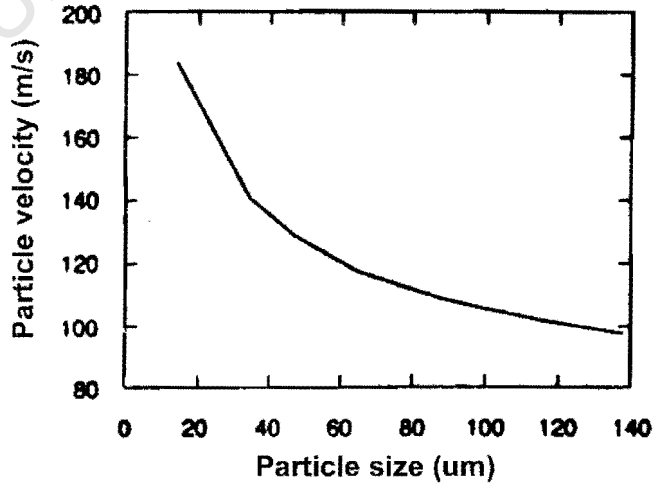

Figure 2-8 Prediction of velocities of different size spheres for the same free stream velocity. (After Sparks & Hutchings 1993[34])

Jin et al.[33] studied the erosion of AISI 304 stainless steel tube banks by coal ash (55% SiO_2, 30% Al_2O_3). Figure 2-9 shows typical particle trajectories for different size particles flowing past two-row staggered tube banks, with free stream velocity, U_∞, of 10 $m.s^{-1}$. Very fine particles ($d_p \leq 20\mu m$), because of their low inertia, rarely impact the surface of the first row of tubes as they are completely entrained by the gas flow. These particles are greatly accelerated in the first row such that almost all the particles strike the second row of tubes. The particle collision frequency decreases with decreasing particle diameter because the particles become more responsive to the gas flow along the tubes.

Although the free stream velocity of the particles may be similar, Jin et al. found that the location of maximum collision frequency in the two rows of tubes was different for different particle sizes. Maximum erosion was noted as being more serious for larger particles, with maximum erosion in the second row three times as high as in the first row, although total erosion was twice that of the first row. At the same location on the tube surface, the impact angles of smaller particles were smaller than those of larger particles.

Gulden[36] found a size-dependent transition between brittle and ductile erosion. She explained this in terms of the higher strain rates produced by smaller particles. At high strain rates, flow stress can be a direct function of strain rate.

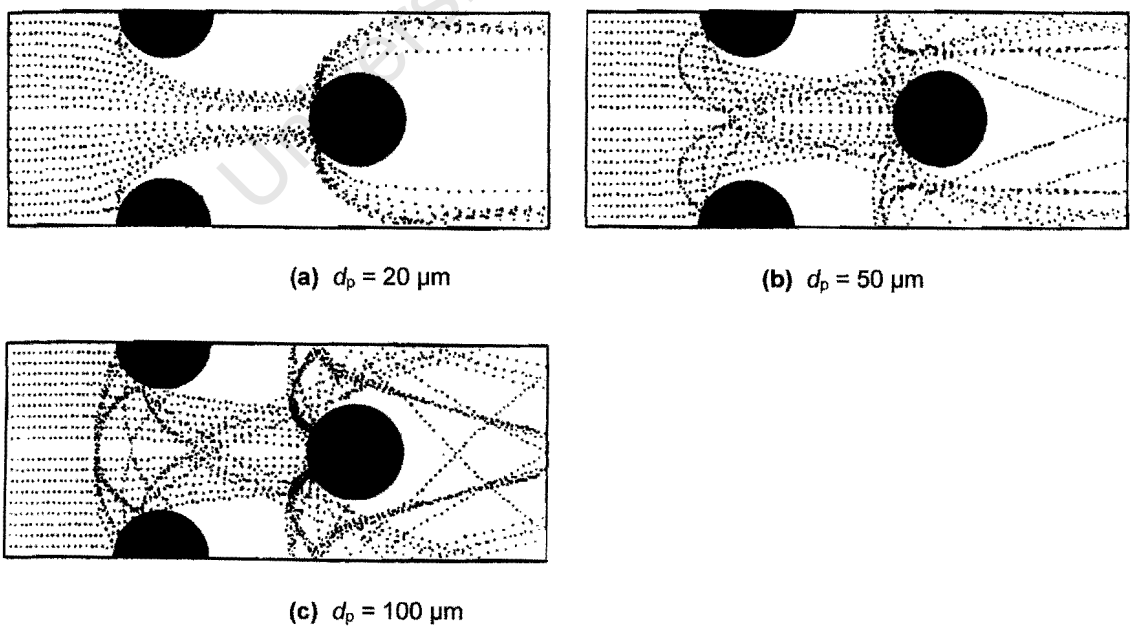

Figure 2-9 Typical particle trajectories for different size particles around two-row staggered tube banks (U_∞ = 10 $m.s^{-1}$). (After Jin et al. 2001[33])

2.3.3. TYPE AND HARDNESS

The hardness of the erodent is an important factor in solid particle erosion. Particles with similar hardness, shape and size cause similar erosion in ductile materials. The erosivity of particles increases with increasing hardness until a threshold hardness is reached above which erosion rate is insensitive to increases in particle hardness. When the hardness of the impacting particle is much in excess of the target material's hardness, differences in hardness are not expected to make any difference to the erosion rate[31].

Based on tests of AISI 1020 steel eroded by SiO_2, SiC and Al_2O_3, Levy and Chik[30] found that above a threshold hardness value of 700 $kgf.mm^{-2}$, mild steel erodes at approximately the same rate regardless of the hardness-strength characteristics of the eroding particle. Hardness is considered a measure of the integrity and strength of the erodent.

The ratio of particle hardness to target hardness is shown below:

$$\frac{H_{erodent}}{H_{target}}$$

This is important because above the threshold value, increasing the particle hardness makes a negligible difference to the erosion rate. It has been reported that the erosion rate drops dramatically when the hardness of the particle falls below that of the target[2].

Levy and Chik[30] found that particles with compositions above a certain threshold level of integrity (generally described by hardness values) that have the same shape as eroding particles in a service environment can be used interchangeably in erosion tests. They also showed that the platelet mechanism was the dominant material loss mechanism regardless of the erosivity of the particle compositions, with the production of shallow craters and platelets being very similar for all three erodents tested.

Documentation of SiO_2, SiC and Al_2O_3 particles revealed that SiO_2 particles were more regular in shape and closer to spherocity than SiC and Al_2O_3 particles[31].

2.4. ERODENT RECYCLING AND PARTICLE FRIABILITY

Recycling of erodent in erosion testing can lead to rounding, or in some cases, significant fracture of the particles, with a concurrent change in erosive conditions. Fragmentation of particles leads to changing erosion rates in subsequent testing.

According to Sparks and Hutchings[34], three factors are responsible:

i. Intrinsic size effect – the reduction in erosion rate with reduced particle size.
ii. Aerodynamic effects, i.e. higher velocities associated with smaller particles.
iii. Changes in particle angularity due to fracture.

The change in the erosion rate is due to competition between these effects. The reduction in size increases the angularity and velocity of the particles, which outweighs the intrinsic size effect and thus an increase in the erosion rate is observed. Further reduction in size is not associated with an increase in angularity, and despite increased velocity, the intrinsic size effect dominates and leads to a reduction in erosion rate.

The interplay of these effects is illustrated by work performed by Rao and Buckley[13], who report a drop-off in erosion rate for prolonged exposures with angular particles typical of those generally encountered in service. For long-term exposures, erosion rates can become lower than the peak erosion rate.

Fragmentation is strongly dependent on velocity, with the strength of the particles and the hardness of the target playing important roles. Hardness of particles and target is often used as a measure of the ability of the particles to maintain structural integrity, and of the target to resist absorption of any but negligible amounts of the particles' energy.

Erosivity of impacting particles is primarily a function of the concentration of force that particles can cause in a local area on the target material. Weak and friable particles shatter, or otherwise lose their integrity when striking target surfaces. Thus they do not transfer as much of their kinetic energy to the target. Most of their energy is utilised in fracture. Smaller pieces also do not have the required mass to provide the localised force necessary to efficiently form and remove platelets by exceeding the local fracture stress of the metal. High integrity particles

cause steady-state erosion to be reached after fewer impacts than low integrity particles that shatter on impact.

Levy and Chik[30] found that SiO_2, SiC and Al_2O_3 particles striking AISI 1020 steel at 80 $m.s^{-1}$ retained their size and shape. They observed striations on the eroded surfaces thought to be imprints of contour facets of the particles as they moved across the metal surface, but no evidence was found of the particles breaking up on impact. Sparks and Hutchings[34] found that SiO_2 particles impacting ceramic specimens at 44 $m.s^{-1}$ and 30° were not fragmented, but at 98 $m.s^{-1}$ and 90°, fragmentation was observed after one cycle of testing. This clearly illustrates how a change in velocity can change the erosive behaviour of the whole system, in this case by causing particle fragmentation at higher velocities.

2.5. TARGET VARIABLES AFFECTING EROSION

2.5.1. DUCTILITY AND DEFORMATION

The erosion of ductile metals is related very closely to the ability of the material to absorb plastic strain associated with particle impact. An improved capacity to absorb this energy equates to a lower erosion rate. The localisation of plastic deformation, which causes highly strained lips (platelets) to form, increases the erosion rate significantly.

Foley and Levy[16] found that the ductility of steels, as measured by their tensile elongation, was shown to correlate most directly with erosion resistance. Their work provides evidence that the greater the ductility of a metal, the greater its erosion resistance. Steels tested in different heat treatment conditions displayed increased erosion resistance in the more ductile conditions. O'Flynn et al.[29] proposed that toughness (as opposed to hardness) is the most influential property with regard to erosion.

Ductility permits the target material to plastically deform to absorb kinetic energy rather than generating a fracture surface that produces particles of debris that are ejected from the surface[3].

Plastic flow, as a mechanism of absorbing the kinetic energy of impacting particles, can play a major role in determining the erosion behaviour of materials. The greater the ductility within a family of alloys of a base metal, the lower the erosion rate can be in spite of the fact that the hardness decreases as the ductility increases. The effect of ductility on erosion rate can be overwhelmed by high kinetic energy levels of the impacting particles or low strength of the material, or both (i.e. there is a finite region where this is useful). Increasing amounts of cold work, which decreases the ductility of the metal, results in an increased erosion rate even though the hardness increases[3].

2.5.2. WORK HARDENING AND HARDNESS

It is well documented that alloy hardness has no correlation with either room temperature or elevated temperature erosion rates[12,15,25]. There is no simple and direct relationship between erosive wear resistance of materials and mechanical properties, including hardness, and others such as yield stress, toughness and elongation[37].

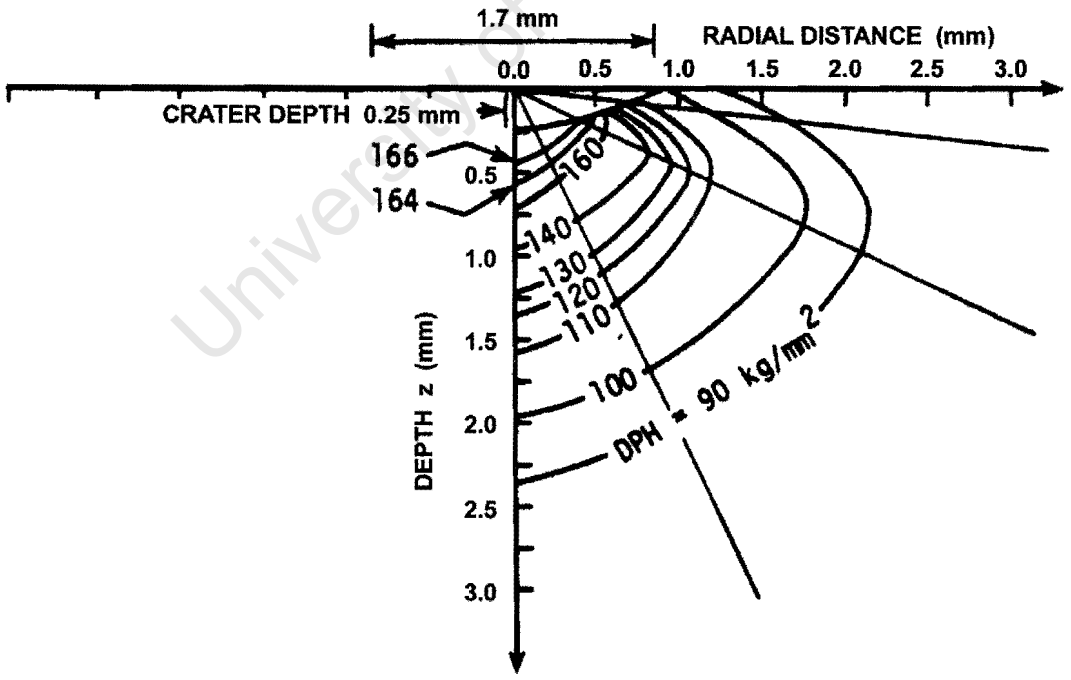

Figure 2-10 Plot of isohardness lines below the impact crater formed in α brass by a 3 mm steel ball. (Naim and Bahadur 1983[22])

Finnie et al. showed that an increase in hardness by cold work or by quenching and tempering steels produced essentially no change in erosion rate[18]. This is because the surface work hardens fully under the high energy / high strain rate erosion conditions[2]. Surface hardness (i.e. the hardness of the target surface under erosive conditions), which is related to work hardening of the metal, has been shown to be important in erosion[29,37].

Naim and Bahadur[22] plotted the variation of hardness observed in an annealed α brass target following a single impact with a 3 mm steel ball at 120 $m.s^{-1}$ at normal incidence (figure 2-10). The maximum hardness was reached just below the central portion of the impact crater, which implies that this region was the most severely work hardened. A gradual decrease in hardness with increasing depth was observed. The field of deformation was approximately three times the radius of the impact crater. Erodent particles interact with this work hardened layer, therefore the erosion resistance of the material is determined by the properties of this layer[25]. Figure 2-11 shows how the work hardening behaviour of the material affects lip formation. Work hardening is expressed as:

$$\frac{d\sigma}{d\varepsilon}$$

where: $d\sigma$ = flow stress

$d\varepsilon$ = plastic true strain

Sundararajan[38] argued that lip formation only occurs at strains higher than a critical strain, ε_c, at which $\frac{d\sigma}{d\varepsilon} = 0$ as shown schematically in figure 2-11(ii),(iii). The material deforms homogeneously below this strain (figure 2-11(i)).

Levin et al.[39] used a nano-indentation method to estimate the restitution coefficient within plastically deformed regions of eroded samples, that provided a measure of the rebounding ability of a material during particle impact. A logarithmic-type relationship was observed between hardness and restitution coefficient, showing that an increase in hardness produced a decrease in the amount of plastic deformation dissipated into the material.

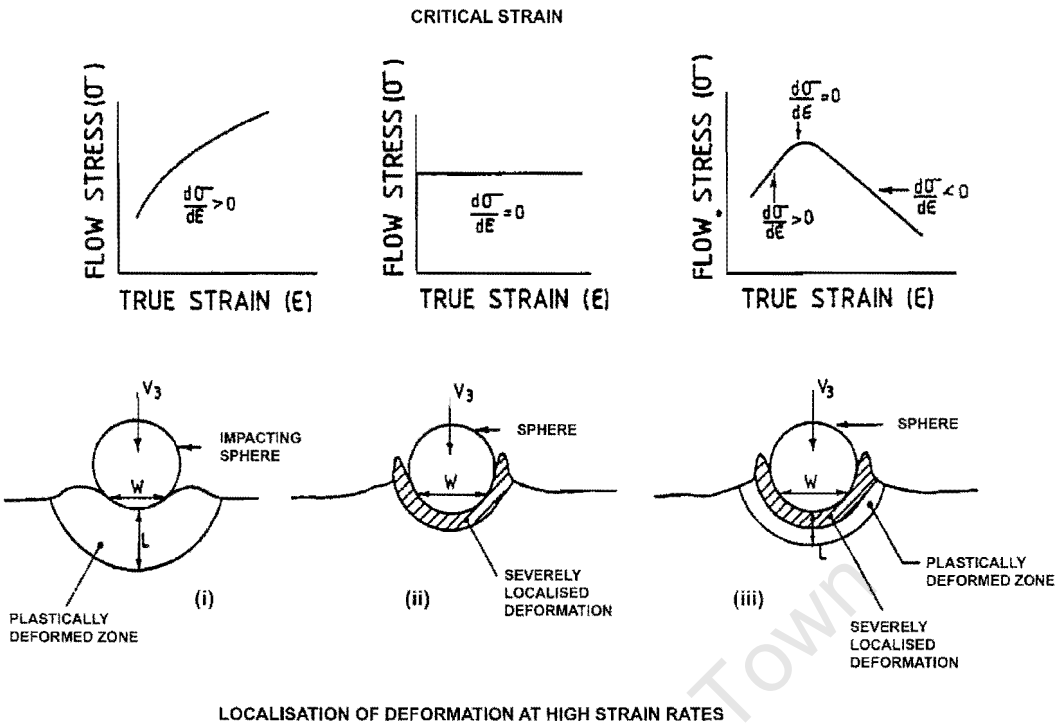

Figure 2-11 The interrelationship between the flow stress-strain (work hardening) behaviour of a material and its tendency to experience localised plastic flow under the impact of a spherical particle.

(i) Strains less than ε_c: $d\sigma/d\varepsilon>0$

(ii) Critical strain: $d\sigma/d\varepsilon=0$

(iii) Strains higher than ε_c: $d\sigma/d\varepsilon<0$ (After Sundararajan 1995[39])

Ball[37] argued that material is lost from the surface by erosive wear when a critical fracture strain is reached. A worn surface is considered to have reached this critical strain, which can be reached after a single impact or through repetitive impacts depending on the system. There is thus a gradient of decreasing hardness (related to plastically strained material) with increasing distance below the surface, with material at the yield point at some depth, beyond which is unaffected (undeformed) material (figure 2-12). Sundararajan[38] rationalised the formation of the uniform deformed surface layer shown by Ball. In figure 2-13(i) the plastic deformation due to a single impacting particle is shown as a hemispherical volume. Under the action of repeated impacts, these plastic zones superpose as in figure 2-13(ii), forming the uniform deformed layer (figure 2-13(iii)) observed in practice.

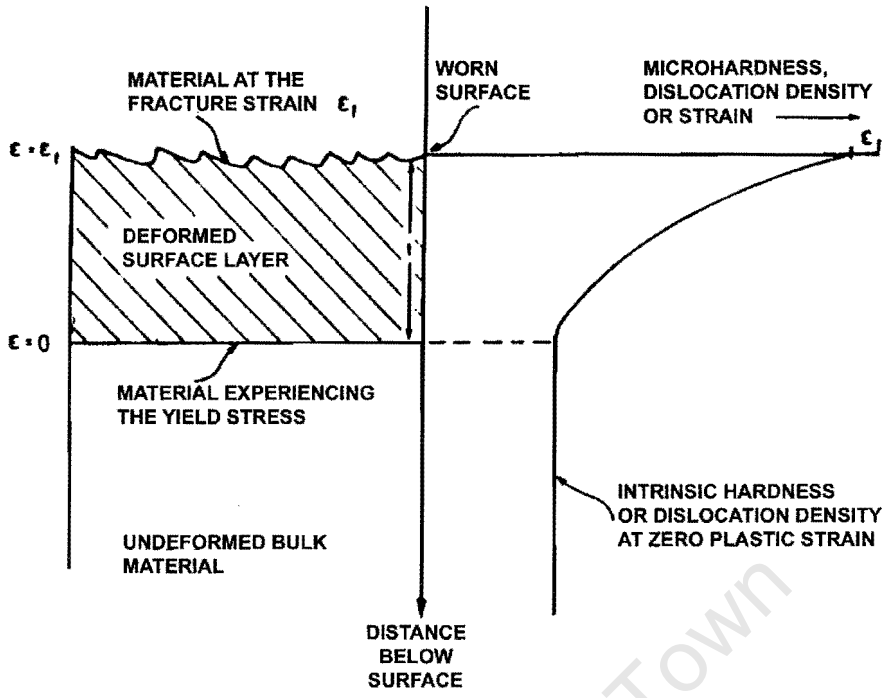

Figure 2-12 Deformed surface layer of an eroded metal, showing decreasing hardness up to a certain depth below the surface. (After Ball 1983[37])

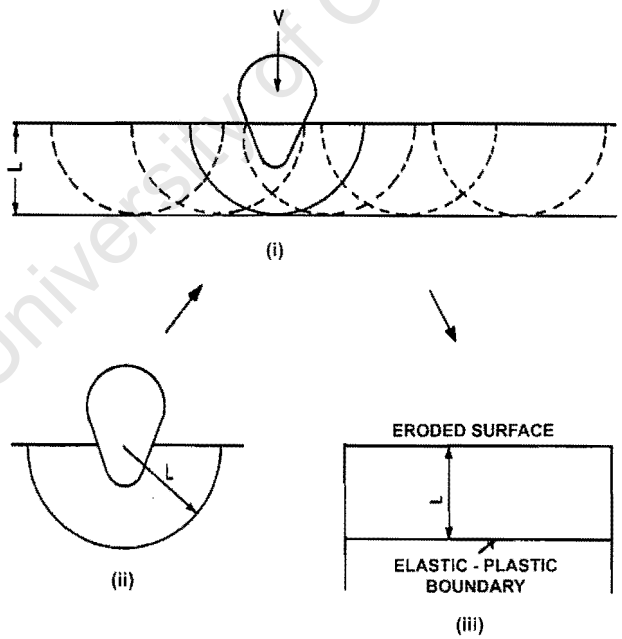

Figure 2-13 A schematic illustration of the formation of the overall plastic zone observed on the surface of metals due to solid particle erosion. This plastically deformed layer is shown to be the sum of the plastic zones formed by individual impacting particles. (After Sundararajan 1995[39])

The heat generated by the impacting erodent can be sufficient to cause softening of the surface of the material. This is illustrated in figure 2-14. The underlying material that is not heated sufficiently, work hardens as expected. Platelets are formed easily in this softened layer, as the impacting erodent deforms the surface against the anvil of the hardened subsurface layer[40]. Figure 2-15 shows the microhardness variation with increasing depth from the surface for an AISI-SAE 1020 impacted by 250 μm silicon carbide particles at 30° and 30 $m.s^{-1}$.

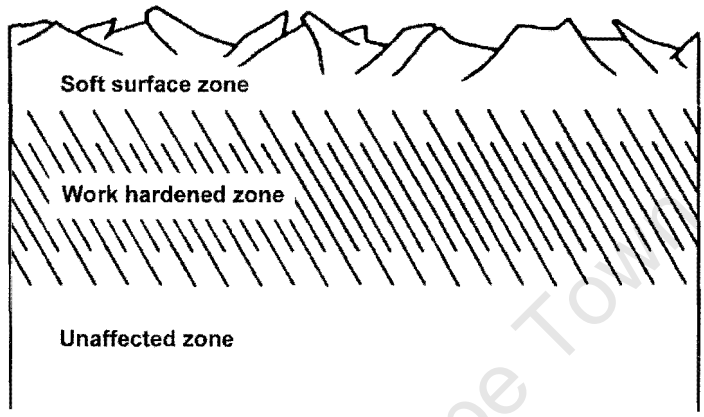

Figure 2-14 Softened surface and work hardened layers due to erosion. Platelets are illustrated in the surface layer. (After Bellman and Levy 1981[40])

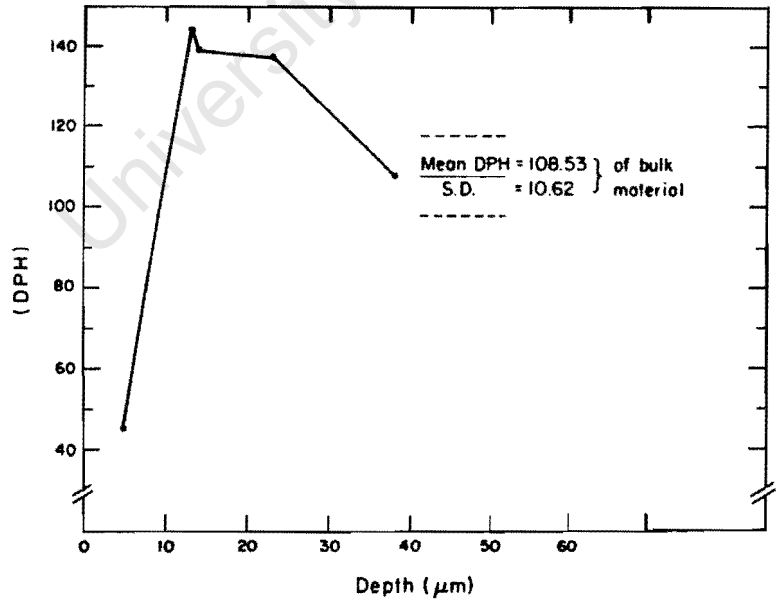

Figure 2-15 Microhardness variation with depth below the surface of an eroded AISI-SAE 1020 steel (250 μm SiC particles; α = 30°; v = 30 $m.s^{-1}$; 25 °C). (After Foley and Levy 1983[16])

According to Foley and Levy[16] the time taken to reach steady-state erosion depends on the work hardening coefficient of the steel. A high strain hardening coefficient is associated with short times to reach steady-state erosion. This correlates with the need (in the platelet mechanism of erosion) for a subsurface cold-worked zone to exist before steady-state erosion occurs. This forms during the incubation period. Naim and Bahadur[22] noted that as the degree of prior coldwork increases, the incubation time decreases, suggesting that severe straining is a prerequisite for material removal, i.e. when the strain induced due to impacting particles exceeds the true tensile fracture strain of the material. For the same number of impacts, the more extensive the prior coldwork, the higher was the steady-state erosion rate.

A metal with a high capacity for work hardening (high work hardening exponent, n, for example a ductile, annealed metal) will 'sink in' because deformation tends to spread to the bulk material, such that a lip is not formed around the crater. By contrast, in metals with a low capacity for work hardening (such as metals already highly deformed, and therefore less ductile), deformation is more localised causing 'piling up' or lip formation. A reduction in the tendency to form lips in turn reduces the number and volume of platelets formed (see section 2.7.1), thereby lowering the erosion rate. Thus, a high work hardening exponent which leads to less platelet formation gives rise to lower erosion rates[29,37].

2.5.3. MICROSTRUCTURE

McCabe et al.[8] studied the erosion of plain carbon steels of eutectoid (AISI-SAE 1078) and hypereutectoid (AISI-SAE 10105) composition by alumina particles with a mean size of 36 μm at 40 – 100 $m.s^{-1}$, 10° - 90° and exposure times of 600 s at a particle feed rate of 0.5 $g.s^{-1}$. Spheroidite was the most resistant to erosion, followed by pearlite and martensite. For both steel compositions, increasing erosion resistance was observed with decreasing hardness. Changing the mean free spacing of ferrite from 2.3 to 4.7 μm in the speroidised microstructure had no effect on the erosion rate. The effect on erosion rate of changes in the microstructure of steel is much less pronounced than the effects of changes in erodent variables.

2.6. ELEVATED TEMPERATURE EROSION

Elevated temperatures, which increase the ductility and decrease the sub-surface work hardening of a metal, decrease the erosion rate, even as the strength decreases[16]. This is true until the temperature is high enough to decrease the yield strength sufficiently that the ductility effect is overcome and fracture surface generation can readily occur.

In work performed by Levy, Yan and Patterson[12], all of the steels tested had constant or decreasing erosion rates as the test temperature was increased until a temperature was reached where a marked increase in erosion rate began to occur with further increases in temperature. Figure 2-16 shows the results for a range of steels impacted by 250 μm silicon carbide particles at 30°. Generally, austenitic steels display superior erosion resistance at elevated temperatures compared with ferritic steels[41].

As the temperature increases, the size of the shallow craters and platelets formed during erosion increases. This is directly related to the decreasing ability of the metal to concentrate the force of the impacting particles in the surface layer, due to the increasing ductility and decreasing work hardening ability[12].

Oxidation effects become important at elevated temperatures[41], particularly at low velocities, with materials that have high scaling rates, such as nickel and cobalt, exhibiting the highest erosion rates. Alumina forming alloy systems have superior erosion resistance, due to the slow growth of the oxide layer (thin layer). Morphology of the oxide layer is also important, with segmented scales outperforming thick, continuous layers that spall over large areas.

Above the temperature at which a metal experiences increasing erosion rates, narrow, elongated gouges form on the surface. They are formed by sharp, angular protrusions penetrating the soft surface of the steel over a horizontal distance brought about by the particle's momentum[12].

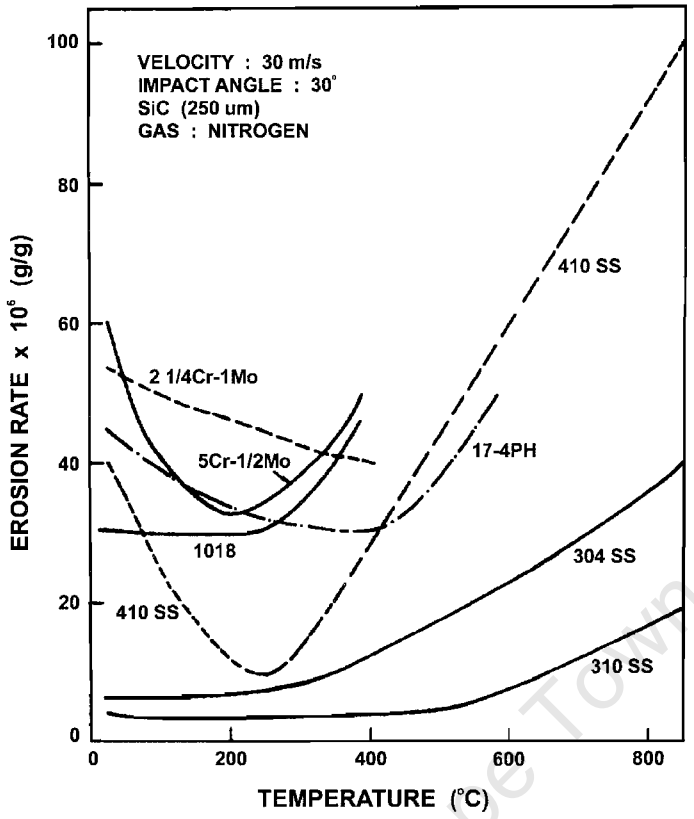

Figure 2-16 Variation of erosion rate with test temperature for 2.25Cr-1Mo, 5Cr-0.5Mo, 1018 steels and 304, 310, 410, 17-4 PH stainless steels. (After Sundararajan & Roy 1997[41])

As the temperature is increased, the increased ductility of the steel compensates for the decrease in strength, such that the erosion rate remains constant, or decreases. At some temperatures, dependent on the steel itself, the erosion rate begins to increase due to the decrease in strength and the increase in oxidation overwhelming the benefits of increased ductility. At high temperatures the higher erosion rates represent erosion of the oxide layer, and are governed by the properties of the oxide layers formed on steel surfaces.

2.7. TARGET RESPONSE TO EROSION

2.7.1. MECHANISMS OF MATERIAL REMOVAL

Material being removed from the target surface constitutes erosion. This material is removed either by a direct cutting action, which machines chips of material from the surface, or by ploughing and the associated platelet formation and removal. Platelets formed on the surface are not removed directly, but rather require subsequent impacting particles to knock them from the material. Figure 2-17 shows piled up material that will form platelets due to subsequent particle impacts. The same mechanism is evident for the velocities shown.

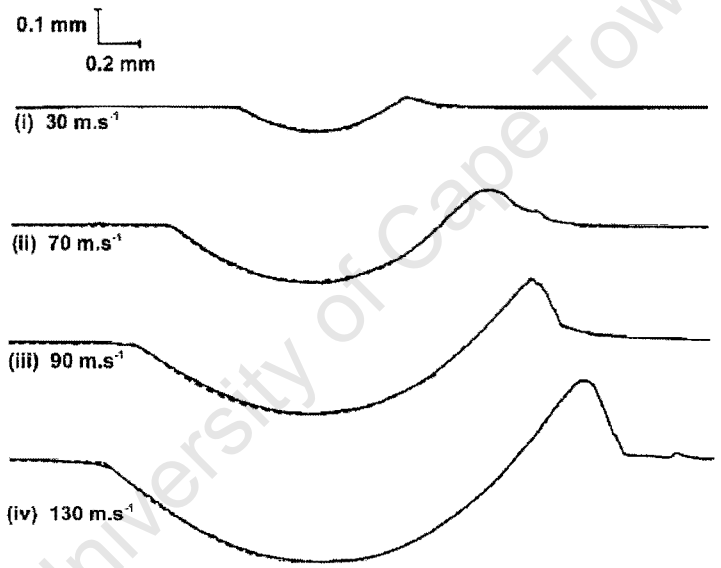

Figure 2-17 Wear profiles produced in aluminium by 1.58 mm spheres at 30° and varying velocity. (After Rickerby and Macmillan 1981[42])

Researchers testing a wide range of steels have shown that all the steels eroded by the platelet mechanism under all conditions (including temperature and impact angle) studied[12,16].

The platelet mechanism of erosive wear originally proposed by Levy[40,43,44] has been widely accepted and observed[3,16,45]. Metal in the immediate surface region is deformed into flat platelets which are extruded from between the impacting particle and target material. These platelets are subsequently highly deformed by continuing particle impacts and are eventually

knocked off the surface when their local fracture strain is exceeded. Beneath the highly deformed surface region a cold-worked zone develops that enhances the ability of the impacting particles to form, deform and knock off platelets. The degree of plastic deformation that each platelet undergoes is a function of the ductility, strength and fracture behaviour of the target material compared to the kinetic energy of the particle[3].

The mechanisms of material removal are generally considered to be different depending on impact angle. This is summarised graphically in figure 2-18. Highly deformed material is removed as chips by cutting at low impact angles and as crater lips at angles close to normal incidence. At normal incidence the formation of flakes (platelets) is maximised, for spherical particles causing maximum erosion at normal impact[21]. Ploughing can be thought of as a transition mechanism that is a combination of the two extremes. Some material is cut from the surface, but other material is extruded to form a crater lip at the trailing edge of the wear scar.

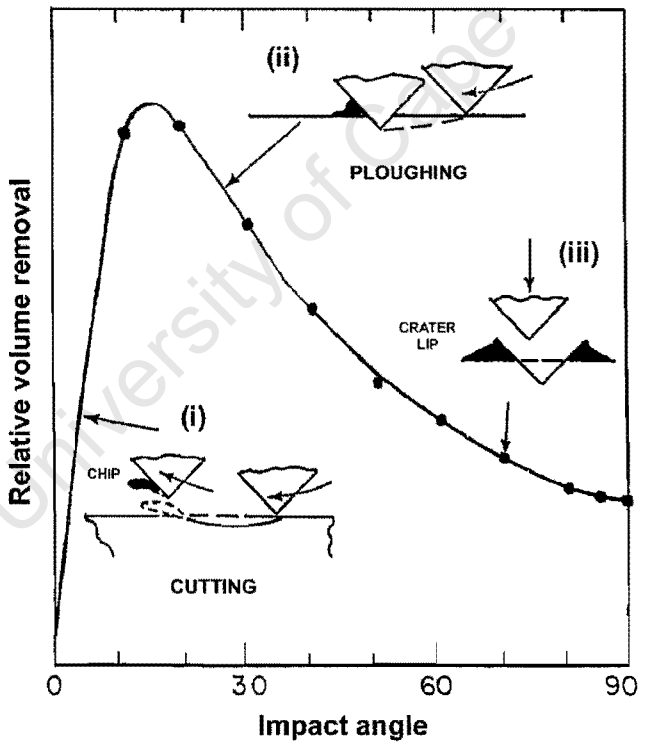

Figure 2-18 Different mechanisms dominant at different impact angles:

(i) Cutting, with material removal as chips, is dominant at low impact angles.

(ii) Ploughing is a combination of the two extremes.

(iii) Crater lip formation, with material removal as platelets from highly deformed crater lips, is dominant at normal incidence. (After Finnie 1995[46])

Not all a particle's kinetic energy is used in removing material from the metal surface. A portion of the volume swept out at low impact angles will be deformed and displaced in a ploughing action. At normal incidence, a significant amount of energy is expended in deforming the sub-surface below the impact crater, where deformation levels are much lower than in the highly deformed crater lips.

Low angle erosion has been compared to abrasion[29]. A critical angle for cutting has been proposed by O'Flynn et al.[29] with chip formation only occurring at angles greater than this critical angle. This angle is not the impact angle, but rather the effective angle that the leading face of the particle (rake angle) makes with the target surface. This angle is thought to depend on the mechanical properties of the eroding surface. High ductility, or high work hardening rates is expected to give rise to high critical angles leading to low wear rates. The concept of uniform strain considers both effects. Uniform strain is defined as the plastic strain required for the onset of localised deformation (necking) in a tensile test specimen. It is also equivalent to the work hardening exponent, n, in the Holloman relationship, and is therefore a measure of the work hardening capacity[29].

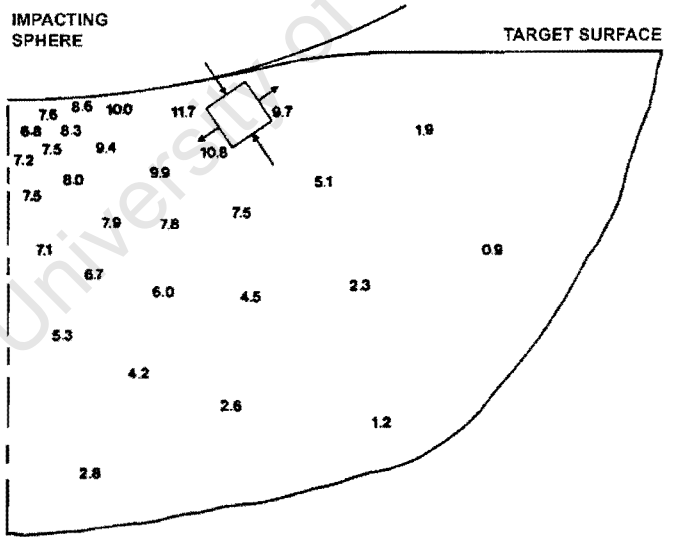

Figure 2-19 Deformation of the surface region as calculated using a finite element model. (After Follansbee et al. 1981[14])

A finite element stress analysis[14] based on an accumulated damage fatigue failure mechanism model used to describe low velocity particle erosion, indicates the strain distribution due to an impacting particle. Figure 2-19 presents these results, which indicate that high plastic strains

(almost pure shear) are found near the surface at the edge of the contact region. The plastic strains rapidly decrease in magnitude with increasing distance beneath the surface. This suggests that platelets worn from the surface would be thin in this dimension, which is confirmed by observation in erosion tests.

2.7.2. SURFACE RIPPLING

The development of surface ripples on metals due to erosion has been observed by several researchers[2,20,21,47-50] in ductile materials at low impact angles. Ripples form normal to the component of the particle velocity parallel to the surface. The appearance of the pattern has been compared to patterns observed in sand dune and water wave motion (figure 2-20).

Ripples are generally observed at low impact angles. Carter et al.[49] noted that the ripples disappear for impact angles greater than 60°. There is some inconsistency in the literature with regard to ripple formation. Green et al.[51] reported extensive surface ripples on plain carbon steel eroded by 250 μm silicon carbide particles at 30°. Under similar test conditions, Stringer and Wright[47] found no evidence of ripples with 50 μm silicon carbide particles.

Stringer and Wright[47] describe the problem as formally that of waves on a surface of discontinuity. This is a standard problem in fluid mechanics and it can be shown that the common boundary is unstable for small wavelengths. The plane surface of the metal target is intrinsically unstable with the net flow of momentum parallel to the surface. A wave pattern forms, provided a mechanism exists whereby a change in shape can take place. The material movement in erosion can thus be regarded as a way in which the surface can change its shape toward the dynamic equilibrium form. Local ductility is therefore not an intrinsic requirement, and ripples have been observed in some brittle materials. If a mechanism exists for preferential erosion of high spots, or some other process which stabilises a planar surface, ripples will not be observed. A high rate of surface movement favours the development of the dynamic equilibrium structure, which explains its widespread observation in ductile metals eroded by solid particles entrained in a gas stream.

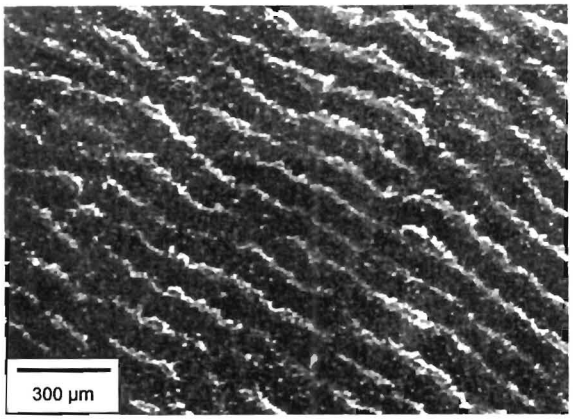

(a) Well-developed ripple structure.
0.06% carbon mild steel
95-105 µm glass beads
30°

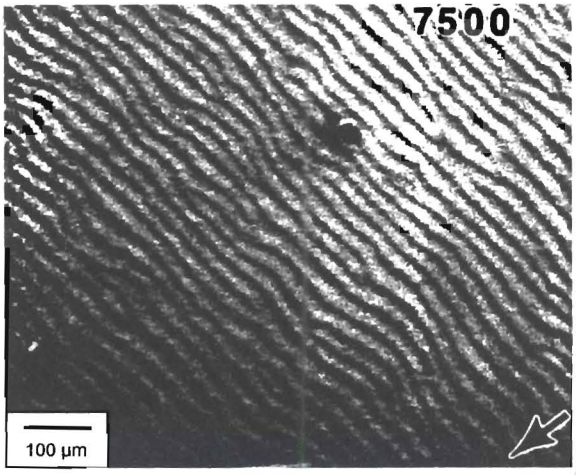

(b) Ripples formed in AISI 446 steel. Arrow indicates direction of erodent.
AISI 446
12 µm alumina
30°
760 °C

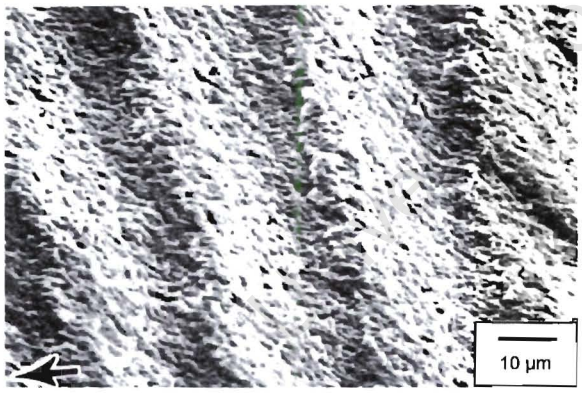

(c) Detail of ripples formed on the steel surface in (b).

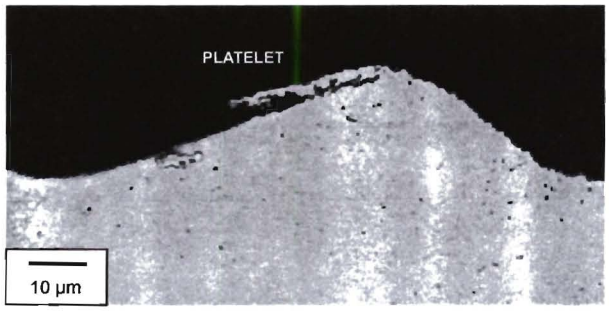

(d) Cross-section through surface shown in (b) & (d). Material at the crest is most susceptible to removal as platelets.

Figure 2-20 Ripples formed on the surface of steel targets by the action of solid particles. (a) Ripples formed in mild steel by 95-105 µm glass beads at 30°. (After Cousens and Hutchings 1983) (b) – (d) Ripples formed in AISI 446 steel by 12 µm alumina particles, at 760°C. (After Stringer & Wright 1987[47])

Carter et al. showed that the scale of the ripples was comparable to the particle diameter, but Stringer and Wright argued that it was more likely a coincidence. In their tests, Stringer and Wright found that wavelengths of ripples ranged from 10 μm to 200±50 μm, using alumina particles with a mean size of 12 μm.

Significant surface movement is necessary. This is favoured by a high rate of energy input to the surface (high particle kinetic energy, high erodent flux) and ease of surface flow (low strength/high ductility, high temperature, absence of impeding microstructural defects). Stringer and Wright found no ripple patterns below 538°C for the alloys Stellite 6B, AISI 446, Inconel MA754 and P22. It would be expected that only at these temperatures would the steel surfaces be able to flow easily enough to form ripples.

The ripples affect actual material removal from material surfaces as follows:

i. They present the erodent with a larger surface area, with a wider range of possible impact angles. A range of erosion micromechanisms is brought into play, depending on local particle trajectories.

ii. It is thought that waves are formed by the upward flow of material from the valleys and the influence of surface work hardening increases from valley to crest, with the material of the crest most susceptible to erosion by brittle fracture.

On an essentially isotropic surface, the ripples precess at a velocity typically of the order 10^{-7} $m.s^{-1}$, with steady-state erosion prevailing[48,49]. The work reviewed here claims that the appearance of ripples is associated with an accelerated erosion rate.

Cousens and Hutchings[21] offer this phenomenon as an explanation for two-stage erosion curves observed in their tests. Initially the whole surface of the target presents the same angle to the particle flow. As the ripples develop, areas of the surface present a higher angle to the flow. Higher impact angles result in more efficient flake (platelet) formation and removal, and consequently the erosion rate increases. Steady-state erosion, which is greater than the initial erosion rate, is thus established when the ripples are fully developed. Cousens and Hutchings found that surface ripples were most noticeable on mild steel specimens eroded at 30° and 45° and to a lesser extent on specimens eroded at 20° and 60° by 95 – 105 μm glass beads at particle velocities of 50 $m.s^{-1}$.

2.7.3. WEAR SCAR GEOMETRY

A continuous stream of particles striking a solid surface will form a crater in the material surface. Lapides and Levy[50] divided the wear damage into an inner area and a halo area, with a definite boundary between the two areas, as shown in figure 2-21. The inner area contains the wear crater, and is the primary region experiencing mass loss in testing. They show that at 15°, the weight loss of the halo region may be as high as 25% of the total weight loss, dropping to 3% at 60°. This is due to the contribution of the more efficient cutting wear mechanisms operating at low angles in the halo region. Particles striking in this region have insufficient energy to cause deformation wear (ploughing), but are able to remove material by cutting.

Shipway[52] developed a mathematical model that describes the divergence of a particle plume as it leaves the nozzle of a gas-blast erosion rig. This enabled calculation of the effect of this divergence on measured erosion rates and the spatial distribution of wear damage.

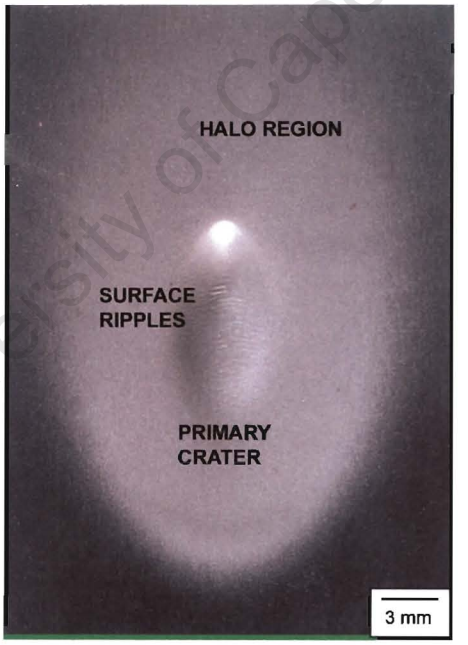

Figure 2-21 Steel sample eroded at 30° showing primary wear crater with surface ripples at the bottom; and encircling halo region.

The depth of the wear crater has a maximum value on the impact axis. The change in depth follows a similar profile to that of the particle velocity across the particle stream (section 2.2.1, figure 2-2). The shallow, halo region is primarily due to the velocity distribution of particles impacting the surface. A secondary effect is the change in actual angle of impact from the

nominal angle. Figure 2-22 shows a schematic of the gas stream exiting the gas stream nozzle. The higher velocity central region, which dictates the size of the primary crater, is indicated. The halo region is associated with the dispersion of the gas stream as indicated.

Lindsey and Marder[6] claim that the formation of a crater on the specimen surface should be avoided in erosion testing because a steady-state erosion rate that is constant across the surface will not be obtained. This may be caused by different particle fluxes, velocities and a range of impact angles, which can increase interactions between particles impacting the specimen and those escaping from the crater.

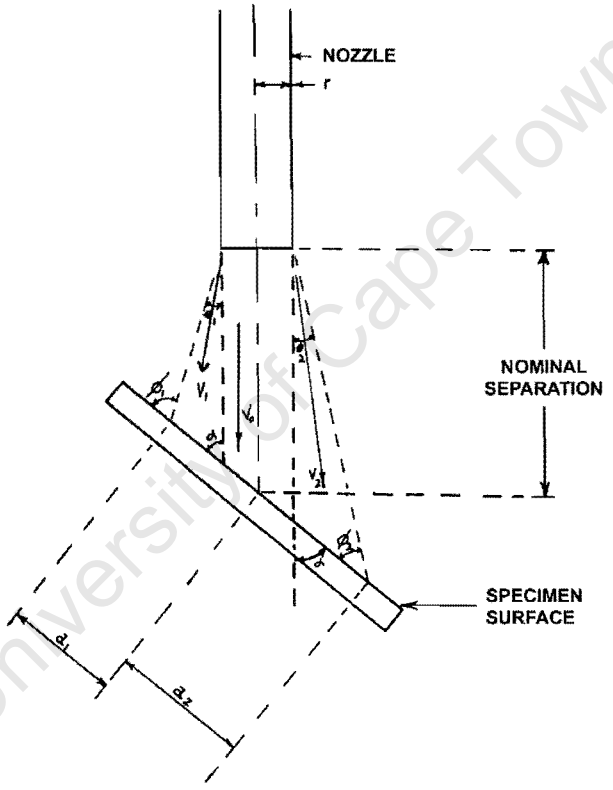

Figure 2-22 Nozzle-specimen area, showing how the divergence of a particle plume as it leaves the nozzle of a gas-blast erosion rig is related to the geometry of the wear scar formed on the specimen surface. (After Lapides & Levy 1980[50])

Rao and Buckley[13] suggest that at long exposure times in erosion testing, the depth of the crater may become sufficient to affect the erosion rate, by means of the following effects:

i. An increase in the distance between the specimen and the nozzle end.

ii. Decreasing the gas stream velocity near the target surface. The momentum of the gas stream must almost reverse to push particles out of a very deep impact crater. Due to its

confined nature, this may lead to a cushion or shield of particles at the bottom of the crater.

Once the crater is very deep, the momentum of the jet has to almost reverse to allow particles to exit the crater. Due to the confined nature of the crater the jet may be cushioned or shielded by a layer of particles at the bottom of the crater. This may reduce the observed erosion rate.

The change in each of crater depth and width with time is similar to the behaviour of cumulative erosion with time for erosion by glass beads. For crushed glass particles, the change in crater depth with time is similar to the behaviour of erosion rate with time. In both cases the impact crater morphology (width, depth and width-depth ratio) strongly controlled the behaviour of the erosion rate with time[13].

2.8. MODELLING EROSIVE WEAR

In its simplest form, the erosion rate is given by:

$$E_R = kV^n$$

where: k = variable containing a target material dependent term
V = particle velocity
n = velocity exponent, varies from 2 to 2.5 for metals
2.5 to 3 for ceramics

The kinetic energy term can be separated out, yielding the exponent, *m*, which is determined by the erosion test apparatus and erodent particle[6]:

$$E_R = kV^{(2+m)}$$

A similar, simple model describing the erosion weight loss per impact for ductile metals in terms of the kinetic energy was proposed by Gulden[36]:

$$E \propto R_p^3 v^2$$

where R_p = particle radius
v = particle velocity

This retains the square relationship of erosion with velocity, but considers only particle size as an additional factor. A strong dependence on particle size is predicted, which is not necessarily true. This simple model cannot explain the increase in erosion sometimes observed with a decrease in particle size.

A recent study by O'Flynn et al.[29] sought to develop a more sophisticated model for predicting erosion rates, with the aim of using material properties obtained by elevated temperature tensile testing, thereby eliminating the need for protracted laboratory erosion simulations. The model proposed that the erosion rate is related to the product of toughness, U_T, and uniform strain, ε_U. Toughness is described as the deformation energy (per unit volume of material) required to produce fracture, and in a tensile test is given by the area under the true-stress-true-strain curve. Uniform strain is described as the plastic strain required for the onset of localised deformation (necking) in a test specimen. It is also equivalent to the work hardening exponent in the Holloman relationship and is therefore a measure of work hardening capacity. While most models use a hardness term to predict depth of penetration of particles and hence volume of material swept out, this model assumes an energy approach in determining material removal rates.

For very low impact angles, cutting is the only mechanism operating, with part of the swept out deformed volume displaced by a ploughing action:

$$E_C = \frac{aV^2}{U_T \varepsilon_U}$$

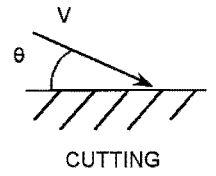

Impact at normal incidence is by lip or platelet formation.

$$E_P = \frac{bV^2}{U_T \varepsilon_U}$$

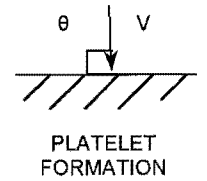

where:

E_C	=	erosion rate due to cutting
E_P	=	erosion rate due to platelet formation
V	=	impact velocity
U_T	=	toughness of the material
ε_U	=	uniform strain (to necking in a tensile test)
a	=	constant for the cutting mechanism
b	=	constant for the platelet or lip formation mechanism

Combining these two equations, and including impact angle dependency, resulted in a model that predicts the erosion rate of ductile metals based on the velocity and impact angle of the erodent particles; and uniform strain and toughness of the target material:

$$E_\theta = \frac{V^2}{U_T \varepsilon_U}[a\cos^4\theta + b\sin^2\theta]$$

where: E_θ = total erosion rate

θ = impact angle

The model's predictions, supported by experimental results, are that erosion resistance increases as the product of tensile toughness and uniform strain (measured at elevated temperatures), $\frac{1}{U_T \varepsilon_U}$, increases.

The novel feature presented in this model, is the use of elevated temperature properties to assess room temperature erosion performance. It is considered by O'Flynn et al. that elevated temperature tensile tests measure the mechanical properties of the steel under conditions closer to those experienced during the high strain/strain-rate deformation typical of erosion. The closest correlation with experimental results for EN42 (eutectoid 0.8% C steel) and EN24 (0.4% C low alloy steel) impacted by fine olivine sand was found by performing the tensile tests at 200°C for impact velocities of 15 and 25 $m.s^{-1}$ and 300°C for an impact velocity of 35 $m.s^{-1}$.

Sundararajan[39] developed a model, based on an energy balance as in the model developed by O'Flynn et al. assuming that erosion occurs due to localisation of plastic flow. The main difference is that Sundararajan assumed that localisation will not occur until a critical strain is reached in the sub-surface zone with zero work hardening rate, that is:

$$\frac{d\sigma}{d\varepsilon} = 0$$

O'Flynn et al. propose in their model that upward flow around the impacting particle (lip formation) will occur without the need for prior work hardening of the sub-surface material. They claim that their model gives better correlation with experimental erosion rates than any other model yet developed. The lack of a fully work hardened surface layer as a requirement

for erosion deformation may allow their model to predict erosion in metals that experience softening in the surface layer due to erosion.

2.8.1. EROSION EFFICIENCY

O'Flynn et al.[29] describe erosion efficiency, η, as the fraction of the impacting particles' kinetic energy used in the removal of material. This is given by the formula:

$$\eta = \frac{2c}{\varepsilon_U}$$

with

$$c = a\cos^4\theta + b\sin^4\theta$$

where:

c	=	constant considering both cutting and platelet formation
a	=	constant for the cutting mechanism
b	=	constant for the platelet or lip formation mechanism
ε_U	=	uniform strain

This equation is derived from the equation for total erosion rate at a given angle θ:

$$E_\theta = \frac{cV^2}{\varepsilon_U U_T}$$

This gave erosion efficiencies of 1.7 – 4.1 % (depending on the value of ε_U) for erosion at 8° and 35 $m.s^{-1}$ for EN24 and EN42. This falls to 0.6 – 1.5 % for similar erosion conditions at 90°, with intermediate values at 30°. Sundararajan et al.[53] achieved similar results; however, they defined erosion efficiency as the ratio of worn volume to crater volume.

Erosion of ductile metals is thus dependent on localisation of plastic deformation, governed by the strength and ductility of the material. Highly localised plastic deformation constrains the force of an impacting particle in a small area of the metal, causing more efficient formation of lips and platelets, and higher wear rates. At lower impact angles, the size of the crater lip at the trailing edge of the wear scar is also related to the plasticity of the material.

Erosion of metals by solid particles is a complicated process, with a wide range of interrelated variables affecting the damage sustained by the material. Erosion can vary considerably with changes in erodent, material and system conditions. Models that can predict erosion in any

erosive system have not yet been developed. Quantitative results need to be obtained for a specific system in order to evaluate its erosive behaviour.

CHAPTER THREE

EXPERIMENTAL METHODS

3.1. MATERIALS

The main materials used in testing were steam coil tube steel specimens serving as targets for milled catalyst erodent particles. Mild steel samples, as well as silica particles were included in the test matrix to provide reference points.

3.1.1. STEELS

A length of unused steam coil tube was supplied for testing. This corresponded to the DIN 1.6580 (30CrNiMo8) specification for low alloy steel for cold extrusion and had the nominal composition shown in table 3-1. Erosion specimens were machined from this tube in such a way that testing could be performed with the gas test stream striking the specimens in the longitudinal direction in a similar manner to that in practice. Mild steel, EN3B samples with a composition as shown in table 3-1 were machined from sheet metal of the same thickness.

Steel		Nominal Composition (%)								
		C	Si	Mn	P	S	Cr	Mo	Ni	Fe
1.6580	Min	0.26	0.15	0.30	-	-	1.80	0.30	1.80	Bal
	Max	0.33	0.40	0.60	0.035	0.035	2.20	0.50	2.20	
EN3B	Min	-	-	-	-	-	-	-	-	Bal
	Max	0.25	0.35	1.0	0.06	0.06	-	-	-	

Table 3-1 Compositions of steel targets used in erosion testing.

Erosion test specimens were 40 mm long, 25 mm wide and 5 mm thick, as shown in figure 3-1. This ensured that the full wear scar was accommodated on the testing surface even at low angles. This specimen geometry enabled the effect of long-term exposure by an impacting erodent stream to be evaluated, while remaining small enough to obtain the accurate mass loss measurements required for calculating erosion rates. The behaviour of the oxidised surface of

the tube steel, as it would be used in practice, was examined. Figure 3-1(b) illustrates the slight curvature of the test surface

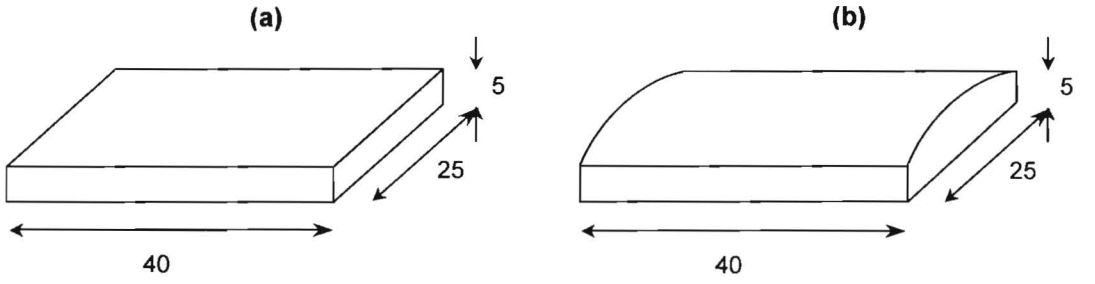

Figure 3-1 Dimensions of steel specimens used in erosion testing **(a)** Dimensions of general test specimens **(b)** Specimen used to test original surface of steam coil tube, displaying **slight** curvature of the test surface. Dimensions in millimetres.

Figure 3-2 **(a)** Length of unused steam coil tube supplied by PetroSA for testing. **(b)** Specimen used to test the effect of the original surface on erosion (geometry as in figure 3-1a).

3.1.2. PLASMA NITRIDED COATING

A commercially prepared plasma nitrided 1.6580 steel plate was supplied for erosion testing. The erosion resistance of the nitrided samples was compared with that of surface ground 1.6580 steel.

3.1.3. ERODENTS

The erodents used in erosion testing were catalyst, as supplied by PetroSA, and silica, which was employed as an erodent for comparison purposes. Both milled and spent catalyst samples were supplied for testing. These two conditions approximate the catalyst before it is reduced and fed into the reaction, and when it is removed and discarded. The catalyst used in the synthol process is 70% iron, with the remaining 30% mostly magnetite. The reduced catalyst is pyrophoric, which precluded its use in erosion testing. Milled magnetite was considered a reasonable approximation to the catalyst used in practice. In the spent condition, the catalyst is covered with petroleum waxes and carbon, which also diffuses into the pores of the catalyst. The catalyst exists as a thick sludge in this condition.

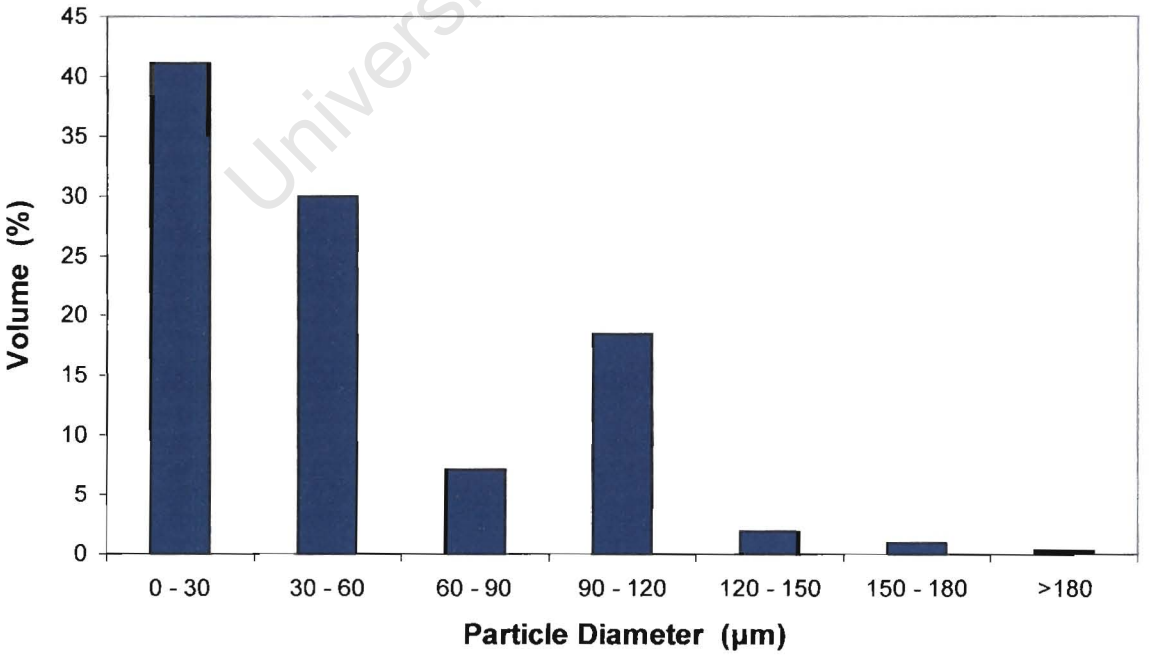

Figure 3-3 Size distribution of milled magnetite particles.

The chemistry laboratory at the PetroSA plant provided the size distribution information for the milled catalyst particles, presented in figure 3-3. A Saturn DigiSizer 5200 V1.03 laser light scattering particle size analyser was used, with a water background, a flow rate of 14.0 $l.m^{-1}$, a circulation time of 45 s, an ultrasonic intensity of 50 and time of 30 s. The average size of the magnetite particles supplied for testing was 38 μm. The particles were very fine, with 41% less than 30 μm, and 71% less than 60 μm in diameter. The magnetite, which was supplied ungraded, was then sieved into the discrete size ranges identified in section 3.4.2 using a laboratory test sieve system.

X-ray diffraction (XRD) was used to confirm the constitution of the supplied catalyst. A personal computer interfaced Copper K_α -radiation Philips X-ray diffractometer was used with a 20 mA current and an accelerating voltage of 40 kV, scanning 2θ from 25° to 100° in interval steps of 0.05 and holding at each interval for 3.85 seconds.

3.2. SOLID PARTICLE EROSION TEST APPARATUS

The gas-blast erosion test apparatus works on the principle of solid erodent particles entrained in a gas stream impacting a specimen in an enclosed testing chamber. The velocity of the particles can be regulated by adjusting the pressure of the carrier gas, the impact angle by changing the angled specimen mounting block, and the mass flux by controlling the amount of erodent entering the gas stream through a venturi per unit time.

3.2.1. GAS-BLAST ROOM TEMPERATURE EROSION RIG

A schematic of the gas-blast erosion apparatus is shown in figure 3-4. Compressed air passes through a regulator which can be adjusted to control the gas velocity, and hence the erodent particle velocity. The air stream flows straight into the test chamber. A venturi draws erodent particles into the air stream from a revolving turntable. Controlling the speed of rotation of the turntable by adjusting power to the electric motor, allows different mass fluxes (feed rates) to be tested. Erodent particles fall through the erodent hopper onto the turntable, from which they are entrained in the air stream through the venturi, and impact the specimen mounted on variable angled blocks in the enclosed, sealed test chamber. The erodent particles are

accelerated along a steel tube 250 mm in length and 4.6 mm in diameter, and strike a sample mounted 20 – 25 mm from the nozzle end. Used particles are removed from the chamber and collected by a Record Power DX750 Extraction Unit. Photographs of the gas-blast erosion apparatus in the Centre for Materials Engineering are included in figure 3-5.

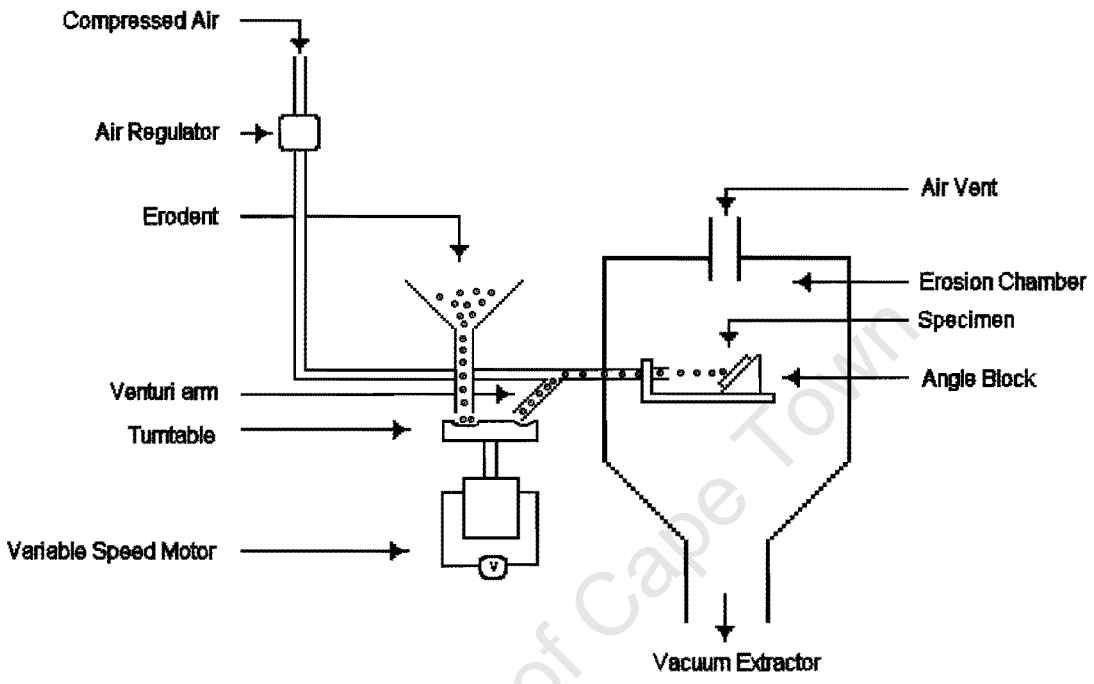

Figure 3-4 Schematic of the room temperature gas-blast erosion apparatus

A variable speed motor can be placed in the test chamber in the path of the gas stream, for use in the double rotating-disc method for determining particle velocity developed by Ruff and Ives[54]. This was used to calibrate the particle velocities for a range of gas pressures. A description of this method is included in section 3.2.2.

Elevated temperature erosion tests were not performed. Previous researchers have shown that, for a wide range of steels tested, erosion resistance does not decrease with moderate increases in testing temperature. The recommended maximum testing temperature of 220°C[55] is within the range of temperatures for which erosion rates do not increase with increasing temperature. This effect is explained in section 2.6.

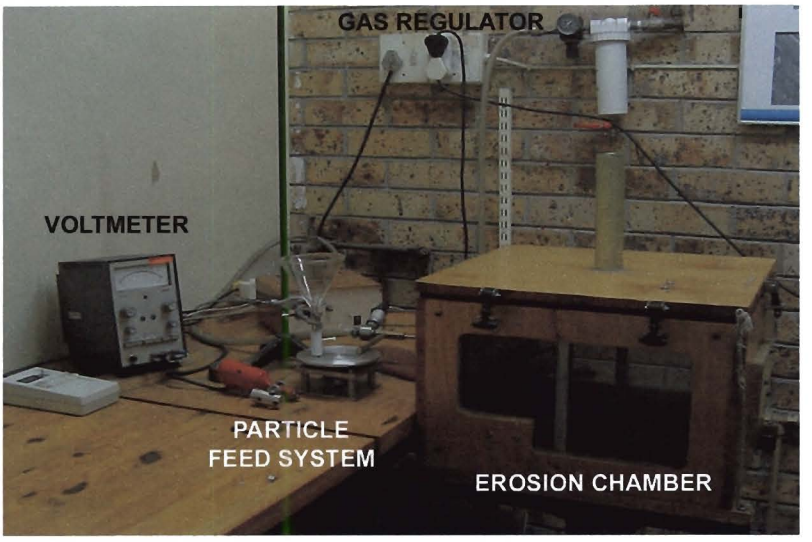

(a) Gas-blast erosion apparatus.

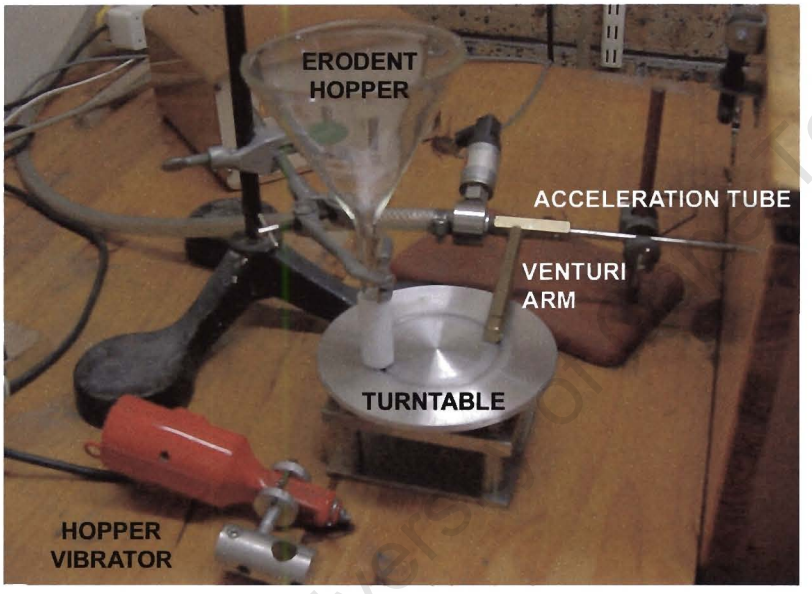

(b) Particle feed system.

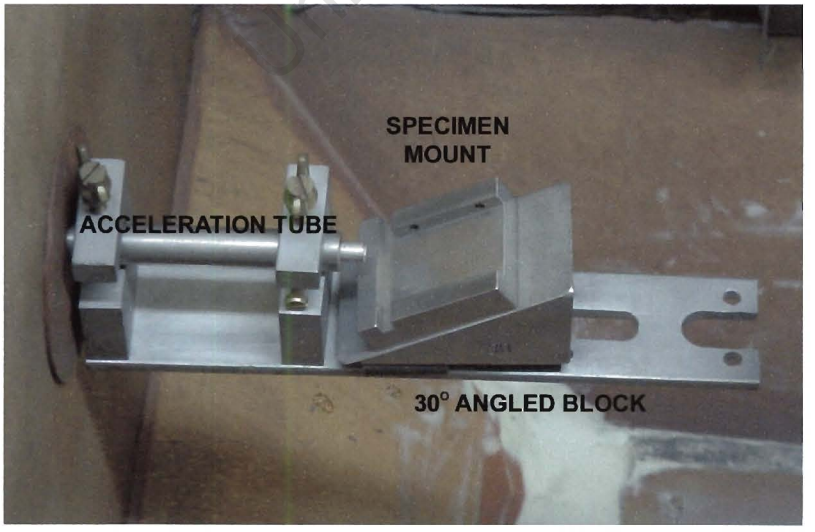

(c) Specimen stage in the erosion chamber. The angled block can be changed to test different impact angles.

Figure 3-5 Gas-blast erosion apparatus in the Centre for Materials Engineering at the University of Cape Town. **(b)** The particle feed system, and **(c)** The specimen stage mounted in the test chamber.

3.2.2. PARTICLE VELOCITY MEASUREMENT

Two methods of measuring particle velocities are widely used – laser Doppler velocimetry (LDV) and the rotating disc method. LDV is perfectly suited to measuring the free stream velocity of particles entrained in a gas stream, but generally measures higher velocities than those measured by the rotating disc method[56]. This may be due to the effect of stagnation on the surface of target materials as explained by Kagimoto et al.[7]. While the random error in the rotating disc method is typically 10%, it estimates particle velocity by measuring wear scars caused by impact with a target, better simulating impact velocity conditions in testing. Kagimoto et al. recommend that particle velocities intended to be reported as impact velocities should be measured no more than a few millimetres from a target surface. Erodent particle impact velocities were measured using the rotating disc method.

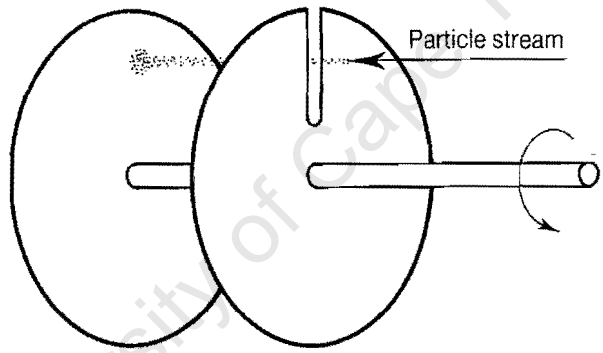

Figure 3-6 Schematic illustration of the double-disc (rotating disc) method of measuring erodent particle velocity in gas-blast erosion testing. (After Hutchings 1992[57])

A schematic of the method is shown in figure 3-6. A particle stream exits the nozzle of the gas-blast apparatus, passes through the slit in the first disc and strikes the second disc. A variable speed motor and electronic counter control the speed and direction of rotation of the discs. The direction of rotation is reversed, and the process repeated to produce two wear scars on the second disc. An appropriate angular speed must be selected for the discs to ensure that the wear scars are separated sufficiently to avoid additional difficulty in recording the separation of the wear scars.

The particle velocity is calculated by relating the displacement of the wear scars to the angular speed of the discs and the time of flight of the particles over the distance separating the discs, using the following formula:

$$V = \frac{4\pi UrL}{\sigma}$$

where: V = calculated particle impact velocity

r = radius at which measurement is taken

L = linear separation of the two discs

U = rotational velocity of the discs

σ = linear separation of the wear scars

Particle velocities achieved in the gas-blast erosion apparatus were calibrated for a range of gas pressures, using 38 – 63 μm magnetite particles. The calibration of the apparatus is presented graphically in figure 3-7.

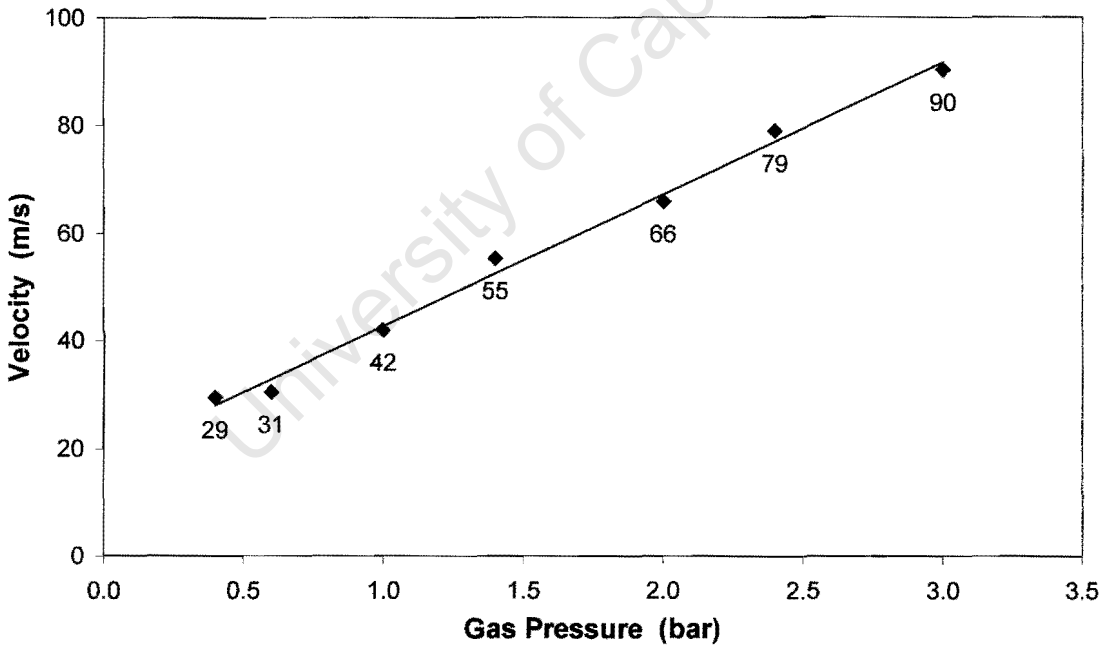

Figure 3-7 Particle velocity calibration in the gas-blast erosion rig using the rotating disc method.

3.3. EXPERIMENTAL MATRIX

System Conditions			Steel Targets
	Min	Max	1.6580
Velocity [m.s^{-1}]	29	90	Plasma nitrided 1.6580
Impact Angle	10°	90°	EN3B
Mass Flux [kg.m^{-2}.s^{-1}]	1.9	32.9	**Erodents**
Temperature [°C]	25		Milled catalyst (magnetite)
Erodent Variables			Spent catalyst
Size	< 25 µm	180 µm	Silica sand
Recycling	Once	5 times	

Table 3-2 Experimental matrix for solid particle erosion testing.

3.4. EROSION TEST METHOD

3.4.1. SPECIMEN PREPARATION

The steel specimens used as targets in erosion testing were machined to the dimensions shown in figure 3-1. Plasma nitrided specimens were cut from the supplied 1.6580 plate to the required thickness, leaving the plasma nitrided surface untouched. Specimens were machined from the supplied steam coil tube, to the same dimensions. The test surface was surface ground, providing a smooth, flat surface for testing on some specimens, while others were prepared with their surface in a similar condition to the steam coil tubes found in the synthol reactor (figure 3-2(b)).

A number of the surface ground specimens were polished using silicon carbide grinding paper and finally polished using ¼ µm diamond paste. A Taylor-Hobson Surtronic 3P surface profiler with a 99.99 µm range for the smoother surfaces and 999.9 µm for the rougher samples, and a cut off of 0.8 mm, was used to report the surface finish of each group of samples.

The preparations described supplied a range of surface finishes and conditions for erosion testing. All specimens were ultrasonically cleaned in ethanol before weighing on a Sartorius R200D digital balance with an accuracy of 10^{-5} grams, i.e. 10^{-2} mg.

3.4.2. ERODENT PREPARATION

The catalyst and silica particles were separated into discrete size ranges suitable for erosion testing using a Fritsch Analysette 06.502 laboratory test sieve. Madison and KingTest stainless steel mesh sieves with the following mesh sizes were used: 38 μm, 63 μm, 106 μm, 125 μm, 150 μm and 180 μm. A charge of particles was sieved continuously for one hour. The sieve mesh was cleared of particles blocking the apertures and the same charge was then resieved. The process was repeated four to seven times. The fine magnetite particles tended to agglomerate due to their magnetic nature. This effect is in addition to the fact that the surfaces of particles of any material, finer than about 75 μm, can develop enough surface charge and show an enhanced tendency to agglomerate[58]. As a result, sieving of particles was a time-consuming and laborious process.

3.4.3. TEST METHOD USING THE GAS-BLAST EROSION APPARATUS

The correct erodent charge was weighed out using a Mettler PC440 electronic balance, accurate to 10^{-3} g. For all tests, except the extended tests, 40 g of erodent was used in 10 g charges. Four cycles of 10 g was shown to be sufficient to establish the erosion rate. This was true for the full range of experimental conditions. The extended tests used either 50 g or 100 g charges, up to a maximum of 1000 g of erodent.

The erodent was poured into the hopper shown in figures 3-4, 3-5(b). The voltage of the variable speed motor controlling the turntable under the hopper was set such that the table turned at the speed required to obtain the correct particle mass flux (particle feed rate). An engraving pen acted as a hopper vibrator and was placed with the vibrating point against the mouth of the hopper to cause the magnetite particles to fall onto the turntable. Maintaining a consistent feed rate through the hopper required patience and practice. The fine, agglomerative

magnetite particles were found to be very difficult to feed. Particles 38-63 μm in diameter did not fall through a 10 mm diameter glass funnel without coaxing.

It was found that heating the milled magnetite particles at 80°C for 30 minutes to one hour in an OptoLab incubator prior to testing caused them to flow more smoothly, with negligible clogging. The same effect was achieved after two to three hours for spent catalyst particles, depending on the shape and size of the container used to hold the sample. A large, flat, open container that exposed the maximum surface area of the sample to the incubator environment proved to be the most efficient geometry for 'drying' the spent catalyst. The same flow problems were not encountered with the silica particles. This agglomeration can be explained by some combination of the following factors:

i. The shape of the erodents.
ii. The magnetic nature of the magnetite particles.
iii. The development of surface charge on very fine particles.

Fine particles can become hygroscopic due to the development of surface charge. Section 4.3.2 presents scanning electron microscope (SEM) images of the erodents used in erosion testing.

The gas pressure was set using the regulator valve, and confirmed using an electronic transducer, to give the desired particle velocity. The prepared and weighed steel test sample was placed in the specimen holder, with the correct angled support already in place and this was then placed in the testing chamber. The chamber was sealed and the extractor fan switched on. The gas flow was then switched on, and finally the turntable. A stopwatch was used to record the test time, which was used to calculate the mass flux.

When the test was finished, the steel specimen was removed, ultrasonically cleaned in alcohol and reweighed. The difference in mass was used to calculate the volume erosion rate, expressed in [$mm^3.g^{-1}$]. The process was repeated four times for all except the long-term tests. Four points were found to be sufficient for determining the linear portion of the volume loss curve. The erosion rate was calculated from the slope of the curve plotting volume lost from the target in [mm^3] versus mass of erodent in [g].

3.5. DETERMINATION OF EROSION RATES

Mass loss values were obtained from the results of erosion testing. A curve of mass lost from the target surface, in milligrams, versus cumulative mass of erodent, in grams, was generated. The slope of the linear part of the curve gives the mass erosion rate. In order to allow comparison of materials of different densities, the mass loss was converted to volume loss, and the volume erosion rate was reported. The densities of the steels were calculated by measuring the dimensions of rectangular specimens and their masses on an electronic balance. These results were related using the equation defining density, ρ:

$$\rho = \frac{m}{V}$$

where: m = mass in grams

V = volume in cubic centimetres.

Steel	Density ($g.cm^{-3}$)
1.6580	7.80
EN3B	7.77

Table 3-3 Densities of steels tested.

3.6. MICROSCOPY

3.6.1. OPTICAL MICROSCOPY

A Reichert MeF3A light microscope with a Leica DC100 digital camera, connected to a personal computer was used for all optical microscopy. A plasma nitrided sample and a sample with the outer surface in the original condition were prepared in order to examine these surfaces. These surfaces were examined directly, and by cross-section. Worn steel specimens were sectioned through the wear scar and mounted in epoxy resin. An untested sample was sectioned to provide a reference. The samples were ground on successively finer grades of emery paper and finally polished using ¼ μm diamond paste and afterwards etched for 20 – 30

seconds in a 2% Nital (2 ml HNO_3, 98 ml methanol/ethanol) solution to reveal the microstructure. The same specimens were used to conduct microhardness tests.

3.6.2. SCANNING ELECTRON MICROSCOPY OF ERODED STEELS

A Leica S440 fully analytical scanning electron microscope (SEM) was used for all electron microscopy. The worn steel specimens were ultrasonically cleaned in ethanol and then mounted on aluminium stubs with conductive carbon-containing glue. The operating conditions were a potential difference of 15 kV with a working distance of 20-25 mm.

Steady-state erosion damage was examined for a range of testing conditions. Single-impact sites were also examined to identify more clearly the mechanisms of material removal at work in the magnetite / steel erosion system tested. Steel samples were polished using ¼ μm diamond paste, yielding a surface roughness of R_a = 0.01 μm that served as the uniform background against which the wear craters caused by individual magnetite particles were observed.

3.6.3. SCANNING ELECTRON MICROSCOPY OF ERODENT PARTICLES

The operating conditions used when examining the different erodent particles were a potential difference of 10 – 20 kV with a working distance of 18 – 25 mm. The particles were mounted on aluminium stubs by carefully sprinkling them onto a layer of conductive carbon-containing glue, and were then gold-palladium sputter-coated. Double-sided tape was stuck to some of the stubs and the particles were sprinkled onto this, before being sputter-coated. This proved a much neater solution. The tape automatically provided a smooth, flat surface which was difficult to obtain by spreading a layer of paste. This was thus the preferred background used in SEM due to its high degree of uniformity.

Both the catalyst and silica particles were examined in each of the sieved size ranges. This enabled the shape of the particles to be compared for the various sizes. Recycled erodent was also examined. A sample was prepared by reclaiming a small quantity of erodent after each subsequent erosion test.

Sections through catalyst and silica particles were examined, to evaluate the integrity of the particles, i.e. the existence of porosity. Particles were mounted in epoxy resin and polished with a ¼ μm diamond paste. The samples were then gold-palladium sputter-coated and mounted on large aluminium stubs using conductive carbon-containing glue.

3.7. HARDNESS TESTING

3.7.1. BULK HARDNESS

An ESEWAY SPVR.2.M hardness tester was used to take hardness measurements of the surfaces of the steel specimens, including the commercially prepared plasma nitrided steel and samples with the original coil tube surface (as-received). Readings were taken on uneroded specimens using a Vickers pyramid indenter with a 30 kg load.

3.7.2. MICROHARDNESS

Microhardness of the erodent particles and subsurface and through-section hardness of the steel specimens were measured using a Matsuzawa MXT-x7 Digital Microhardness Tester. Results were reported as Vickers (HV).

The erodent particles were mounted in an epoxy resin and carefully ground using a 1200 grit silicon carbide polishing wheel, to provide flat surfaces suitable for indentation. Loads of 25 and 50 gf were used for the very fine catalyst particles and silica particles respectively. Higher loads resulted in a large degree of scatter. At higher loads, the very small, irregular particles (especially the magnetite particles) make it difficult to contain the indenter and its associated strain field within the particle being tested. The indenter may also crack the particles, leading to errors in reading the lengths of the indent diagonals. Some silica particles were shattered by the indenter, making those results worthless. At least ten readings were taken and the average reported.

Cross-sections of both worn and untested steel specimens were mounted in epoxy resin and polished with ¼ μm diamond paste using a Struers RotoPol-22 automatic polisher with a Struers RotoForce-4 specimen mounting. A 1000 gf load was used to generate the required hardness profiles.

CHAPTER FOUR

RESULTS

4.1. CALCULATION OF REACTOR CONDITIONS

The velocity of the gas and the mass flux of catalyst through the reactor were calculated using relevant plant monitoring data supplied by PetroSA. Details of the calculations are included in Appendix II. Table 4-1 summarises the calculated gas velocities and mass fluxes at three different cross-sections through the synthol reactor. These positions were chosen to provide a range of cross-sectional areas, and are described in Appendix II. The velocities reported in table 4-1 represent the maximum values expected to exist in the reactor.

Steel Targets	Velocity [$m.s^{-1}$]	Mass Flux [$kg.m^{-2}.s^{-1}$]
Max. internal diameter	8.5	4.81
Through steam coil tubes	10.7	6.08
Lower transfer line	41.7	23.66

Table 4-1 Calculated velocity and mass flux within the synthol reactor.

Higher velocities were used to accelerate erosion testing due to the limited quantity of catalyst available. The effect of velocity on erosion is quantified in section 4.2.2. It is widely recognised that the higher energy associated with higher impact velocity merely accelerates erosion. Once the behaviour of the system with respect to velocity is known, results at higher velocities may be extrapolated back to estimate erosion at velocities approximating those encountered in practice.

4.2. EROSION SYSTEM VARIABLES

4.2.1. THE EFFECT OF IMPACT ANGLE

The angle of maximum impact lies between 30° and 40°. Limited work performed at Sasol observed a maximum erosion rate at 35° using similar conditions[59]. A flattened peak is observed and the erosion rate drops to 60 % of the maximum at 10° and at normal incidence. These tests were performed at a particle velocity of 90 $m.s^{-1}$ and a mass flux of 5.92 $kg.m^{-2}.s^{-1}$ (mass feed rate 0.09 $g.s^{-1}$) with erodent in the size range 125 – 180 μm.

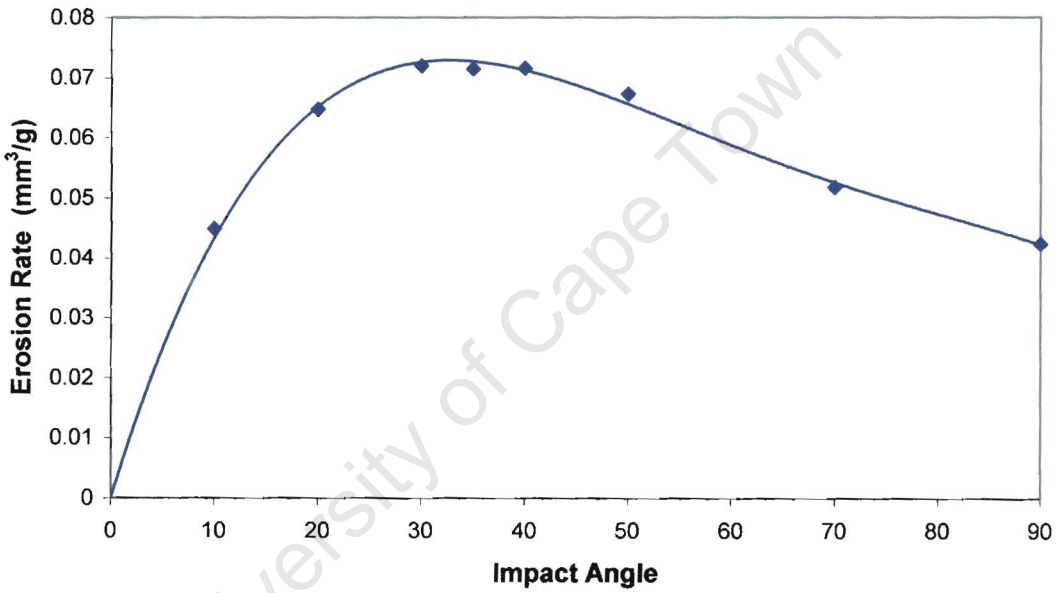

Figure 4-1 Dependence of erosion rate on incident angle of impact for silica particles impacting 1.6580 steel. Similar results were obtained using magnetite on 1.6580 steel[59].

4.2.2. THE EFFECT OF PARTICLE IMPACT VELOCITY

The tests to investigate the effect of particle impact velocity were performed at an impact angle of 30°, with 38 – 63 μm magnetite particles, at a mass flux of 5.7 $kg.m^{-2}.s^{-1}$. An equation of the form, $E_R = kV^n$, was generated by fitting a curve to the experimental erosion rates as shown in figure 4-2. This predicted a velocity exponent of 2.07, which is similar to values predicted in the literature. The following is the resultant equation relating velocity to erosion rate:

$$E_R = 1 \times 10^{-5} V^{2.07}$$

To confirm the validity of this calculation, manual manipulation of the erosion results was performed, using the equation described in section 2.2.1:

$$\frac{E_1}{E_2} = \left(\frac{V_1}{V_2}\right)^n$$

This yielded an average velocity exponent of $n = 2$.

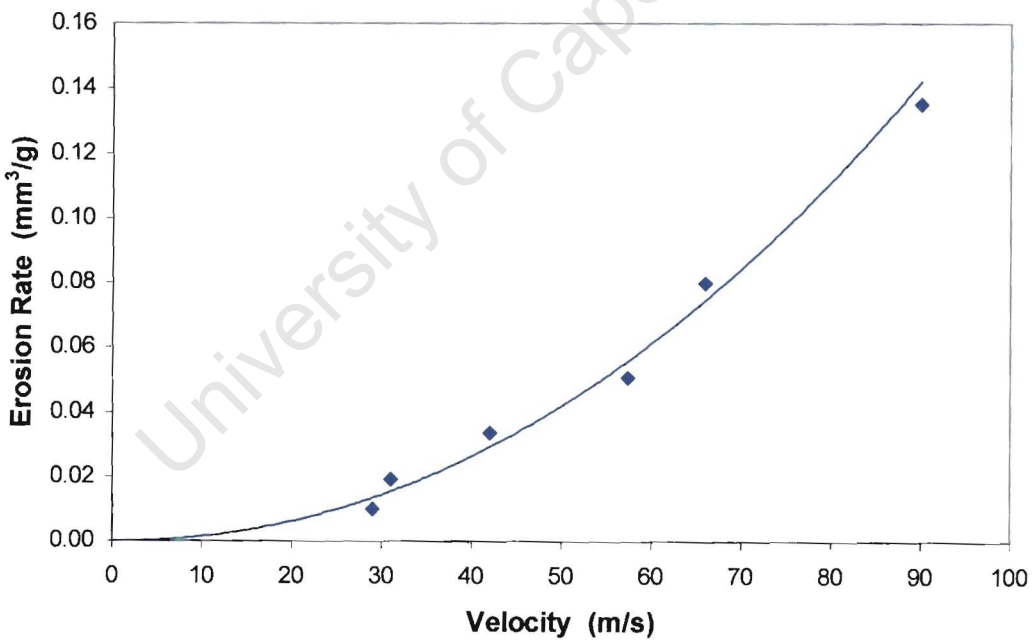

Figure 4-2 The effect of particle impact velocity on erosion rate for 1.6580 steel specimens impacted by 38 – 63 μm magnetite particles.

4.2.3. THE EFFECT OF MASS FLUX

The effect of variation in the erodent mass flux on the erosion rate was investigated for mass flux values between 1.9 and 32.9 $kg.m^{-2}.s^{-1}$, corresponding to mass feed rates between 0.075 and 1.312 $g.s^{-1}$. These values were chosen to encompass the expected mass fluxes in the synthol reactor (table 4-1), predicted by the calculations presented in Appendix II.

1.6580 steel samples were impacted by magnetite particles 63 – 106 μm in diameter, at 30° and 90 $m.s^{-1}$. Figure 4-3 illustrates the results of these tests. A dramatic change in erosion rate with varying mass flux of erodent was not observed. A consistent, but very slight decrease in erosion rate was observed as the flux was increased from 14.4 $kg.m^{-2}.s^{-1}$ to 30.9 $kg.m^{-2}.s^{-1}$ (feed rate from 0.55 $g.s^{-1}$ to 1.20 $g.s^{-1}$). The difference between the extreme values, i.e. lowest and highest fluxes tested, was just less than 10%.

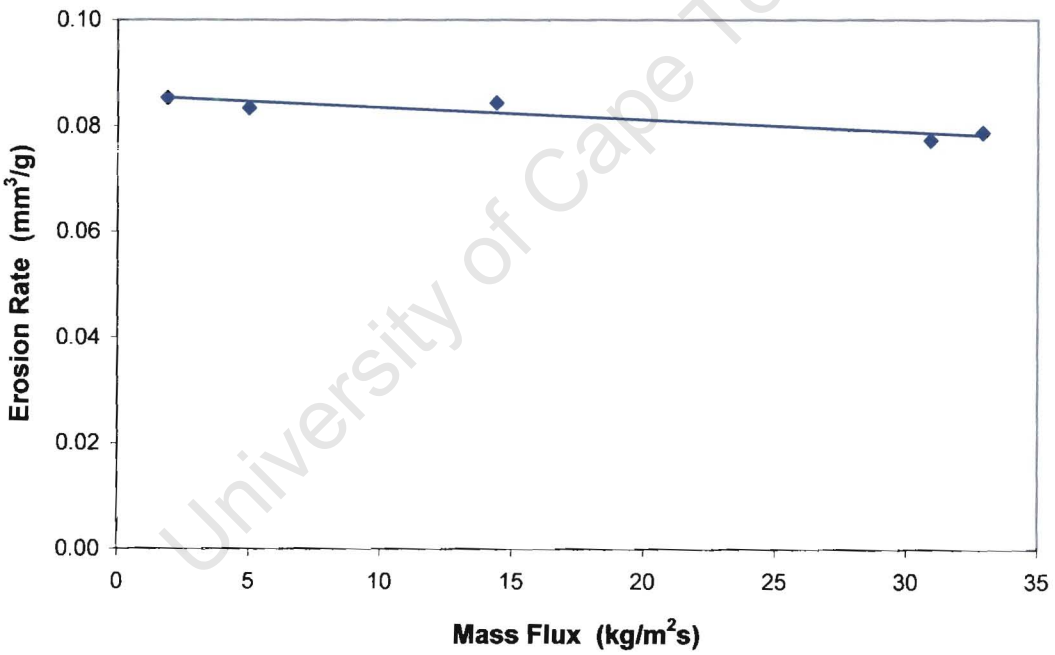

Figure 4-3 The effect of mass flux of magnetite particles on the erosion rate of 1.6580 steel.

4.3. ERODENT FACTORS

4.3.1. THE EFFECT OF ERODENT TYPE AND CONDITION

The erodent used in most of the erosion testing was milled catalyst, which was confirmed as magnetite (Fe_3O_4) by X-ray diffraction (XRD). The XRD plot in figure 4-4 has all the peaks corresponding to the positions expected for magnetite. Although much less significant, there are two unidentified peaks at 42° and 61°2θ, but the volume fraction contribution is very small. Silica was used for comparative purposes. The morphology of the erodents tested is shown in figures 4-6 and 4-7.

The magnetite particles had a microhardness of 900 HV using a 25 gf load. A low load was used with the very fine magnetite particles to ensure that the entire indent was formed in the particle being tested. Accepted values of hardness for silica are 1040 – 1230 HV, depending on the lattice orientation[60]. The results obtained using mounted silica particles revealed a high degree of scatter depending on the load employed in the microhardness tester. Using a 50 gf load, the average hardness was found to be 1182 HV.

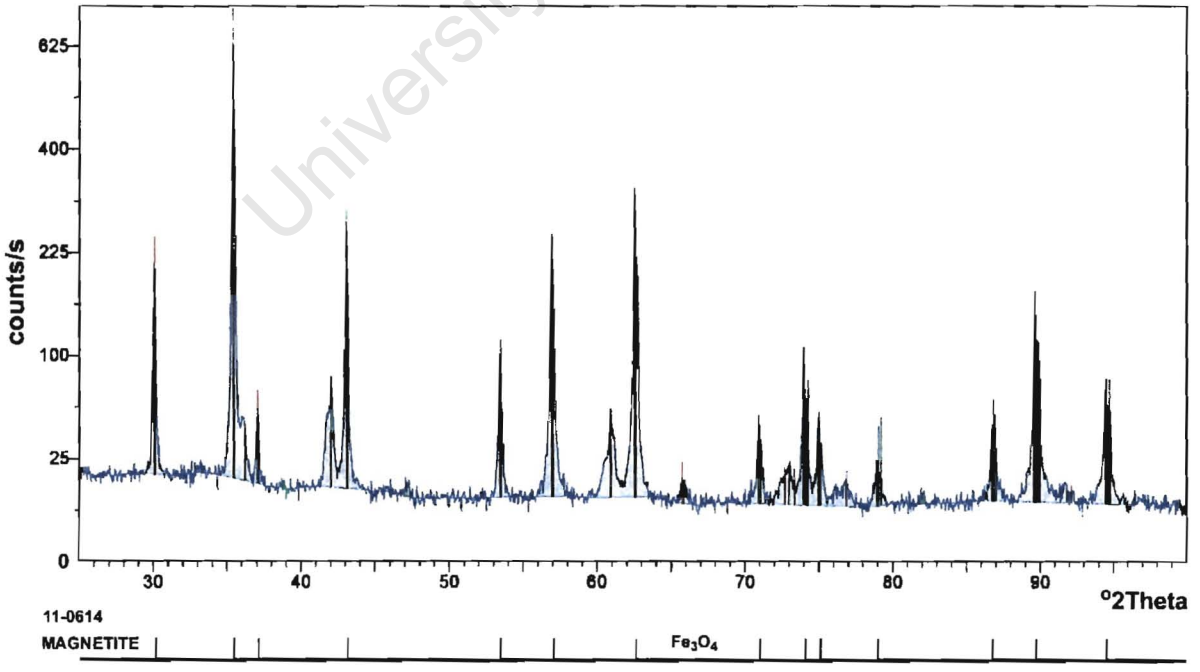

Figure 4-4 XRD plot confirming composition of milled catalyst as magnetite (Fe_3O_4).

The erosivity of magnetite and silica particles were compared. A surface ground (R_a = 0.73 μm longitudinal and R_a = 0.83 μm transverse) EN3B steel sample was impacted by 125 – 180 μm silica particles and as-received milled catalyst. The erodents impacted the steel at 30°, 90 $m.s^{-1}$ and particle fluxes of 3.62 $kg.m^{-2}.s^{-1}$ (feed rate of 0.11 $g.s^{-1}$) for magnetite and 2.96 $kg.m^{-2}.s^{-1}$ (feed rate of 0.09 $g.s^{-1}$) for the silica particles. The flux is difficult to control precisely, especially with the recalcitrant magnetite particles. However, the difference in flux was shown to have a negligible effect on erosion rate (see results presented in section 4.2.3).

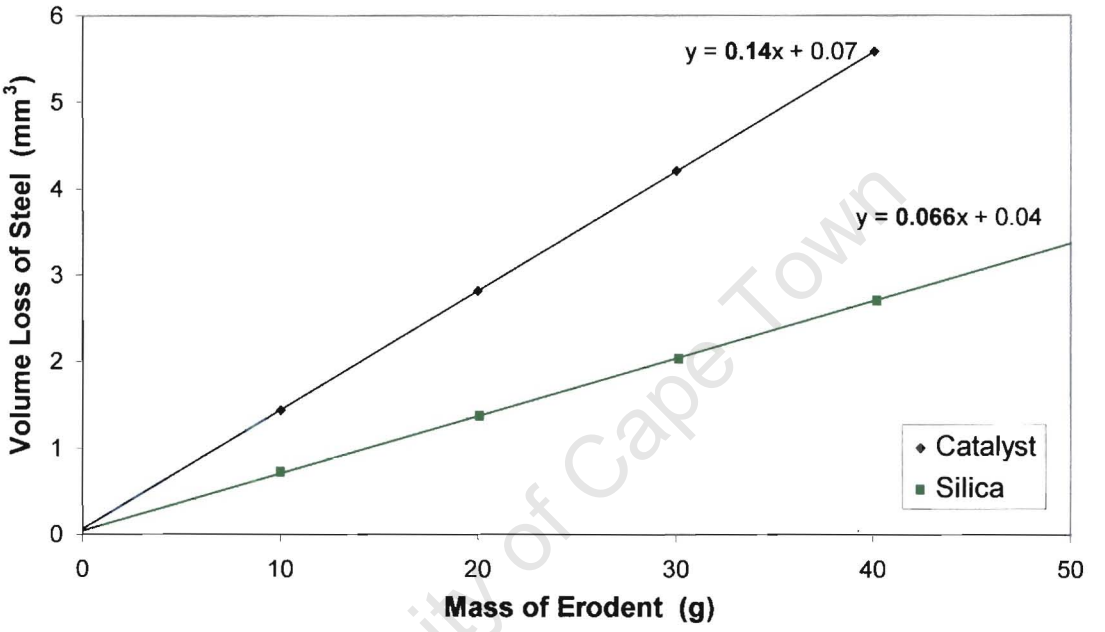

Figure 4-5 Comparative volume loss curves for EN3B impacted by different erodents. The slopes of the curves, highlighted in bold font, represent the erosion rates.

The erosion rate for magnetite was approximately double that for silica particles, as shown in figure 4-5. Further tests were conducted in which the erosivity of the magnetite catalyst was determined in two different conditions (figure 4-8), namely:

i. Milled catalyst (as-received)

ii. Spent catalyst (as-received)

The morphology of these particles is shown in figure 4-6. The spent sample is more spherical with less angular protrusions than the milled catalyst (figure 4-6(b)). Cross-sections of magnetite and silica particles are shown in figure 4-7. The particles are solid and non-porous. For a given particle size, the effective erosive mass is thus high.

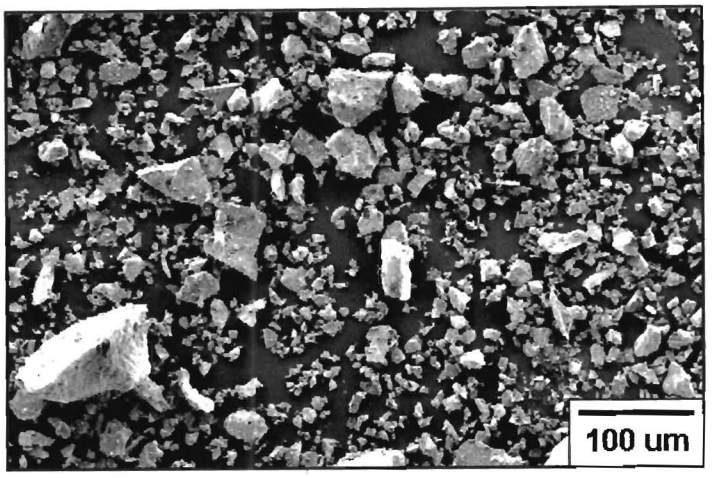

(a) Morphology of milled catalyst (Fe_3O_4).

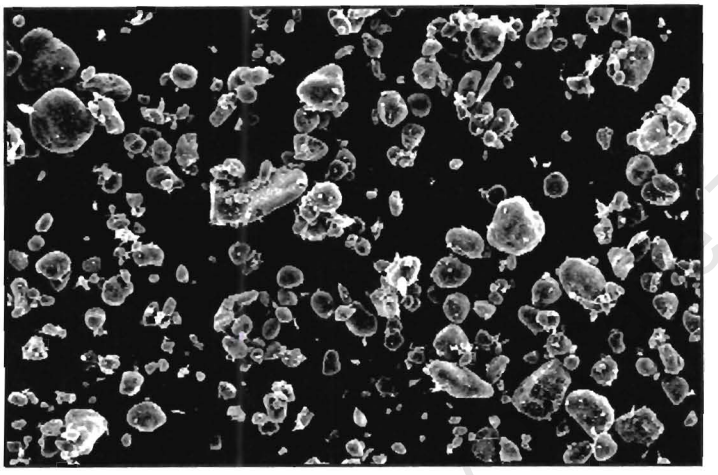

(b) Morphology of spent catalyst.

(c) Morphology of silica (SiO_2) particles.

Figure 4-6 Morphology of erodent particles used in erosion tests: **(a)** Fresh (milled) catalyst, **(b)** spent catalyst and **(c)** silica particles.

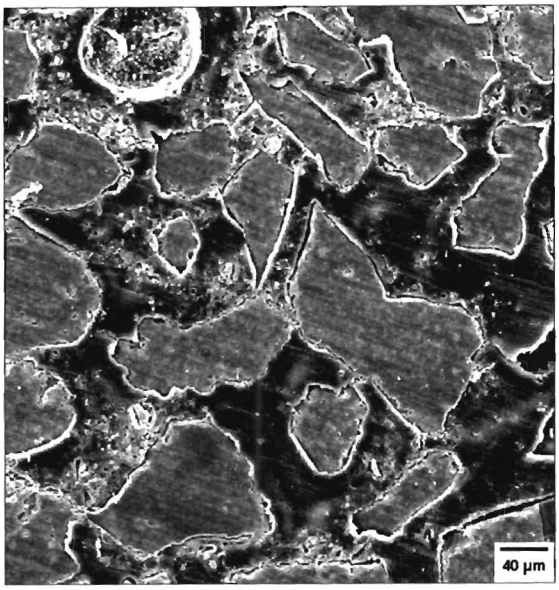

(a) Sections through milled magnetite particles.
- Highly irregular.
- Low porosity.

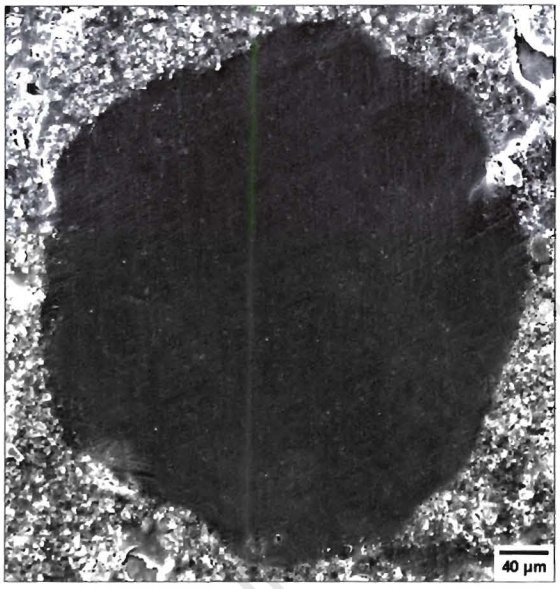

(b) Section through a typical silica particle.

Figure 4-7 Erodent morphology: Sections through **(a)** Magnetite particles and **(b)** Silica particle.

The spent catalyst had been removed from the reactor following use. Over the life of the catalyst, it becomes coated with carbon, with carbon also diffusing into the pores of the particles. Waxes (products of the catalysed reaction) are also found in the pores and adhere to the surfaces of the particles. The intrusive carbon and waxes lead to a degeneration of the particles, which is desirable in terms of the reaction, because it keeps the catalyst active by exposing fresh reaction surfaces.

Erosion tests were performed using 38 – 63 μm particles of milled and spent catalyst impacting 1.6580 steel specimens at 30° and 90 $m.s^{-1}$. The volume loss curves in figure 4-8 show that the spent catalyst is less erosive than the milled catalyst. The appearance of the milled and spent catalyst is shown in figure 4-6(a),(b). The spent catalyst particles are more spherical, with fewer angular protrusions than the milled catalyst. A decrease in erosivity of synthol catalyst with increasing carbon content has been observed before[58].

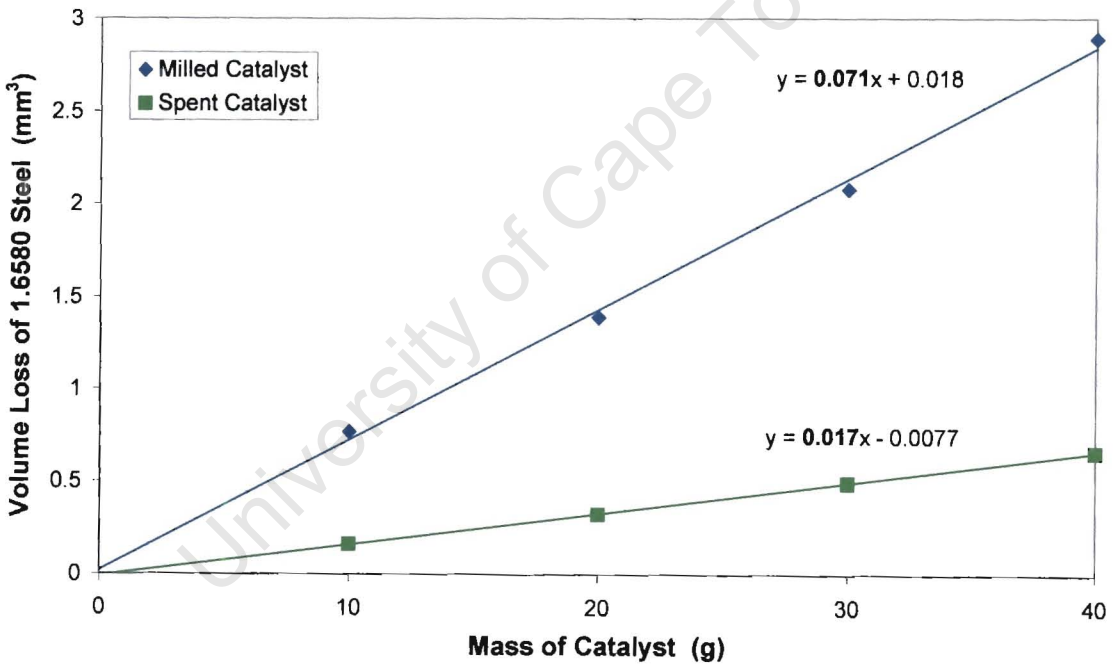

Figure 4-8 Comparative volume loss curves for milled and spent catalyst conditions. The erosion rates are given by the slopes of the curves.

4.3.2. THE EFFECT OF SIZE AND SHAPE

An examination of the particle morphology was conducted using SEM. Figures 4-11 – 4-13 compare magnetite and silica particles, across the range of sizes of the supplied catalyst. The variation of particle shape with size for each erodent can also be evaluated. The figures clearly reveal the angular nature of the particles, particularly the very fine ones. A large fraction of very fine magnetite particles was observed in samples that were nominally of a much larger size. These fine particles were found loose, but many were found attached to the larger particles. The finer particles shown in figure 4-11 appear to be more angular than the larger particles shown in figures 4-12 and 4-13. Very fine particles were also observed in the larger size intervals despite careful sieving. Many fine particles could be observed clinging to larger particles.

The fine silica particles are highly angular, though less so than the fine magnetite particles, becoming more spherical with increasing diameter. Very few fine particles could be observed in the higher size ranges, compared to those seen in the magnetite sample. The magnetic nature, charging of the particle surfaces and very high degree of angularity of the magnetite particles may explain the difficulty experienced in separating the particles into discrete size intervals.

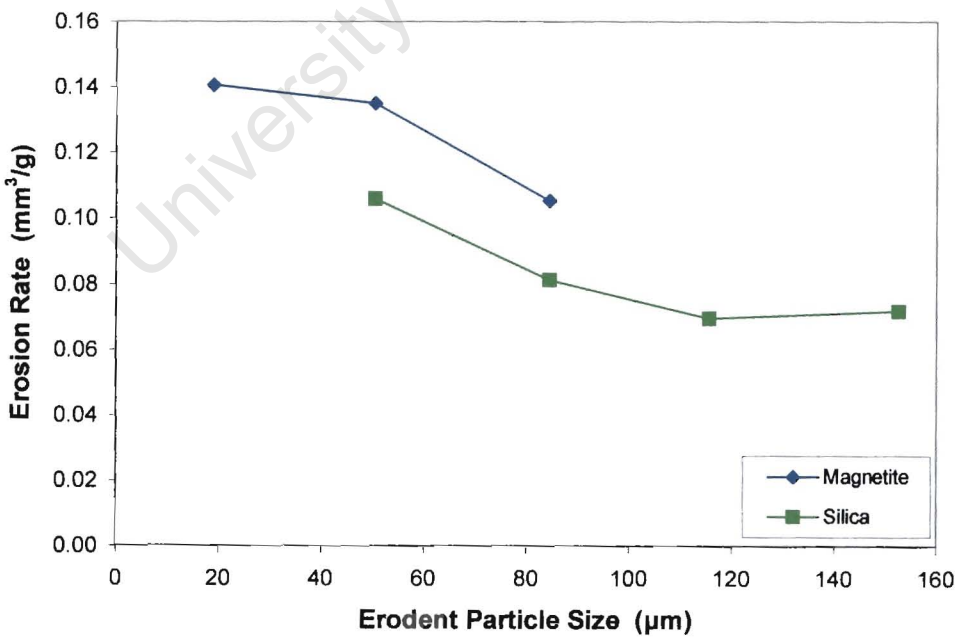

Figure 4-9 Variation in erosion rate with increasing particle size for magnetite and silica particles.

The effect on erosion rate of using different particle sizes in erosion testing is illustrated in figure 4-9. The results show a general trend of decreasing erosion rate with increasing particle size, for the size range considered. 1.6580 steel samples were impacted at 30° with a mass flux within the range 2.63 – 4.28 $kg.m^{-2}.s^{-1}$ (feed rates of 0.08 – 0.13 $g.s^{-1}$). The tests were performed with a constant free stream velocity, i.e. a fixed gas pressure. This equated to an impact velocity of 90 $m.s^{-1}$ for 38 – 63 μm magnetite particles. The variation in impact velocity with particle size for a constant free stream velocity, is shown in figure 4-10.

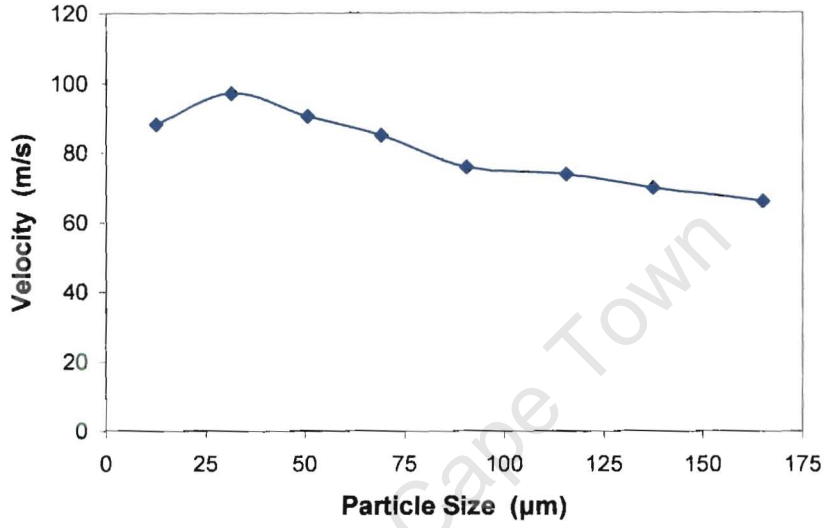

Figure 4-10 The effect of particle size on impact velocity for constant free stream velocity.

The steady-state erosion damage observed on the surface of 1.6580 steel by magnetite of various particle sizes is shown in figure 4-33 in section 4.7.4, Mechanisms of Material Removal. There is evidence of significant deformation of the eroded surfaces. Individual tracks left by particles in removing material from the surface by cutting can be identified. The scale of the observed damage is affected by the particle size, as may be expected. Larger particles cause larger impact craters, resulting in a rougher surface. Finer particles cause predictably "smoother", less undulating surfaces at the same magnification, with smaller platelets (and lips) formed.

MAGNETITE

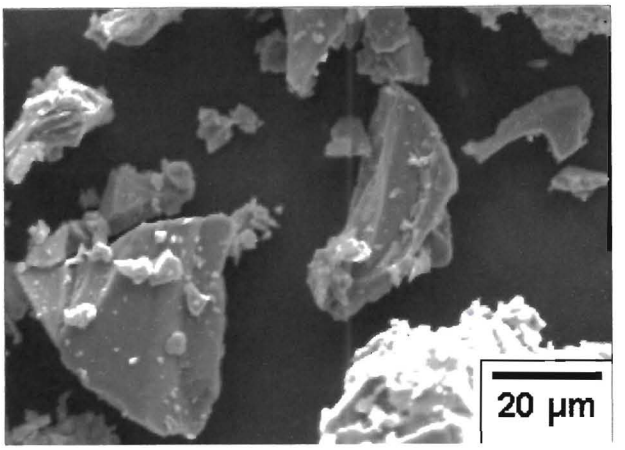

(a) < 25 µm

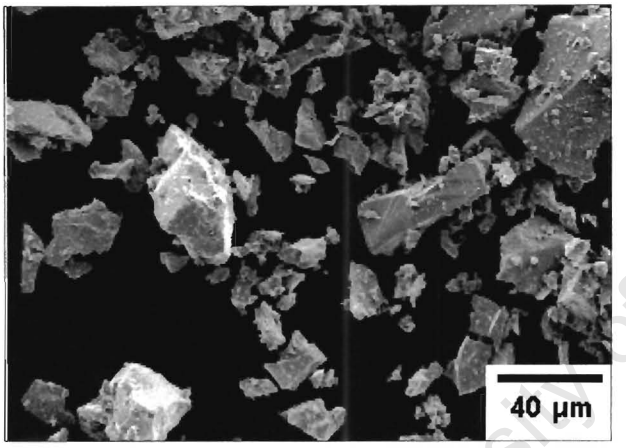

(b) 25 – 38 µm

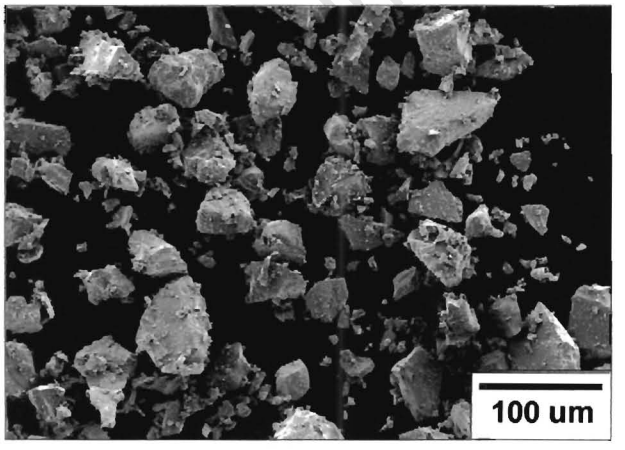

(c) 38 – 63 µm

SILICA

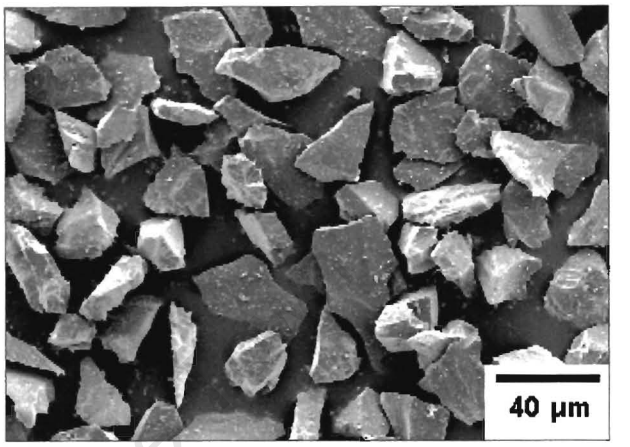

(d) < 38 µm

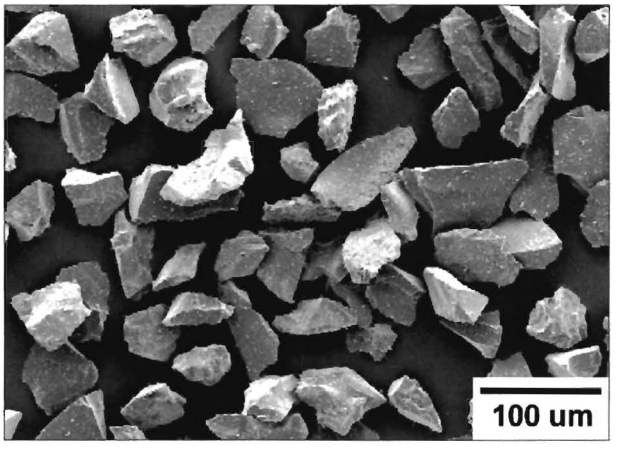

(e) 38 – 63 µm

Figure 4-11 Morphology of the very fine erodent particles in the indicated size ranges, for **(a) – (c)** magnetite particles, and **(d) – (e)** silica particles.

MAGNETITE

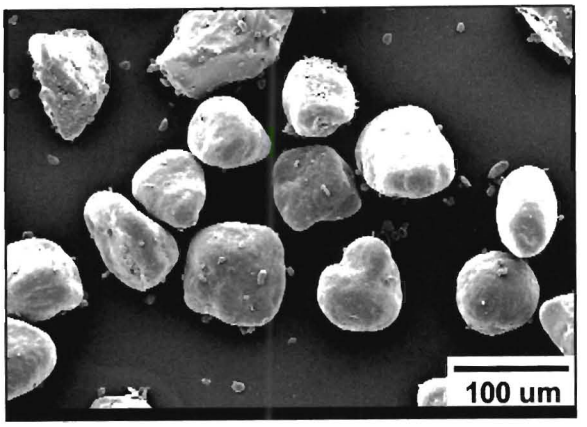

(a) 63 – 75 µm

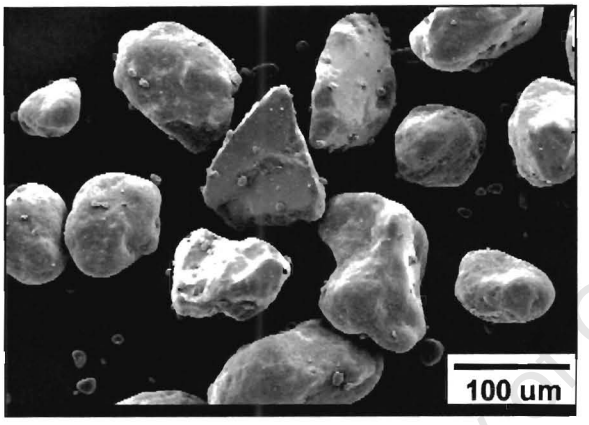

(b) 75 – 106 µm

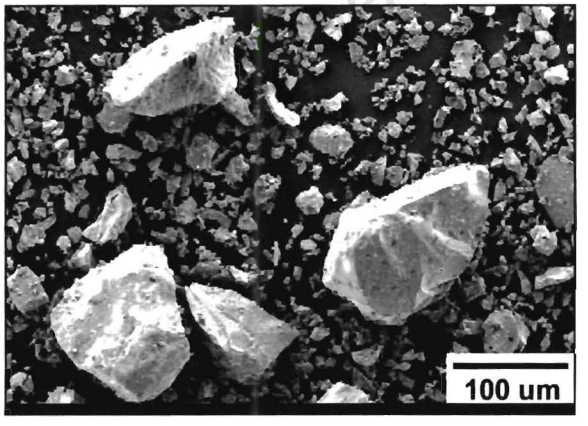

(c) 106 – 125 µm

SILICA

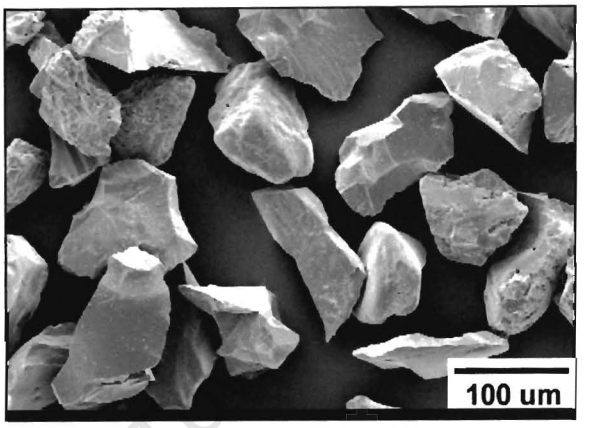

(d) 63 – 106 µm

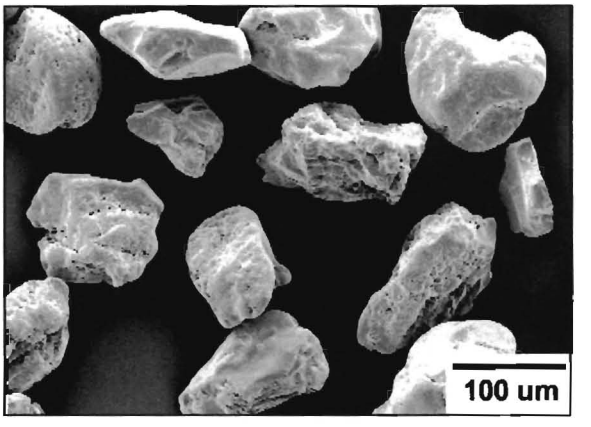

(e) 106 – 125 µm

Figure 4-12 Morphology of the intermediate erodent particles in the indicated size ranges, for **(a) – (c)** magnetite particles, and **(d) – (e)** silica particles.

MAGNETITE

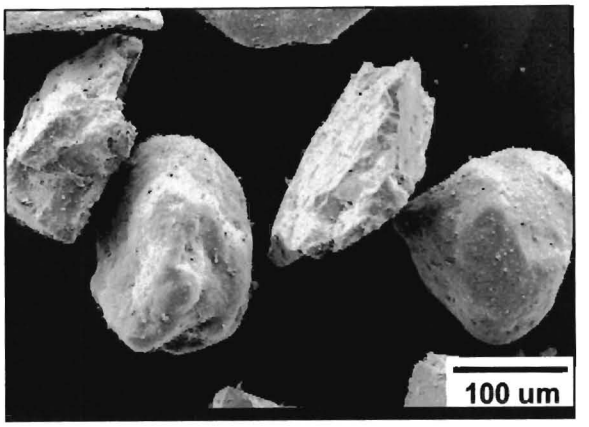

(a) 106 – 125 µm

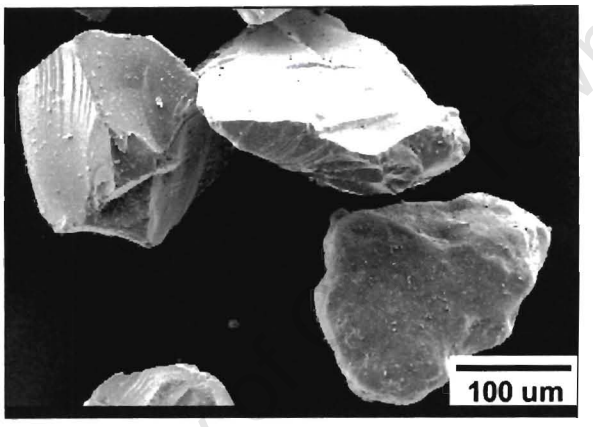

(b) 150 – 180 µm

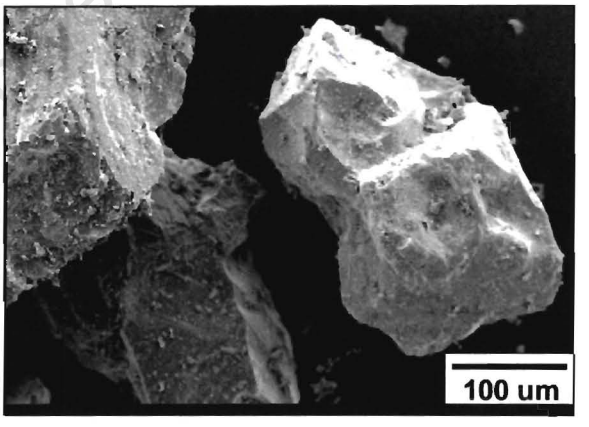

(c) > 180 µm

Figure 4-13 Morphology of the largest magnetite particles considered in testing, in the indicated size ranges. A very small percentage of the catalyst is within these size ranges (see figure 3-3).

4.4. PARTICLE FRIABILITY AND THE EFFECT OF ERODENT RECYCLING

A number of erosion tests were performed with the same sample of magnetite. This was achieved by recovering the particles after each test and reusing them on untested steel specimens. The behaviour of the magnetite particles when repeatedly striking a solid surface is important because of the circulating action of the catalyst particles in the synthol reactor, i.e. the same particle may strike the steam coil tubes and other reactor components numerous times. Magnetite particles 38 – 63 μm in diameter were used in testing, impacting the steel specimens at 30°. The change in erosion rate with each subsequent test is illustrated in figure 4-14. The erosion rate shows a consistent decrease with each subsequent test.

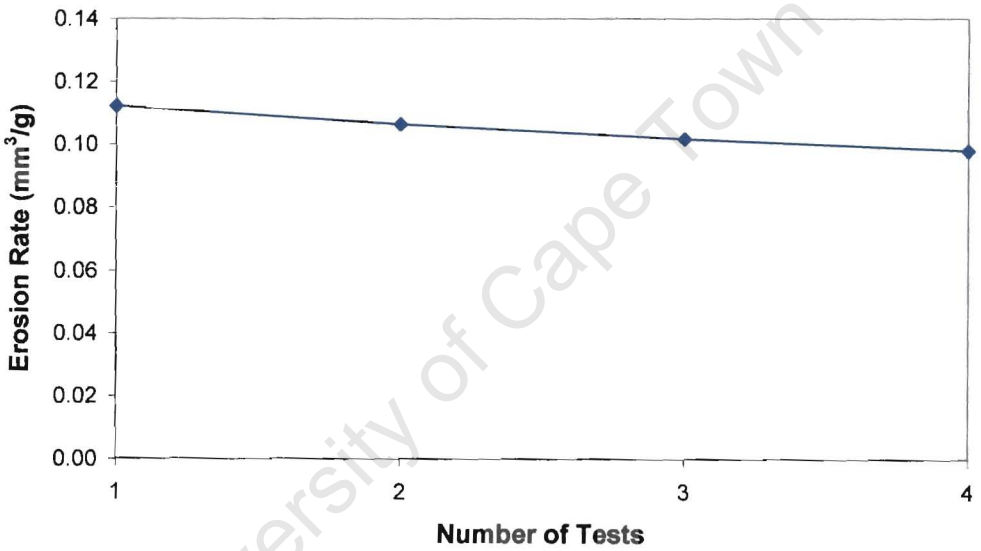

Figure 4-14 The effect on erosive wear rate of repeated erosion tests using the same erodent sample.

The SEM images in figure 4-15 illustrate the morphology of the magnetite particles following each subsequent erosion test. Negligible mechanical degradation can be observed. The very fine particles were progressively lost, because the test chamber was not perfectly sealed. After the third test, the fine particles seemed to be almost entirely absent.

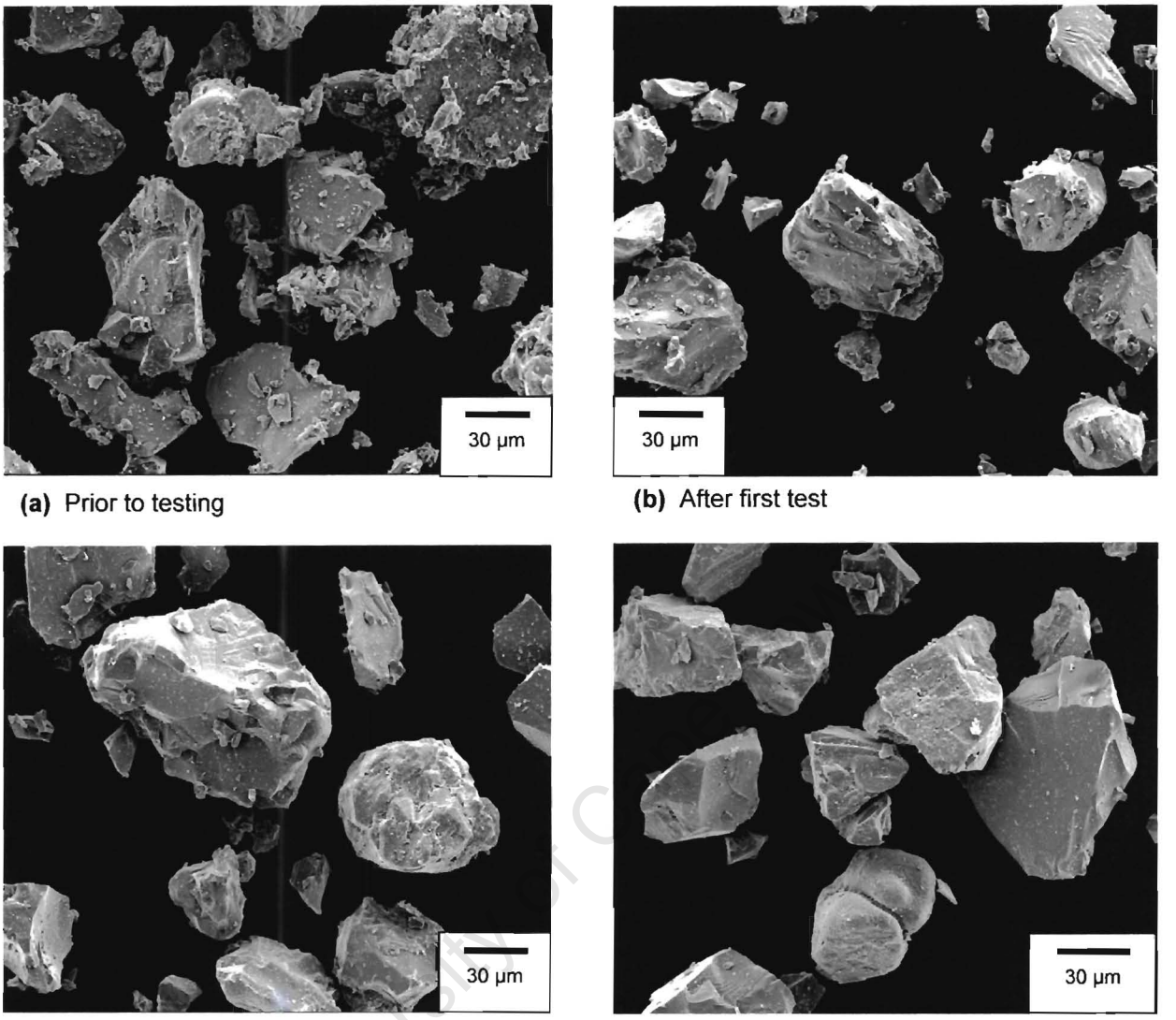

(a) Prior to testing

(b) After first test

(c) After second test

(d) After third test

Figure 4-15 Morphology of magnetite particles subjected to repeated erosion testing. Negligible mechanical degradation is observed, but there is a noticeable loss of the finer particles.

4.5. EFFECT OF DIFFERENT STEEL TARGETS

Mild steel (EN3B) was chosen as the control sample for comparing erosion rates of the reactor steel. Figure 4-16 shows the erosion rates obtained by testing EN3B and 1.6580 steels with 125 – 180 μm silica particles at 30° and an average velocity of 80 $m.s^{-1}$. The curves representing cumulative volume loss have very similar slopes. The erosion rates, which are represented by the slopes of the curves in figure 4-16, are similar, with a negligible difference of approximately 4% between them.

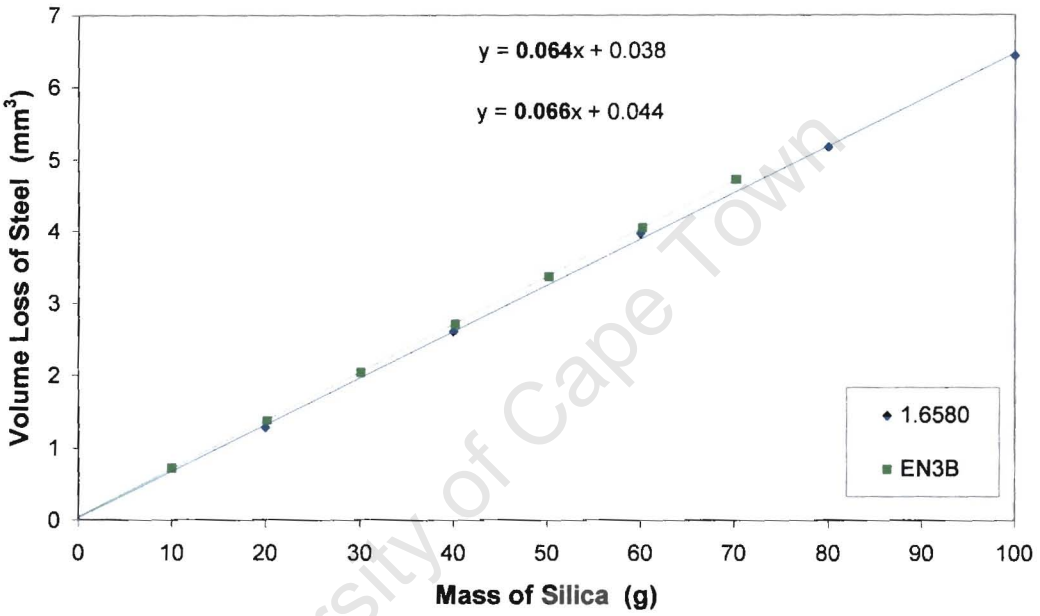

Figure 4-16 Comparative volume loss curves for EN3B (reference material) and 1.6580 steel (tube steel) impacted by silica particles.

The microstructures of the steels used in erosion testing are shown in figure 4-17. The 1.6580 steel samples were found to have an equiaxed microstructure in both the longitudinal and transverse directions. The grains were of comparable size in both directions. The structure of the steam coil tube steel is ferrite and pearlite, typical of a low carbon annealed steel. The microstructure of the EN3B steel is consistent with its designation as a low carbon (max. 0.25%) mild steel.

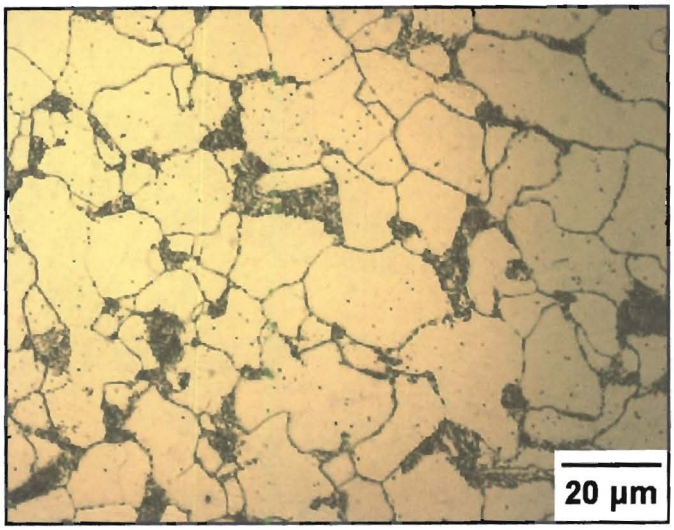

(a) Longitudinal section 1.6580 steel

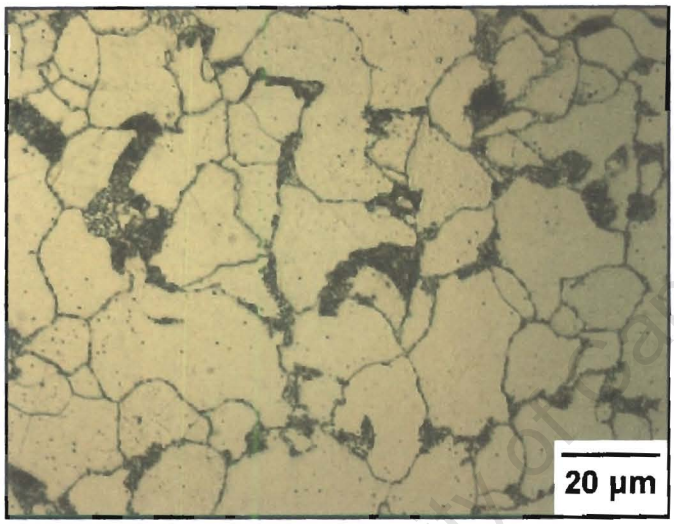

(b) Transverse section 1.6580 steel

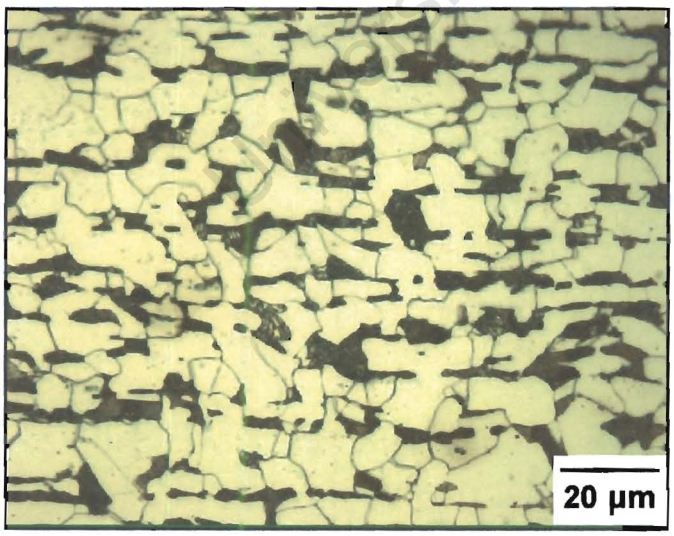

(c) EN3B

Figure 4-17 Microstructure of steels used in erosion testing. **(a), (b)** 1.6580, steam coil tube steel **(c)** EN3B, reference material.

4.6. EFFECT OF SURFACE CONDITION ON EROSION

Further erosion testing was performed to evaluate the effect of surface condition and surface engineering on erosion rates. Steel specimens were tested with a range of surface conditions (with corresponding surface roughness values):

i. Original, or as-received, steam coil tube surface ($R_a \approx 7.1$ μm, with a wide range of values, 2 – 14 μm)

ii. Surface ground, as received from the workshop ($R_a = 0.73$ μm longitudinal and $R_a = 0.83$ μm transverse)

iii. Polished using 1000 grit emery paper ($R_a = 0.04$ μm)

iv. Plasma nitrided ($R_a = 10.9$ μm)

4.6.1. GROUND AND POLISHED SURFACE

Figure 4-18 compares the erosion rates for a specimen that had been surface ground ($R_a = 0.73$ μm in the direction of erosion; $R_a = 0.83$ μm perpendicular to particle stream), and a similar specimen polished using 1000 grit emery paper ($R_a = 0.04$ μm). Silica particles 125 – 180 μm in diameter impacted 1.6580 targets at 30° and 80 $m.s^{-1}$. A negligible difference was observed between the slopes of the curves, which represent the erosion rates.

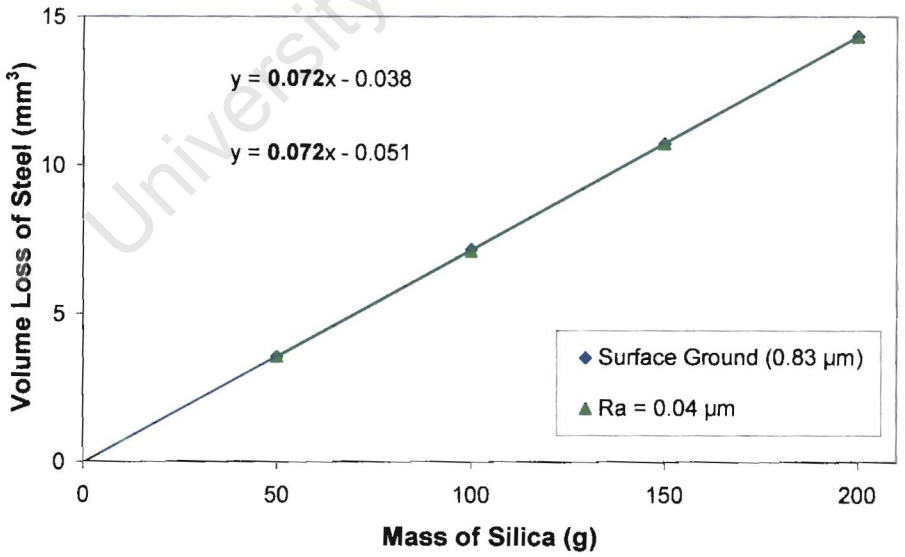

Figure 4-18 Effect of surface finish on volume loss for ground and polished 1.6580 steel specimens.

A similar test was performed for a surface ground specimen (R_a = 0.73 – 0.83 μm) compared with an as-received surface ($R_a \approx$ 7.1 μm). Magnetite particles 38 – 63 μm in diameter impacted 1.6580 steel targets at 30° and 90 $m.s^{-1}$. A negligible difference in the erosion behaviour of these specimens was observed, as indicated by the similar erosion rate curves shown in figure 4-19. A measurable deviation of one of the curves from the initial steady-state erosion behaviour cannot be identified for 400 g of erodent tested. The difference in appearance of the tested surfaces is shown in figure 4-20. Erosion was thus insensitive to changes in the surface finish of the steel. Subsequent testing was performed using surface ground specimens, as received from the workshop, for convenience and ease of testing.

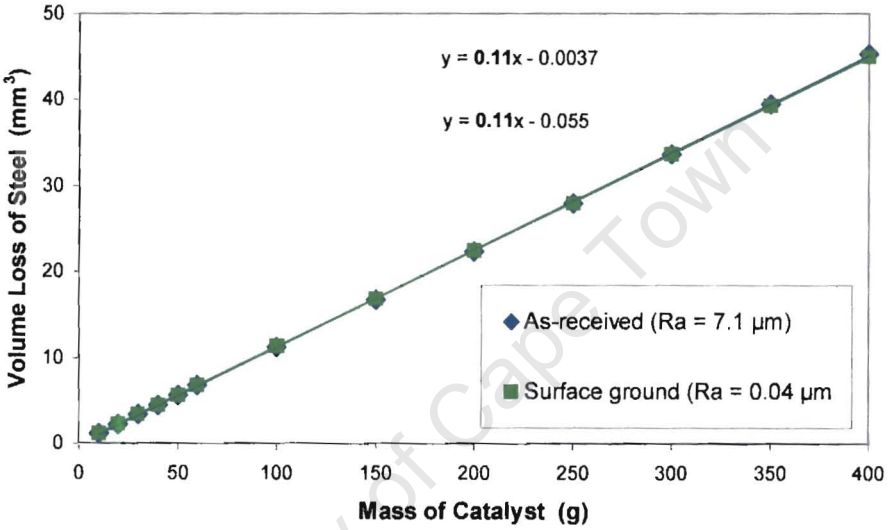

Figure 4-19 Erosion rates produced in 1.6580 steel with surface ground surface finish, and original steam coil tube surface.

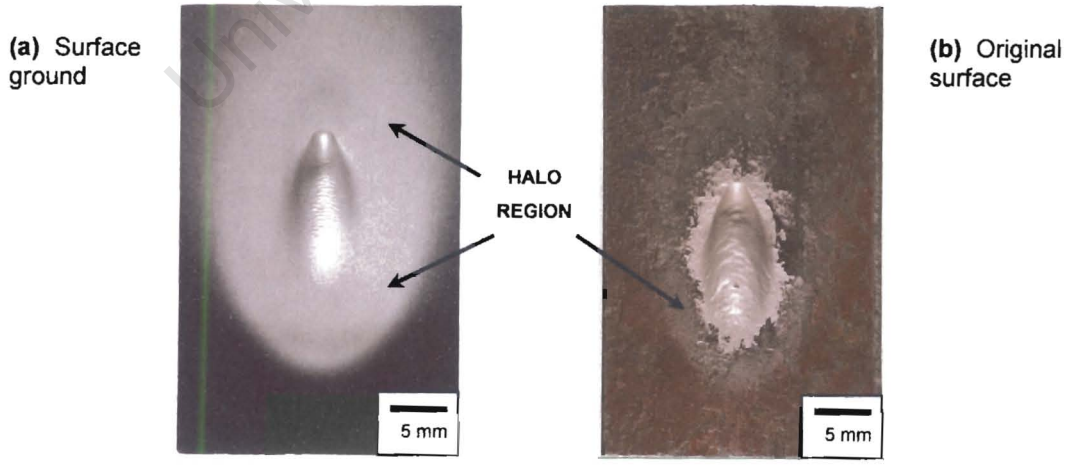

Figure 4-20 Surfaces of 1.6580 steel specimens as eroded in figure 4-19.

4.6.2. ORIGINAL STEAM COIL TUBE SURFACE

Figure 4-20 compares a surface ground specimen (figure 4-20a) with a specimen cut from a steel tube similar to those used in the reactors on the PetroSA plant (figure 4-21b). The surface of the latter specimen was left in its original condition, i.e. a thin layer of corrosion scale with a decarburised surface layer beneath it as shown in figure 4-21. This surface layer was found to have a negligible effect on the erosion rate of the steels tested (figure 4-19).

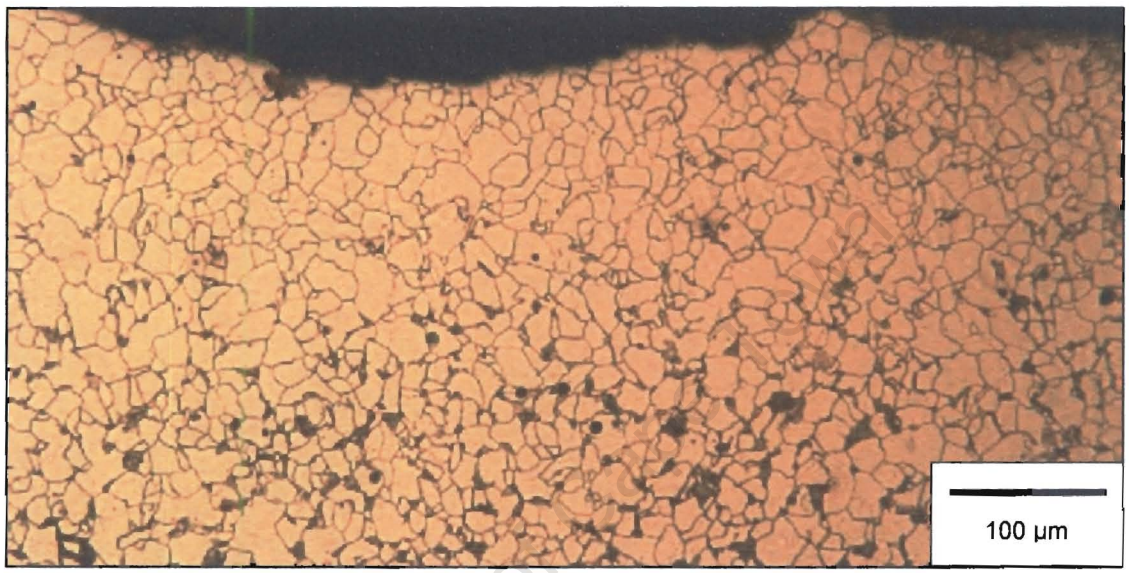

Figure 4-21 Structure of the steam coil tube surface, as received from PetroSA. A 150 µm deep decarburised layer is evident on the tube surface.

The hardness of the bulk steel was approximately 135 – 154 HV. The decarburised surface layer (depth = 0.15 mm) displayed a slightly higher hardness value of between 167 and 171 HV.

This may be explained by the apparent smaller grain size in this region, but the difference is considered too small to be of significance.

4.6.3. PLASMA NITRIDED STEEL

Commercially prepared plasma nitrided steel plates were supplied for erosion testing. The specimens were machined to the same dimensions as described in figure 3-1(a). Magnetite particles 38 – 63 μm in diameter impacted surface ground and plasma nitrided 1.6580 targets at 30°, and velocities of 38 $m.s^{-1}$ and 90 $m.s^{-1}$; generating the volume loss curves shown in figure 4-23. Erosion rates are given by the slopes of the curves, highlighted in bold font.

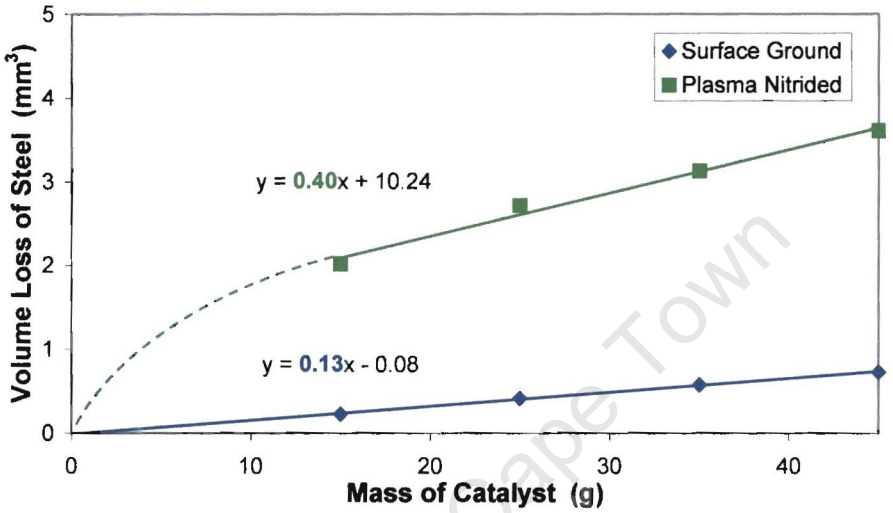

(a) Particle impact velocity = 38 $m.s^{-1}$

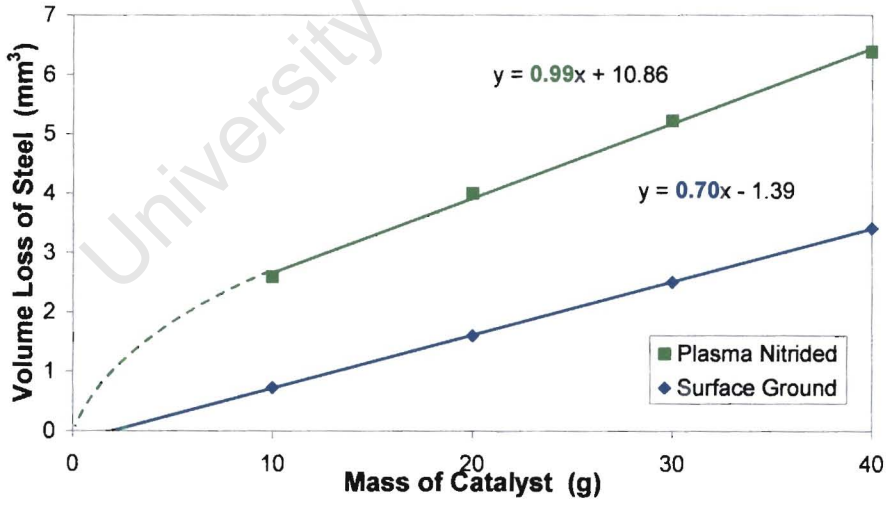

(b) Particle impact velocity = 90 $m.s^{-1}$

Figure 4-22 Volume loss curves for plasma nitrided 1.6580 compared with surface ground 1.6580 impacted by magnetite at particle impact velocities of **(a)** 38 $m.s^{-1}$, and **(b)** 90 $m.s^{-1}$.

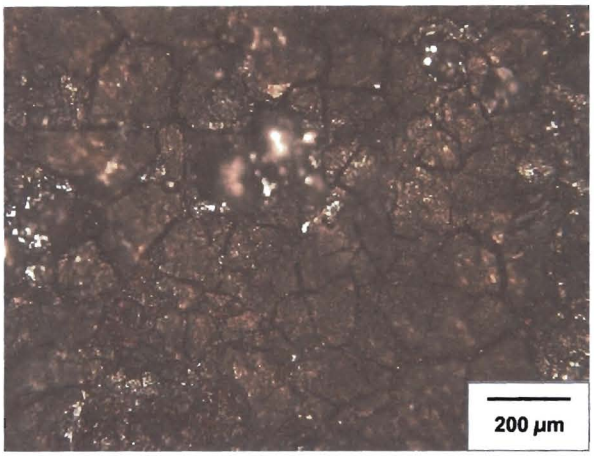

Figure 4-23 Surface of the plasma nitrided 1.6580 steel.

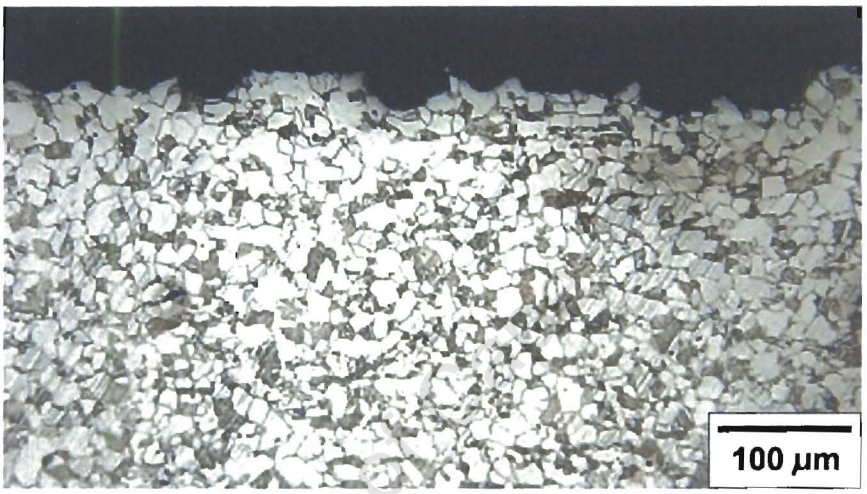

Figure 4-24 (20X) Cross-section of surface of plasma nitrided tube steel

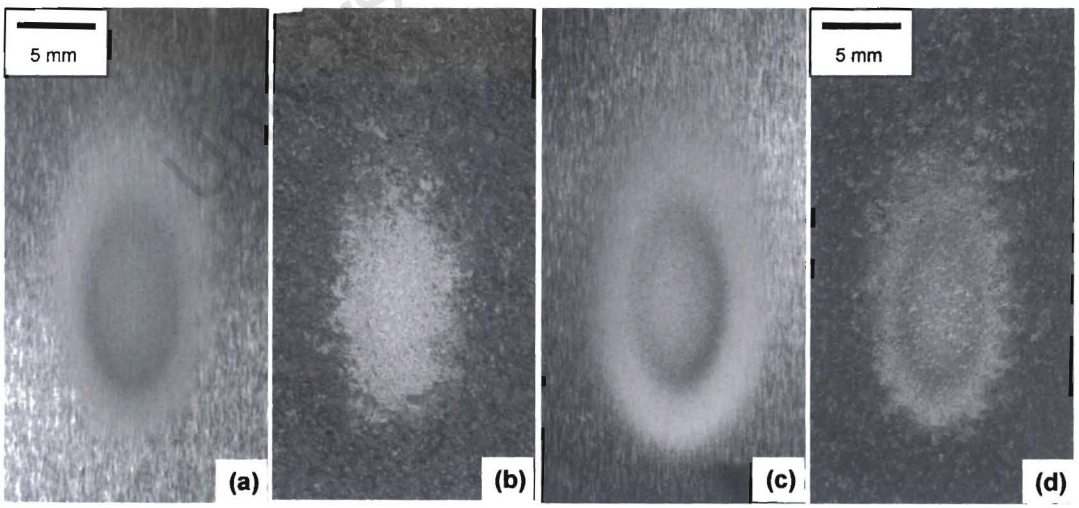

Figure 4-25 Plasma nitrided tube steel specimens **(b), (d)** and surface ground tube steel **(a), (c)** eroded by 38 – 63 µm magnetite at 30° and **(a), (b)** 36 $m.s^{-1}$ **(c), (d)** 90 $m.s^{-1}$.

Optical microscopy revealed the surface of the plasma nitrided sample to be cracked and uneven (figures 4-23 and 4-24). The surface roughness was R_a = 10.9 μm, which approximated the roughness of the oxidised original tube surface and had a hardness of 1100 HV. The response of the specimens to erosion is illustrated in figure 4-25. The documented damage is the result of the erosion tests described above (figure 4-23). The very uneven surface led to the formation of an uneven wear scar, and much higher initial, and steady-state erosion behaviour. The hard, brittle protrusions on the nitrided surface were easily removed by impacting catalyst particles, explaining the higher erosion rates observed.

Steel target	HV
Plasma nitrided 1.6580	1100
Original tube surface 1.6580	167
Surface ground 1.6580	144
Surface ground EN3B	169

Table 4-2 Surface hardness values for the steels tested, measured using a Vickers pyramid indenter.

The results suggest that the plasma nitriding was unsuccessful. No benefits could be discerned from using this treatment in the erosive environment considered in this work. The plasma nitrided surface treatment was not considered further.

4.7. RESPONSE OF STEEL TO EROSION

4.7.1. SURFACE RIPPLES

The characteristic ripple structure observed at 30° at the bottom of the wear scars of eroded 1.6580 steel specimens is shown in figure 4-26. The appearance of surface ripples followed the formation of a distinct wear crater. They became more pronounced until the crater was very deep. There were no ripples observed on the surface of the specimen tested with 1600 g of magnetite (figure 4-30b). Beyond a certain depth of wear scar, the favourable conditions for the formation and precession of surface ripples do not exist.

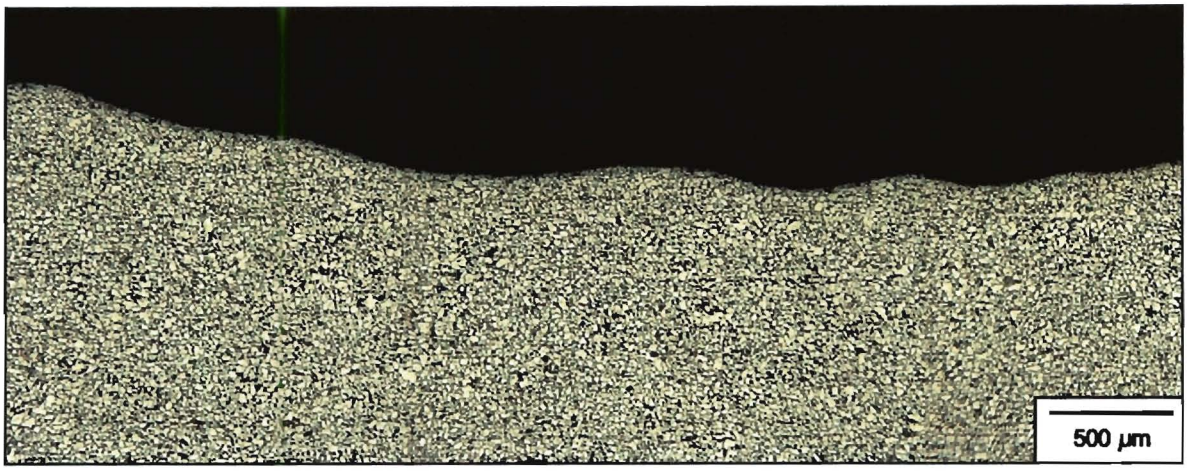

Figure 4-26 Cross-section through surface ripples at the bottom of a wear scar formed by impacting surface ground tube steel with 38 – 63 µm magnetite particles at 30° and 90 $m.s^{-1}$.

4.7.2. LONG-TERM EROSION AND EVOLUTION OF THE WEAR SCAR

It was observed in practice that erosion of the steam coil tubes was uneven, and long, elongated wear scars were produced on the tube surfaces. In an effort to reproduce such characteristics and evaluate the effects of long-term testing on erosion rates, larger quantities of erodent were employed.

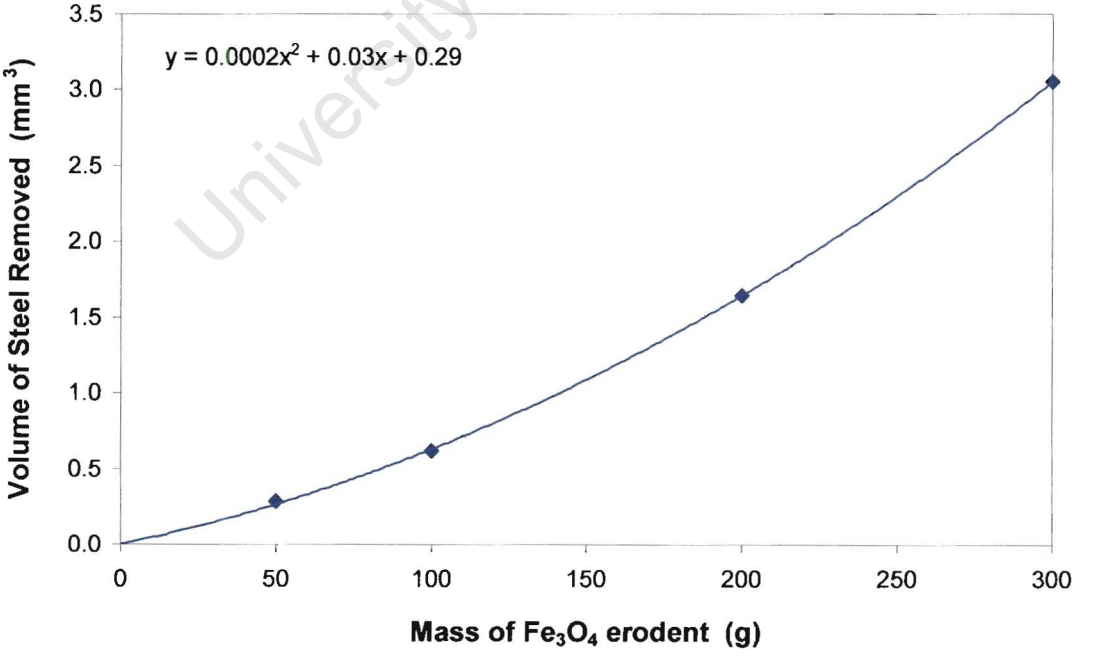

Figure 4-27 Effect of large quantities of magnetite on the volume loss of 1.6580 steel.

Four steel specimens were used to generate the set of results shown in figure 4-27. Volume loss was determined for each 50, 100, 200 and 300 g of erodent. This compared to a total charge of only 40 g for general erosion testing. These tests were conducted at 60 $m.s^{-1}$ and 30°, with an average particle mass flux of 7.24 $kg.m^{-2}.s^{-1}$, with 38 - 63 μm magnetite particles impacting a steam coil tube steel specimen with a R_a = 0.01 μm surface finish. The erosion rate shows a gradual increase with increasing erodent charge, as indicated by the non-linear volume loss curve.

Figure 4-28 shows the results of erosion tests using 38 – 63 μm magnetite particles impacting a 1.6580 steel specimen with test surface in the original condition of the steam coil tubes, at 30° and 90 $m.s^{-1}$. A constant erosion rate of 0.88 $mg.g^{-1}$ was observed until 450 – 500 g of erodent had been fed through the rig. From that point onward the erosion rate began to increase slightly. The test was stopped at 700 g due to a lack of erodent. This corresponded to a test time of 86 minutes. The curve for a surface ground specimen is included with an extrapolated best-fit curve to show the deviation of the erosion rate from a constant value (as represented by the slope of the linear volume loss curve). After 700 g of erodent, a 4.7% deviation was observed. Even a slight increase in erosion may prove significant, because over a long period of time the difference in wastage of the steel may become substantial.

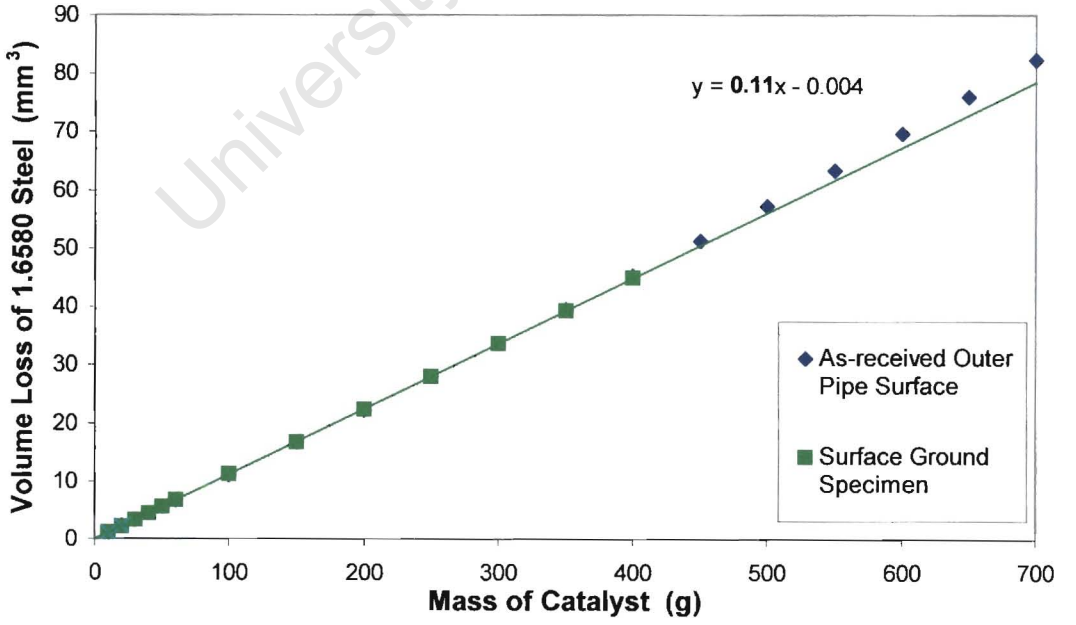

Figure 4-28 Extended erosion test, showing the effect of large quantities of erodent on the volume loss of the steel target. The slope of the curve represents the erosion rate.

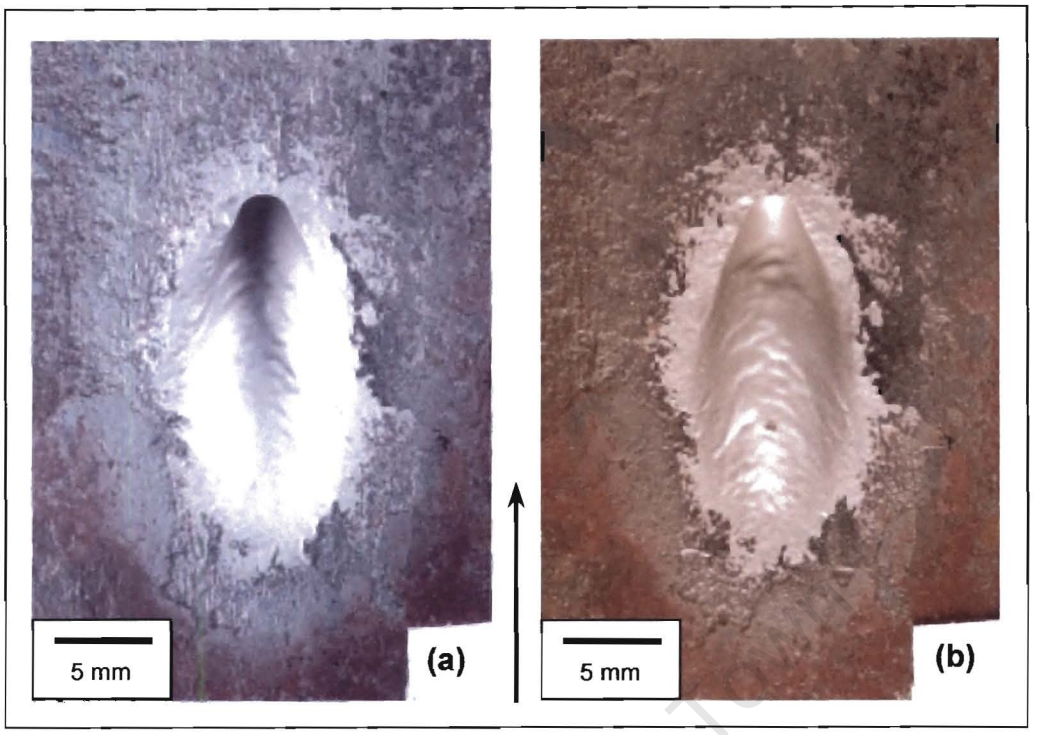

Figure 4-29 Wear scar formed by 700 g of magnetite impacting a 1.6580 steel surface. An undercut is observed at the top of the wear scar. **(a)** and **(b)** represent the same specimen under different lighting conditions.

The photographs in figure 4-29 show a steel specimen with the as-received outer surface as eroded with 700 g of erodent. The arrow indicates the direction of the erodent. The erodent undercuts the surface of the steel at the end of the wear scar. The damaged area is shown, with different lighting, to highlight different parts of the wear scar. The photograph in figure 4-29(a) highlights the undercut, while the flow lines of the steel (surface ripples) are more easily noticeable in figure 4-30(b). A cross-section through the center-line of the wear crater in figure 4-29 is shown in figure 4-30(a).

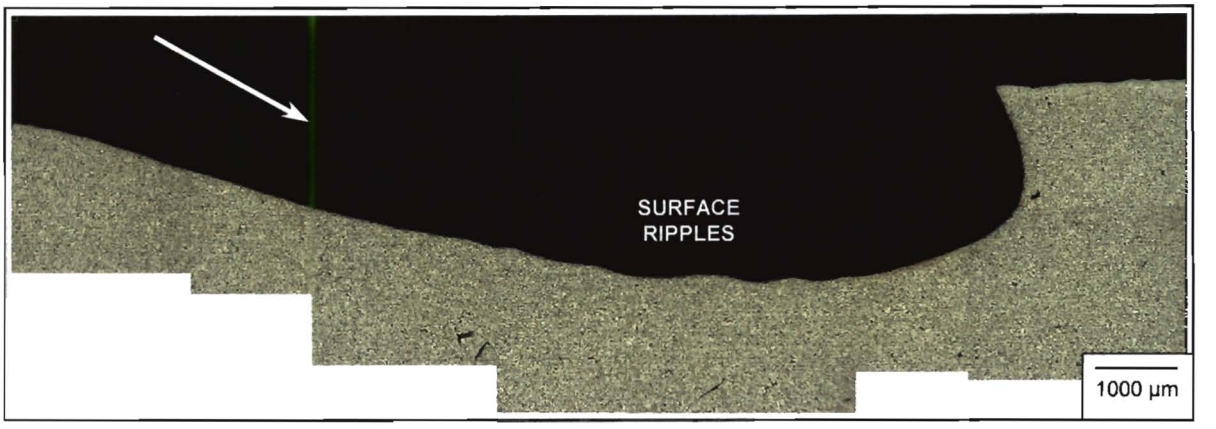

(a) Crater formed by 700 g of magnetite particles. Well developed ripple structure evident at the bottom of the crater. Particles have been directed into the front of the crater, forming an undercut.

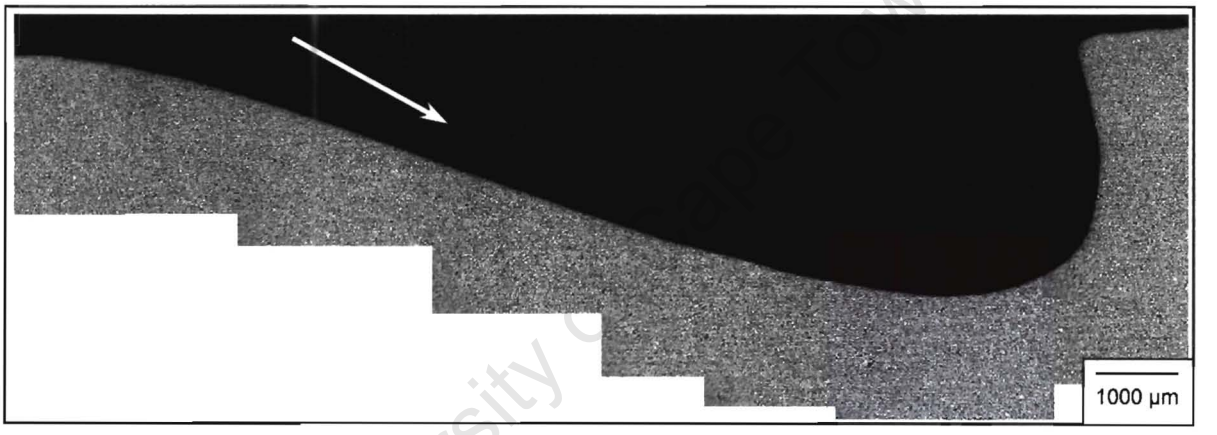

(b) Crater formed by 1600 g of magnetite particles. The approach to the crater has stabilised, with wear proceeding in the front of the crater. The 'nose' of the crater becomes deeper and the crater elongates by erosion of the undercut.

Figure 4-30 Cross-section through wear craters formed by the impact of **(a)** 700 g and **(b)** 1600 g of catalyst at 30° and 85 $m.s^{-1}$. Arrows indicate the direction of the erodent.

The formation of ripples and an undercut in the wear scar was considered in more detail. Erosion tests were performed using 800 g of catalyst at 30°, average particle impact velocity of 85 $m.s^{-1}$ and mass flux of 1.8 $kg.m^{-2}.s^{-1}$. The catalyst was tested without first separating it into size intervals by sieving. The test was an attempt to simulate as closely as possible the conditions experienced in the reactor. The 800 g were tested in a total time of 74 minutes. After testing with each charge of 100 g of catalyst, taking an average of 9 minutes and 15 seconds each, the target was removed for photographic documentation of the wear scar, the

results of which are shown in figure 4-32. This test allowed the formation of the constrained wear crater, including the undercut at the trailing edge, to be observed. A constant wear rate was observed for 600 g of erodent striking the target. Above 600 g of erodent, the erosion rate began to increase slightly. This is in agreement with the results presented in figure 4-29. The erosion rate began to increase slightly from about 500 – 550 g of erodent (figure 4-29). The results presented in figure 4-31 for similar conditions show a slight increase in erosion rate around 600 – 700 g. It is considered that figure 4-31 is less sensitive to subtle changes due to the larger intervals (larger catalyst charges) between measurements of volume loss.

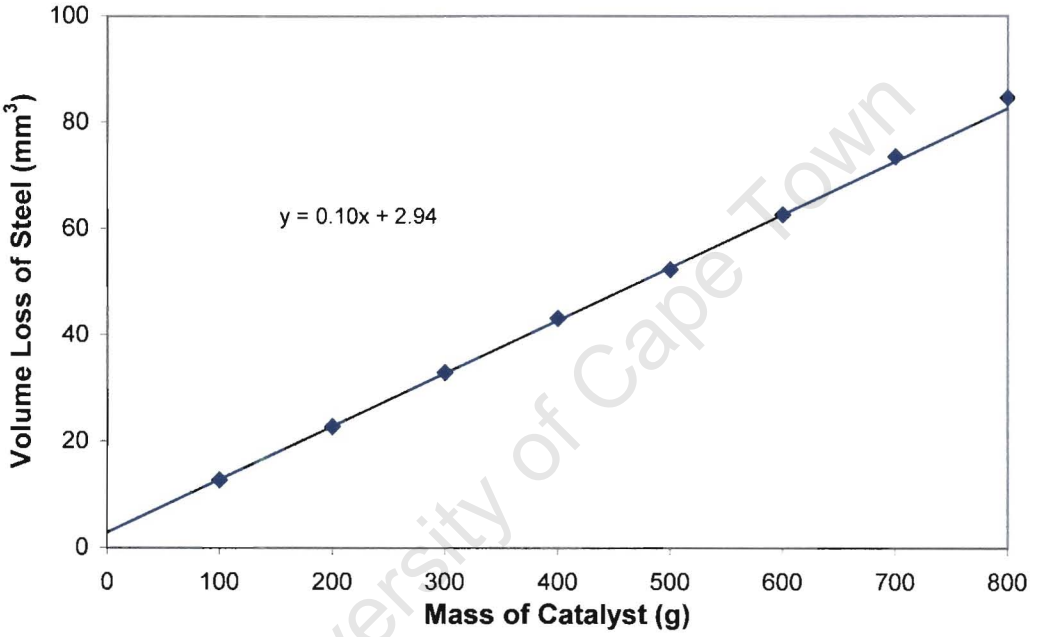

Figure 4-31 Long-term erosion test of 1.6580 steel eroded by 800 g of magnetite particles.

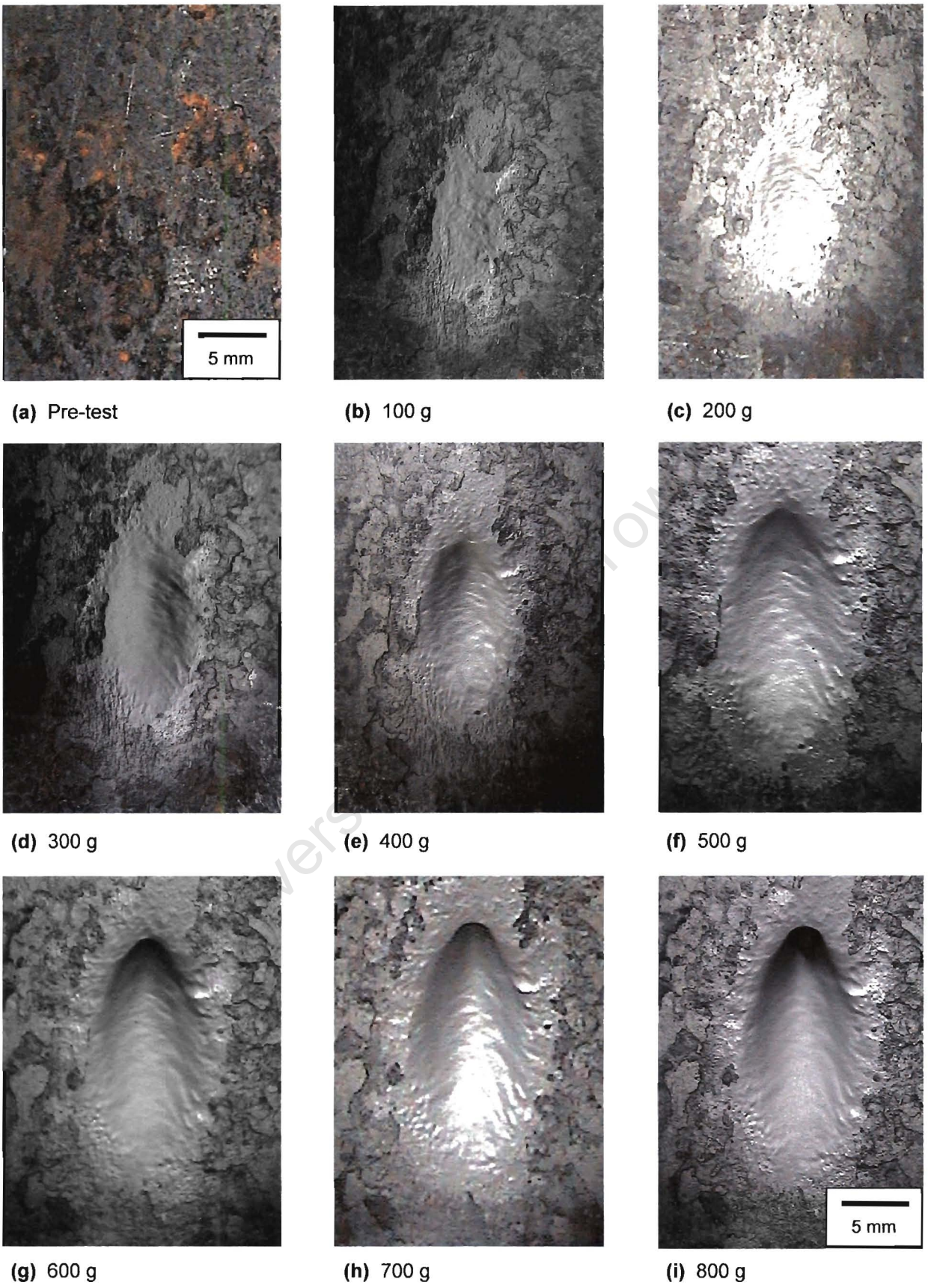

Figure 4-32 Evolution of the wear scar for 1.6580 steel impacted by magnetite particles in 100 g increments.

4.7.3. HARDNESS AS A FUNCTION OF DEPTH BELOW THE SURFACE

The microhardness of an eroded 1.6580 steel surface was found to be slightly lower than that of the base metal. A specimen impacted by 38 – 63 μm magnetite particles at 30° and 90 $m.s^{-1}$ displayed a softened surface zone less than 10 μm thick. There was a work hardened zone directly beneath this softened surface, below which the hardness of the bulk material was unaffected.

4.7.4. MECHANISMS OF MATERIAL REMOVAL

The response of the steels to erosion was typical of the ductile erosion of steels by hard angular particles. Figure 4-33 shows steady-state wear damage for 1.6580 steel impacted by magnetite particles less than 38 μm (figure 4-33a) and particles 38 – 63 μm in diameter. The surfaces showed evidence of severe plastic deformation, with evidence of both cutting; and wear by ploughing and platelet formation. The size of the individual strikes in the steel surface is dependent on the size of the impacting particles. Extensive cutting by the highly angular magnetite particles can be observed in figure 4-33.

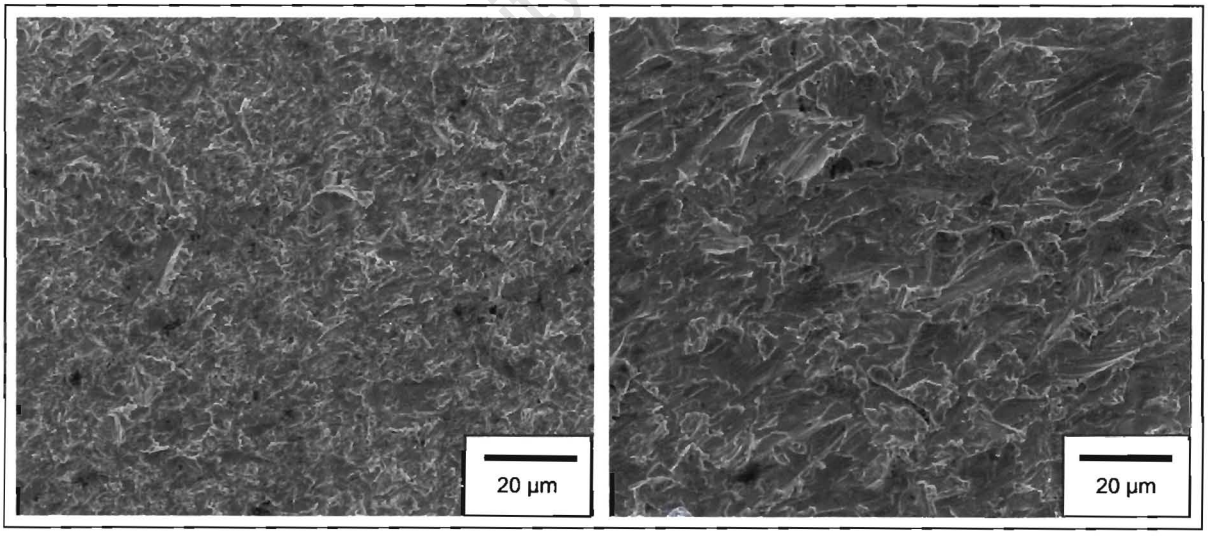

Figure 4-33 Steady-state erosion damage in a 1.6580 steel specimen impacted by magnetite particles **(a)** < 38 μm and **(b)** 38 – 63 μm in size.

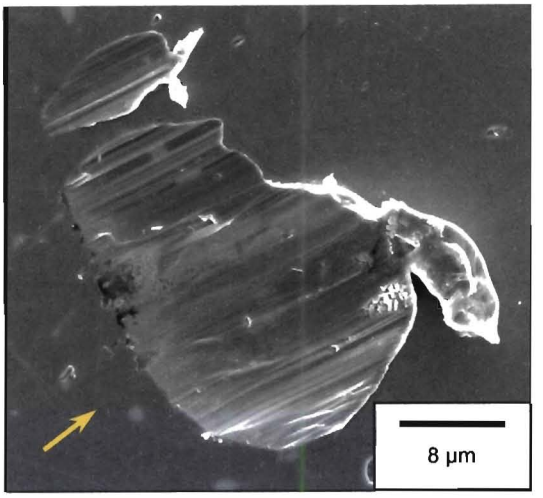

(a) Low angle ploughing / cutting damage in steel, with loosely attached platelet.

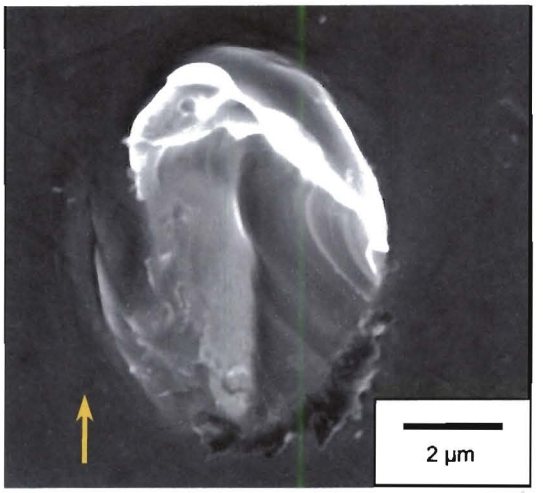

(b) Ploughing damage in steel, with a large crater lip formed at trailing edge of the wear scar.

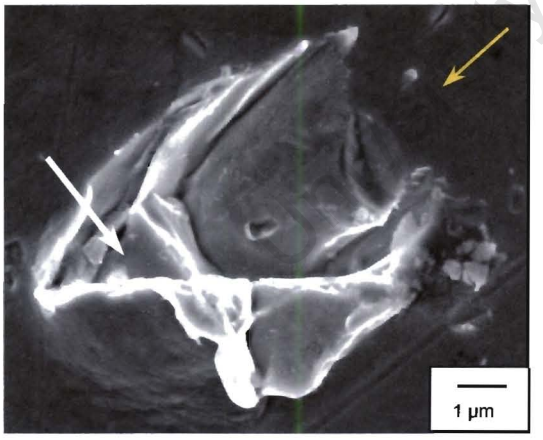

(c) Embedment of catalyst particle.

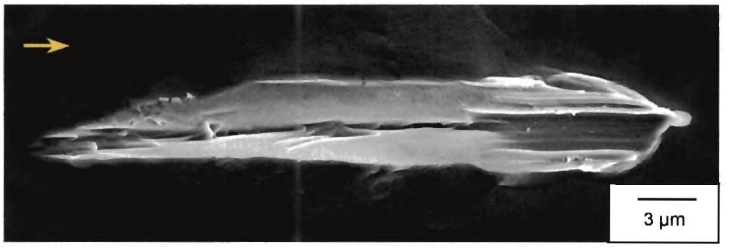

(d) Cutting erosive wear.

Figure 4-34 Erosive wear in 1.6580 steel due to single impacts by < 38 µm magnetite particles at 30° and 90 $m.s^{-1}$. The yellow arrows indicate the direction of the erodent particles.

At low angles (30°), evidence of both cutting and ploughing was observed. Figure 4-34 shows different impact events for the same steel specimen impacted by a controlled number of magnetite particles less than 38 μm in diameter. Figure 4-34(a) can be considered a combination of cutting and ploughing. Material has been swept from the steel surface, with a small, loosely attached lip thrown up at the trailing edge of the wear scar.

Although not widespread, there was evidence of particle embedment of small particles. Figure 4-34(c) shows a very fine catalyst particle embedded in the front tip of a wear scar. The particle did not have sufficient energy due to its small size to peel back the layer of metal it had ploughed beneath. Some of the crater lip has been peeled back, but the particle cut deep enough for it to remain wedged in the surface.

Figure 4-34(d) shows an example of classic cutting wear by angular particles in ductile materials at low impact angle. A neat chip of metal has been removed from the surface, leaving an almost imperceptible crater lip.

CHAPTER FIVE

DISCUSSION

5.1. INTRODUCTION

It is clear from the present experimental work that the erosive wear of the steel heat exchanger tubes is critically dependent on the process variables within the synthol reactors. This is not an unexpected result since it has been documented previously that erosion is highly systems dependent[1,2,4,9]. Nevertheless, any attempt to quantify and understand the influence of the specific variables involved is important, as it allows a prediction of likely wear in practice. It is then possible to predict the effect on erosion of changes that are made in the process and reactor conditions. Of particular importance in this work is the effect of the catalyst particles, magnetite, on the erosive wear of steel.

5.2. THE EFFECT OF SYSTEM CONDITIONS

Room temperature erosion tests using magnetite to impact steam coil tube steel samples revealed a maximum on the erosion rate versus impingement angle curve of between 30° and 40° (figure 4-1). The shape of the curve was consistent with the accepted curve of erosion of ductile materials by solid particle impact[9,15-17,20] (figure 2-4). The exact position of and relative sharpness of the peak are determined by the erosive system. For this system, the maximum in the erosion peak is flattened, with similar erosion rates for impact angles between 30° and 40°. The erosion rates drop to approximately 40% of the maximum at both extremes of the curve, i.e. at 10° and at normal incidence. Since the relative shape of the peak gives an indication of the ductility of the steel[16], it is clear that the steel used for the steam coil tubes is highly ductile. A flattened curve of erosion rate versus impact angle indicates that the material is better able to absorb the energy of impacting particles in a manner less dependent on the impact angle.

The effect of velocity on erosion is perhaps the most critical consideration in this system. The dependence of erosion rate on velocity followed a power law relationship (figure 4-2):

$$E_R = 1 \times 10^{-5} V^{2.07}$$

The value of around 2 for the velocity exponent lies within the range 2 – 2.5 generally found for metals[9,10,57]. The effect of velocity is thus of great significance, and steps that limit the velocity of the catalyst, or eliminate regions of high velocity in the reactor will cause an associated decrease in erosion of the reactor internal components.

Laboratory testing was performed at velocities higher than those experienced in the synthol reactor. This was due to limited quantities of magnetite catalyst being made available for testing. It was considered acceptable to use the known dependence of erosion rate on velocity to extrapolate the reported erosion to velocities similar to those found in the reactor. Regions may exist within the reactor where the local velocity is much higher than the general velocity of the gas and catalyst in the reactor. This can lead to streaming, where the erodent stream impinges on the tube walls at a much higher velocity and with a higher concentration of catalyst particles than in the surrounding areas. While it has been shown here that erosion rates decreased slightly with increased mass flux of catalyst, due to increasing interference of rebounding particles with incident particles, the effect is small, and may be overwhelmed by the increase in velocity of the stream. The result of this streaming would be non-uniform erosion, with erosion rates of certain components or areas within the reactor being much higher than those expected considering the nominal operating conditions.

It is thought that the severe, largely localised wear damage observed in the synthol reactors may be due to streaming of the catalyst particles. The synergistic effects of localised increase in velocity and particles impacting the steam coil tubes near the angle for maximum wear, may explain the deep gouges formed in the steel surface in practice. Mathematical modelling of the gas flow in the reactor may confirm this theory, but has yet to be performed. A method of limiting erosive wear in the synthol reactors by attaching rib baffles to the steam coil tubes, thereby eliminating streaming, is proposed in Chapter Seven, Recommendations.

Elevated temperature erosion tests were not performed. The results presented in the literature agree that up to 250 – 400°C, the erosion rate for a wide range of steels either decreases or remains constant. The erosion rate of 1.6580 steel was not expected to increase with increasing temperature up to the proposed test temperature of 220°C.

5.3. THE EFFECT OF ERODENT SIZE, MORPHOLOGY AND CONDITION

It is clear from the experimental work presented that catalyst shape and size are of considerable significance for this erosive system. The results have shown that as the particle size decreases, the erosion rate increases. A change in magnetite particle size from 63 – 106 μm to < 38 μm resulted in a 27% increase in the erosion rate. While this change is small, it is nonetheless important in a system such as this that runs for long periods of time without inspection. It would be expected that the erosion would decrease with decreasing particle size, due to the so-called size 'effect'[11,31,33]. A larger particle has more momentum and can transfer its kinetic energy to the target more efficiently, resulting in larger volume loss. The reason for this apparent inconsistency with published work is the change in angularity of the catalyst particles with size. It was shown that the angularity of the magnetite particles increases as the size decreases. Very fine magnetite particles are highly angular, often spear shaped or platelike, as shown in figure 5-1. The size effect is valid for particles that have the same morphology regardless of size.

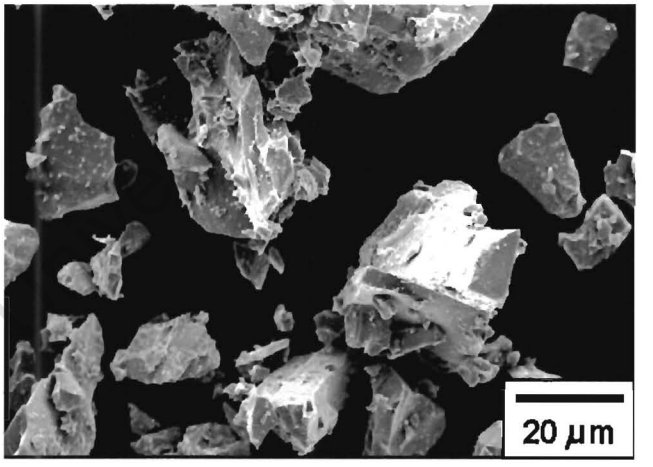

Figure 5-1 Angular nature of fine milled catalyst (magnetite) particles.

It is widely accepted that angular particles are more aggressive than spherical particles, due to the cutting action of these particles[24-26]. Spheroidal particles remove material by accumulated damage. Platelets are formed by impacting spheres by means of a ploughing action. Subsequent particles continue to deform these platelets until the fracture strain is reached, and they are removed from the surface[3,16,45]. Cutting is a much more efficient mechanism of

erosive wear. Chips of material are removed directly from the surface by each particle, with some material displaced as crater lips that are removed by the platelet mechanism of erosion. As the erodent becomes less rounded, the rake angle changes from a large negative angle to a large positive angle for highly angular particles with sharp protrusions[29]. Thus it is reasonable that the increase in angularity of the catalyst and the associated increase in the contribution of cutting to the wear of the steel with decrease in size is sufficient to overwhelm the effect of momentum considering the additional mass of larger particles.

The smaller particles, with their lower mass, are also more easily accelerated in the nozzle of the test apparatus. Thus, for the same free stream velocity, smaller particles will have a higher velocity than larger particles (figure 4-10). Previous researchers[31,32] claim that there is a cut-off size below which the small particles are not able to transfer sufficient energy to the target to cause plastic damage. If the particles are not massive enough, and the velocity not high enough, the impacting particles will elastically deform the surface of the metal, causing negligible observable damage. This assumes that the particle shape does not change with size. The smallest magnetite sizes tested caused measurable damage, with no observable decrease in erosion rates observed for the very fine particles. This is due to the very high degree of angularity of these fine particles.

The importance of particle angularity in erosion can be demonstrated by the differences in erosion observed for the milled and spent catalyst and the silica particles. The nominal hardnesses of the particles are between 81% and 86% harder than 1.6580 steel. These particles would be expected to erode the steel at similar rates. Despite this, the erosion rates for the three different erodents are different. The angularity of the particles can explain this unexpected result, with the most angular particles eroding the steel at higher rates. Silica particles are also more likely to degrade mechanically during impact with the target than magnetite particles, which may contribute to the lower erosion rates compared to those observed for milled magnetite particles.

Magnetite reclaimed after repeated impact with steel targets showed very fine particles clinging to the surface of larger particles even after two cycles through the erosion apparatus. If this is the case, it may artificially increase the angularity of the particles, causing increased erosion. It is worth noting that the finest catalyst particles are removed from the reactor with the reaction product and need to be filtered out at a later stage. It can thus be recommended that exclusion

of the very fine catalyst sizes would be desirable for limiting the erosion experienced in practice.

The milled catalyst used in testing was confirmed to be fully magnetite using XRD. A sample of spent catalyst, which had been removed from the reactor, was also used in erosion testing. During the reaction, waxy products and free carbon that is a by-product of the reaction, coat the catalyst particles. Some carbon also diffuses into the pores of the catalyst, splitting it open to reveal fresh reaction surfaces[55]. It would be expected that the fracturing of the catalyst in situ, which increases the angularity, should result in higher erosion rates compared to the fresh, milled catalyst. However, the build-up of carbon and waxes on the catalyst surfaces appears to negate such effects and leads to an overall lowering of erosive wear rates as shown in the results (figure 4-8). Based on the results presented, it may be expected that the erosivity of the catalyst decreases steadily with time in the reactor. Catalyst is replaced on-line, with the result that there is always fresh (milled and reduced) catalyst circulating through the reactors. Any decrease in the erosivity of the milled catalyst may lead to marked decrease in the erosion observed within the synthol reactors.

5.4. THE EFFECT OF SURFACE CONDITION

The effect of surface condition was tested, using the original tube surface ($R_a \approx 7.1$ μm), specimens machined to a 0.83 μm finish, and specimens polished to a 0.04 μm finish. Erosion rates were found to be similar for all the above conditions (figures 4-18, 4-19). There was a negligible difference in erosion of the decarburised and hardened outer layer of the tube compared to carefully prepared polished samples. The uneven surface and slight curvature of the specimen (as cut directly from a steel tube) also seemed to have little effect on erosion rates. The initial behaviour may be affected, until an eroded surface is developed, but this initial stage in the wear process was not noticeable for the conditions used in the erosion testing performed. Once the surface has been worn sufficiently, the erosion resistance is dependent on the performance of the bulk material. Of more interest, considering the long-term use of the steam coil tubes in the erosive environment of the synthol reactors, was the steady-state erosive behaviour of the steel.

A commercially prepared plasma nitrided 1.6580 steel plate was tested to investigate the effect of surface engineering on the erosion rate. A clean, machined steel surface eroded less than a plasma nitrided sample. Normally diffusion layers/zones perform well because of their greater strength and hardness, until they are breached. Nitriding is used extensively for wear parts. Clearly this sample was defective and thus no strong conclusions can be drawn.

5.5. THE EFFECT OF LONG-TERM TESTING

The synthol reactor is a circulating bed reactor. The catalyst thus cycles through the reactor repeatedly. Periodically some catalyst is removed and a fresh charge introduced into the process. Repeated tests were performed by reclaiming the magnetite particles after each test and using a new steel sample to determine each erosion rate. The erosion rate decreased steadily with each subsequent test. This was an interesting result, because it might be expected that as the hard, brittle magnetite particles recycle, they suffer structural degradation by chipping or splitting. If this were the case, the erosion rate should increase due to the increasing angularity and decreasing size of the particles. Conversely, if the particles experienced only slight chipping of the sharpest protrusions, recycling may produce more rounded particles, which would be expected to lower the erosion rate. Examination of the particles revealed neither gross degradation, nor apparent chipping. Rounding of the particles may occur in practice because the particles impact the reactor internal components far in excess of the four times tested. Most notable was the progressive loss of the very fine particles clinging to the larger particles. Magnetite particles agglomerate due to their ferromagnetic nature and the tendency of very small particles to develop surface charge. These factors contributed to the fact that the magnetite used in erosion testing was very difficult to separate into neat, discrete size ranges. A quantity of very fine particles was observed in samples of a much larger nominal size. These very fine particles are lost to the atmosphere during erosion testing. It seems that the decrease in erosion rate is associated with the loss of these more aggressive particles. These extremely erosive particles should be filtered out of the system.

The steel of the steam coil tubes is subject to this detritive environment for long periods of time and large quantities of erodent were used to determine the effect of continuous testing on the erosion rate. Surprisingly, the erosion rate remained constant for much longer than might be expected since a deep crater is formed, which results in the magnetite impacting the surface at

changed angles and interfering with other particles to a greater degree. Most erosion testing proceeds until a steady-state erosion rate can be determined and is then stopped. This generally causes a slight depression in the surface in the shape of an oval, with its centre on the blow axis (section 2.7.3). As testing continues, ripples are formed on the surface and the wear scar deepens. The ripples precess across the wear scar in the direction of the gas flow (figure 4-20). The movement of these ripples is analogous to that of sand in contact with a flowing liquid. Gradually, as the wear scar becomes deeper, it develops a slope from the front to the back. Interestingly, the erosion rate appears to remain constant in spite of differences in actual impact angle, and particle interactions. The ripples act to provide a surface for particles to interact with that is parallel to the original surface, albeit at an increasing distance from the nozzle end. This may explain why the erosion rate remains constant in spite of what, at first glance seems to be continually changing conditions. However, this aspect needs to be examined in more detail than in this work.

It may be expected that the wear scar would continue to become uniformly deeper until the sample is perforated, but the walls of this gouge begin to direct more of the particles toward the back of the wear scar, causing the undercut observed. While this must surely be associated with an increase (or any change) in the erosion rate, the slope remains unchanged. As testing continues, the undercut becomes more pronounced and a small deviation of the curve from linear is observed. While this increase in the erosion rate may seem negligible, if extrapolated over the useful service life of the component, the accelerated erosion experienced once these gouges have been formed may explain the long gouges observed along the steam coil tubes. The volume loss measured by erosion testing is removed from the front of the wear crater. The wear crater elongates by the formation and removal of an undercut by rebounding particles. Negligible erosion is observed for the approach to the crater. The magnetite particles cause very little damage at low impact angles, as predicted in figure 4-1. Little erosion is experienced by the side walls and tail of the wear scar at this advanced stage because the particles are striking the steel at low enough angles for the steel to largely resist the impact elastically. Once formed, it seems that these gouges are associated with an increase in erosion. Avoidance of the initial formation of these gouges is therefore critical in the reduction of erosion damage to the steel tubes.

CHAPTER SIX

CONCLUSIONS

The following conclusions can be reached based on this work:

6.1 Maximum erosion rates were found at impact angles of 30° to 40°.

6.2 There was a strong dependence of erosion rates on particle impact velocity, with a velocity exponent of near 2.

6.3 Erosion rates decreased very slightly with increasing mass fluxes for the range considered.

6.4 The loss of material occurred through the ductile mechanisms of erosive wear.

6.5 Surface ripples were observed in 1.6580 steel at 30°.

6.6 Milled catalyst was highly angular. Spent catalyst was more spherical, with few angular protrusions.

6.7 The size of the magnetite particles had a great effect on erosion rates.

6.7.1 Smaller particles were more erosive than larger particles for the particle size range considered.

6.7.2 Smaller particles were highly angular, with sharp protrusions. Angularity decreased with increasing particle size.

6.7.3 Particle impact velocity decreased with increasing particle size, for a constant free stream velocity.

6.8 Magnetite particles were up to twice as erosive as silica particles.

6.9 Milled catalyst was more erosive than spent catalyst.

6.10 Erosion rates decreased when the magnetite erodent was recycled due to the progressive loss of the finest particles.

6.11 Magnetite particles were not friable and maintained their structural integrity on impact with the steel.

6.12 Erosion rates were insensitive to surface condition.

6.13 Commercially supplied plasma nitrided steel performed poorly in erosion testing.

6.14 Erosion rates for EN3B and DIN 1.6580 steels were similar.

6.15 Elongated grooves tend to form in the steel when impacted by large quantities of magnetite by the repeated formation and elimination of an undercut at the front of the wear scar.

6.16 Erosion rates increased slightly with continuous testing.

6.17 A softened surface zone was created by erosion, below which the steel work hardened.

CHAPTER SEVEN

RECOMMENDATIONS

It is recommended that attention be paid to the following if erosion in the synthol reactor is to be reduced:

7.1 The smallest catalyst particles are the most angular, and are accelerated to higher velocities than larger particles, for a constant free stream velocity. This results in higher wear rates. It would seem appropriate to filter out these particles to minimise erosive damage of the synthol reactor internal components by the catalyst particles.

7.2 Lowering the velocity will lead to lower erosion rates and streaming in the reactor should be avoided. If an overall decrease in the velocity of the gas and catalyst through the reactor is not possible due to process considerations, the use of baffles around the steam coil tubes should encourage turbulent flow, thus eliminating streaming. Local velocities will also be reduced and regions of high velocity can be avoided.

Baffle plates have long been used to prevent localised erosive wear in facilities such as coal-fired boilers[61]. Ribs, which act like baffles, but on a much smaller scale in terms of fluid flow disruption, have been proposed for use in decreasing the erosive wear damage sustained by pipe bends[62]. Ribs were fixed inside a pipe along the outer wall, causing a turbulent layer that reduced the velocity of particles in a gas stream, and changed their trajectories.

It is proposed that fixing rib baffles to the lower 500 mm of the steam coil tubes will promote turbulent flow and eliminate streaming; and also reduce the velocities of catalyst particles impacting the steel tubes. The installation time and cost of this solution are both favourable. The ribs may be easily and quickly fixed to the tubes in situ. The proposed geometry of the rib baffles and proposed positions along the steam coil tubes within the synthol reactor are shown in Appendix III. Relative height and separation of the ribs are important parameters that must be finalised based on an assessment of the flow conditions within the synthol reactor.

CHAPTER EIGHT

REFERENCES

1. CS Yust, *Tribology and Wear*, International Metals Reviews, Vol.30 No.3 (1985) 141.
2. TH Kosel, *Solid Particle Erosion*, ASM Handbook Vol.18 Friction, Lubrication and Wear, 199.
3. A Levy, *The Role of Plasticity in Erosion*, Proc. 5th Int. Conf. on Erosion by Solid and Liquid Impact, Cambridge, UK (1979) 39-1.
4. P Shewmon, G Sundararajan, *The Erosion of Metals*, Ann. Rev. Mater. Sci. 13 (1983) 301.
5. JA Williams, *Engineering Tribology*, Oxford University Press, 1994, 190.
6. BA Lindsey, AR Marder, *The effect of velocity on the solid particle erosion rate of alloys*, Wear 225-229 (1999) 510.
7. Y Kagimoto et al., *Experimental Study on the Relation Between Erosion Wear Rate and Particle Impact Velocity Measured by LDV*, Proc. 7th Int. Conf. on Erosion by Liquid and Solid Impact, Cambridge, UK (1987) 69-1.
8. LP McCabe, GA Sargent and H Conrad, *Effect of microstructure on the erosion of steel by solid particles*, Wear 105 (1985) 257.
9. CM Preece, NH MacMillan, *Erosion*, Annual Review of Materials Science 7 (1977) 95.
10. M Suckling, *High Temperature Erosive Wear of a Boiler Tube Steel*, PhD Thesis, University of Cape Town (1996).
11. W Tabakoff, *High Temperature Erosion Study of AM355 Steel*, Proc. 7th Int. Conf. on Erosion by Liquid and Solid Impact, Cambridge, UK (1987) 52-1.
12. AV Levy, J Yan and J Patterson, *Elevated Temperature Erosion of Steels*, Proc. Int. Conf. on Wear of Materials, New York, USA (1985) 708.
13. PV Rao and DH Buckley, *Time Effect of Erosion by Solid Particle Impingement on Ductile Materials*, Proc. 6th Int. Conf. on Erosion by Liquid and Solid Impact, Cambridge, UK (1983) 38-1.
14. PS Follansbee, GB Sinclair and JC Williams, *Modelling of Low Velocity, Particulate Erosion in Ductile Materials*, Proc. Int. Conf. on Wear of Materials, San Francisco, USA (1981) 577.

15. AW Ruff and GF Schmitt Jr, *Erosion*, Encyclopaedia .of Materials Science and Engineering, Vol. 2, Pergamon Press Ltd. (1986) 1573.
16. T Foley and A Levy, *The Erosion of Heat-Treated Steels*, Wear 91 (1983) 45.
17. IM Hutchings, *Some comments on the theoretical treatment of erosive particle impacts*, Proc. 5th Int. Conf. on Erosion by Liquid and Solid Impact, Cambridge, UK (1979) 36-1.
18. I Finnie, GR Stevick and JR Ridgely, *The influence of impingement angle on the erosion of ductile metals by angular abrasive particles*, Wear 152 (1992) 91.
19. RM Branch, Int. J. Impact Eng. 7 (1988) 37; as referenced in: I Finnie, GR Stevick and JR Ridgely, *The influence of impingement angle on the erosion of ductile metals by angular abrasive particles*, Wear 152 (1992) 91.
20. KH Yee, PJ Shayler and N Collings, *Erosion of metals by flyash particles*, Wear 91 (1983) 161.
21. AK Cousens and IM Hutchings, *Influence of Erodent Particle Shape on the Erosion of Mild Steel*, Proc. 6th Int. Conf. on Erosion by Liquid and Solid Impact, Cambridge, UK (1983) 41-1.
22. M Naim and S Bahadur, *Work hardening in Erosion due to Single Particle Impacts*, Proc. Int. Conf. on Wear of Materials, Reston, Virginia, USA (1983) 340.
23. PH Shipway and IM Hutchings, *A method for optimising the particle flux in erosion testing with a gas-blast apparatus*, Wear 174 (1994) 169.
24. M Liebhard and A Levy, *The effect of erodent particle characteristics on the erosion of metals*, Wear 151 (1991) 381.
25. J Salik and DH Buckley, *Effect of Mechanical Surface and Heat Treatments on Erosion Resistance*, Proc. Int. Conf. on Wear of Materials, San Francisco, USA (1981) 592.
26. IM Hutchings, *Single Particle Impact Erosion Mechanisms*, Proc. of ASTM Symposium, Erosion Prevention and Useful Applications STP664 (1978).
27. RE Winter and IM Hutchings, *Solid particle erosion studies using singular angular particles*, Wear 29 (1974) 181.
28. N Gane and MJ Murray, *The transition from ploughing to cutting in erosive wear*, Proc. 5th Int. Conf. on Erosion by Solid and Liquid Particle Impact, Cambridge, UK (1979) 40-1.
29. DJ O'Flynn, MS Bingley, MSA Bradley, AJ Burnett, *A model to predict the solid particle erosion rate of metals and its assessment using heat-treated steels*, Wear 248 (2001) 162.
30. AV Levy and P Chik, *The Effects of Erodent Composition and Shape on the Erosion of Steels*, Wear 89 (1983) 151.

31. S Bahadur and R Badruddin, *Erodent Particle Characterisation and the Effect of Particle Size and Shape on Erosion*, Proc. Int. Conf. on Wear of Materials, Denver, Colorado, USA (1989) 143.
32. Goodwin, Sage and Tilly, *Study of Erosion by Solid Particles*, Proc. of Institute of Mechanical Engineers 184 (1969) 279.
33. J Jin et al, *Numerical simulation of the tube erosion resulted from particle impacts*, Wear 250 (2001) 114.
34. AJ Sparks and IM Hutchings, *Effects of erodent recycling in solid particle erosion testing*, Wear 162-164 (1993) 139.
35. AJ Ninham and IM Hutchings, *A computer model for particle velocity calculation in erosion testing*, Proc. 6th Int. Conf. on Erosion by Solid and Liquid Particle Impact, Cambridge, UK (1983) 51-1.
36. ME Gulden, *Influence of Brittle to Ductile Transition on Solid Particle Erosion Behaviour*, Proc. 5th Int. Conf. on Erosion by Solid and Liquid Particle Impact, Cambridge, UK (1979) 31.
37. A Ball, *On the importance of work hardening in the design of wear-resistant materials*, Wear 91 (1983) 201.
38. BF Levin, JN DuPont and AR Marder, *Indentation analysis of sub-surface deformation in ductile materials after solid particle erosion*, Materials Science & Engineering A283 (2000) 203.
39. G Sundararajan, *The solid particle erosion of metallic materials: The rationalisation of the influence of material variables*, Wear 186-187 (1995) 129.
40. R Bellman, Jr. and A Levy, *Platelet mechanism of erosion of ductile metals*, Proc. Int. Conf. on Wear of Materials, San Francisco, California, USA (1981) 564.
41. G Sundararajan and M Roy, *Solid particle erosion behaviour of metallic materials at room and elevated temperatures*, Tribology Int. Vol.30 No.5 (1997) 339.
42. DG Rickerby and NH Macmillan, *Erosion of aluminium and magnesium oxide by spherical particles*, Proc. Int. Conf. on Wear of Materials, San Francisco, California, USA (1981) 548.
43. AV Levy, *Erosion mechanisms in ductile and brittle materials*, Proc. 6th Conf. On Erosion by Liquid and Solid Impact, Cambridge, UK (1983) 39-1.
44. A Levy, M Aghazadeh and G Hickey, *The effect of test variables on the platelet mechanism of erosion*, Wear 108 (1986) 23.

45. M Naim and S Bahadur, *Effect of microstructure and mechanical properties on the erosion of 18 Ni (250) Maraging steel*, Proc. Int. Conf. on Wear of Materials, Vancouver, Canada (1985) 586.
46. I Finnie, *Some reflections on the past and future of erosion*, Wear 186-187 (1995) 1.
47. J Stringer and IG Wright, *Some Views on the Formation of Ripples on Eroded Surfaces*, Proc. 7th Int. Conf. on Erosion by Liquid and Solid Impact, Cambridge, UK (1987) 47.
48. I Finnie and YH Kabil, *On the formation of surface ripples due to erosion*, Wear 8 (1965) 60.
49. G Carter, MJ Nobes and KI Arshak, *The mechanism of ripple generation on sandblasted ductile solids*, Wear 65 (1980) 151.
50. L Lapides and A Levy, *The halo effect in jet impingement solid particle erosion testing of ductile metals*, Wear 58 (1980) 301.
51. GM Green, R Taggart and DH Polonis, Metallography 14 (1981) 191.
52. PH Shipway, *The effect of plume divergence on the spatial distribution and magnitude of wear in gas-blast erosion*, Wear 205 (1997) 169.
53. G Sundararajan, M Roy and B Venkataraman, *Erosion efficiency – a new parameter to characterise the dominant erosion micromechanism*, Wear 140 (1990) 369.
54. AW Ruff and LK Ives, *Measurement of solid particle velocity in erosive wear*, Wear 35 (1975) 195.
55. Werner Grond, Process Engineer, PetroSA, Private Communication.
56. Z Feng, *The erosion of materials*, PhD Thesis, University of Cape Town (1998).
57. IM Hutchings, *Tribology: Friction and Wear of Engineering Materials*, Edward Arnold, 1992.
58. A Jillavenkatesa, SJ Dapkunas and LH Lum, *Particle Size Characterisation*, Natl. Inst. Stand. Technol., Spec. Publ. 960-1, 2001.
59. Louis Boshoff, SASOL Secunda, Private Communication.
60. JF Shackelford (ed), The CRC Materials Science and Engineering Handbook, CRC Press, © 1992, 644.
61. E Raask, *Impact erosion wear caused by pulverized coal and ash*, Proc. 5th Int. Conf. On Erosion by Liquid and Solid Impact, Cambridge, UK (1979) 41-1.
62. J Yao, B Zhang and J Fan, *An experimental investigation of a new method for protecting bends from erosion in gas-particle flows*, Wear 240 (2000) 215.

APPENDIX I

LAYOUT OF THE SYNTHOL REACTOR

THE SYNTHOL REACTOR

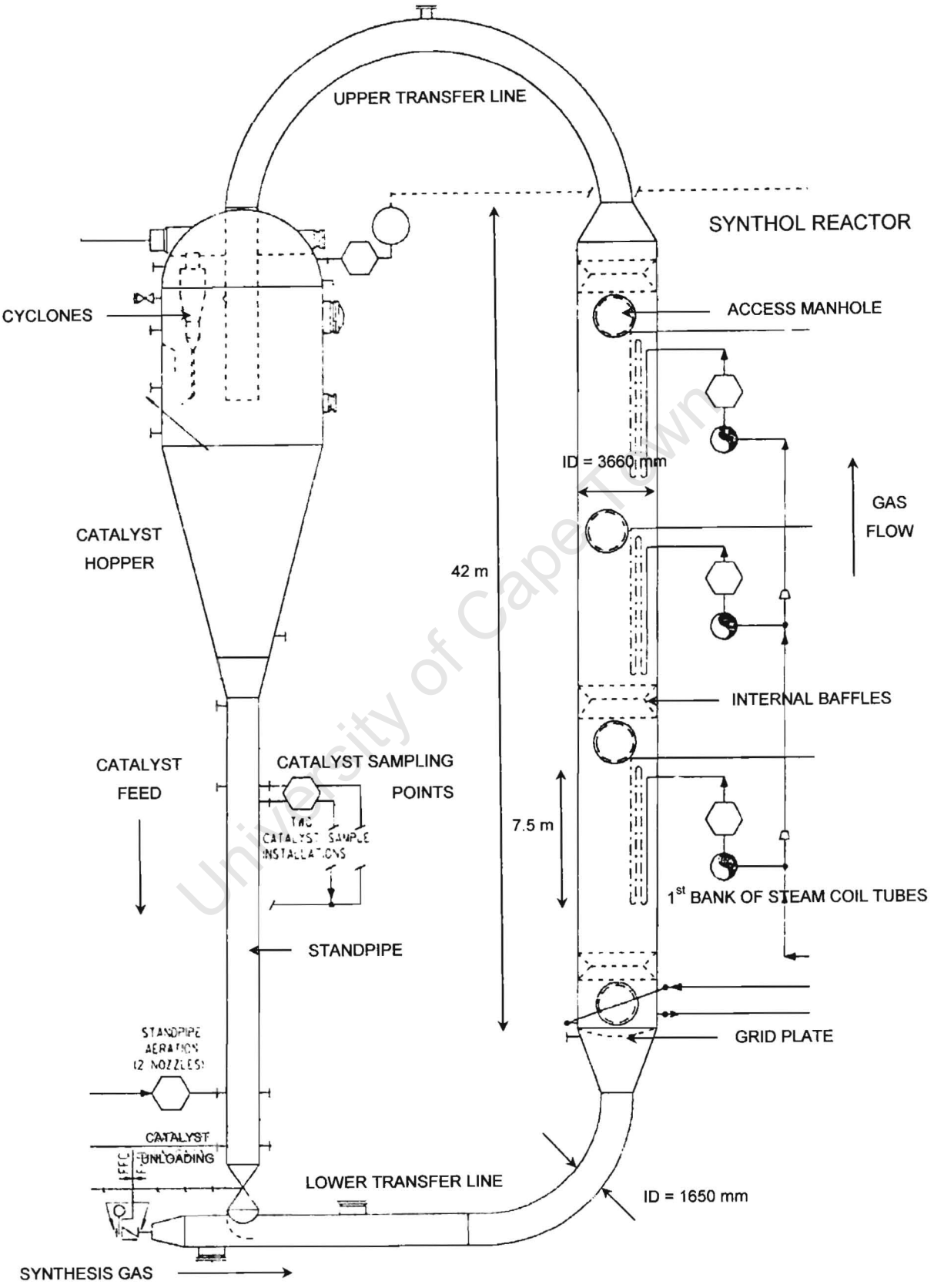

Figure A-1 Schematic of the synthol reactor, showing catalyst hopper on the left.

INTERNAL STEAM COIL TUBES

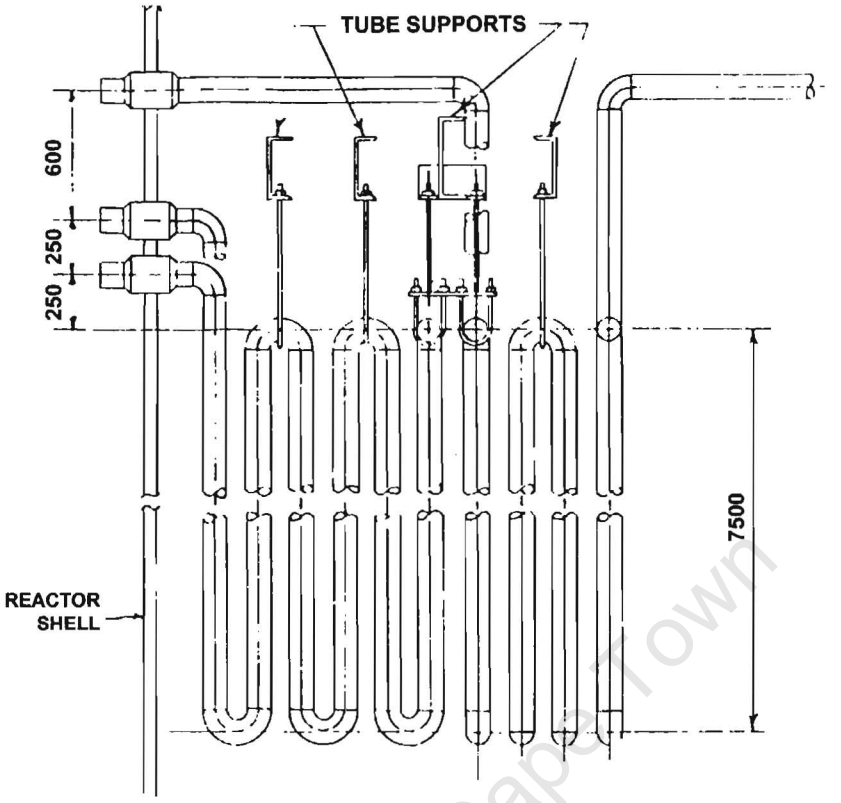

Figure A-2 Schematic of a steam coil tube.

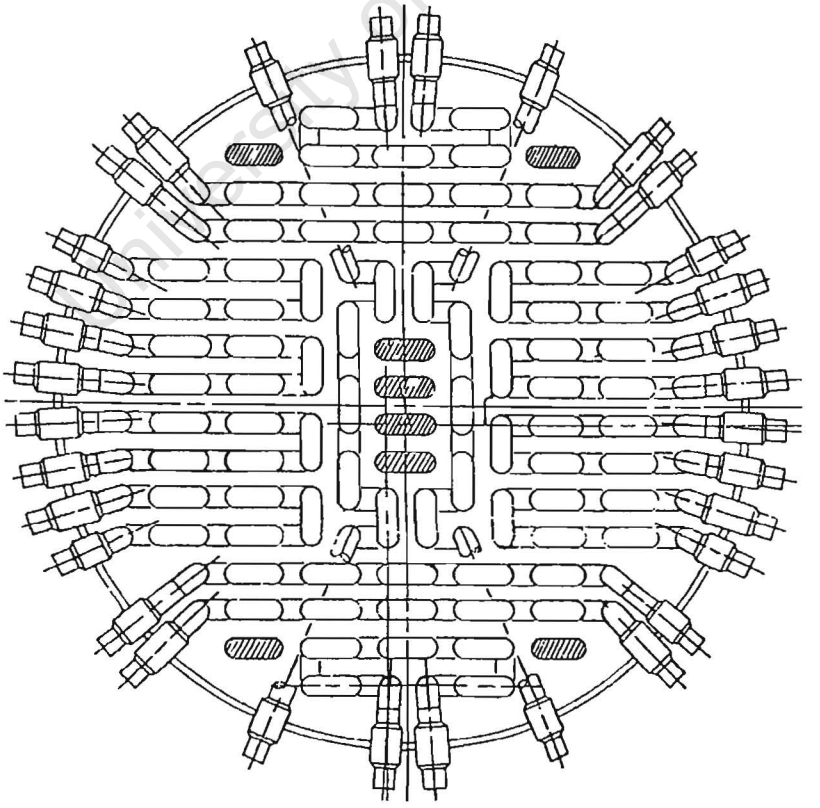

Figure A-3 Reactor cross-section, showing layout of steam coil tubes.

APPENDIX II

CALCULATION OF REACTOR CONDITIONS

MASS FLUX OF CATALYST THROUGH REACTOR

Mass flux can be calculated from plant data, and geometry of the synthol reactor as follows:

$$\frac{\textit{Total mass in}}{\textit{Cross-sectional area}} \qquad [kg.m^{-2}.s^{-1}]$$

Synthol train	[kg.h^{-1}]	[kg.s^{-1}]
1	177918	49.42
2	181482	50.41
3	187421	52.06
Average	182273.7	**50.63**

Table A-1 'Total mass in' as obtained from the mass balance and general plant monitoring information for the period 14/04/2001 – 15/04/2001.

Values for 'total mass in' used in calculating the mass flux are shown in table A-1. An average value for the three synthol trains was taken and converted to [kg.s^{-1}] for use in the above equation. Mass flux was calculated for three cross-sections at different places along the reactor, selected to provide the range of values encountered in practice:

i. Lower transfer line
ii. Unobstructed (maximum) internal diameter of the synthol reactor
iii. Cross-section of a bank of steam coil tubes

i. LOWER TRANSFER LINE

$$A = \pi r^2$$

$$A = \pi(0.825)^2$$

$$A = 2.14m^2$$

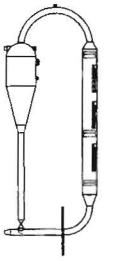

$$Flux = \frac{50.63}{2.14} = 23.66kg.m^{-2}.s^{-1}$$

ii. CROSS-SECTION OF A BANK OF STEAM COIL TUBES

A cross-section through a bank of steam coil tubes will see the tubes in section. The tubes present a reduction in the available cross-section for gas-catalyst flow equal to their cross-sectional area. This area value was multiplied by the number of tubes and the result subtracted from the cross-sectional area of the reactor:

$$A = \pi r^2 - 216(\pi r^2)$$

$$A = \pi(1.83)^2 - 216(\pi(0.057)^2)$$

$$A = 8.32m^2$$

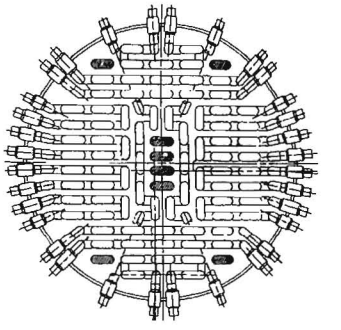

$$Flux = \frac{50.63}{8.32} = 6.08kg.m^{-2}.s^{-1}$$

iii. REACTOR MAXIMUM INTERNAL DIAMETER

$$A = \pi r^2$$

$$A = \pi(1.83)^2$$

$$A = 10.52m^2$$

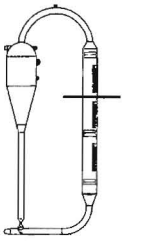

$$Flux = \frac{50.63}{10.52} = 4.81kg.m^{-2}.s^{-1}$$

GAS FREE STREAM VELOCITY

The Ideal Gas Law:

$$\frac{P_1V_1}{T_1} = \frac{P_2V_2}{T_2}$$

was used to calculate the actual volume per unit time, from the normalised value of 900 000 $N.m^3h^{-1}$. Normalised values have been "normalised" using standard temperature and pressure.

Std conditions: T = 25 °C

P = 101.325 kPa

Conditions in the reactor providing a good estimate of the maximum free stream velocity within the reactor:

T = 220 °C

P = 2500 kPa

$$V_2 = \frac{P_1V_1T_2}{P_2T_1} = \frac{(101.325)(900000)(220)}{(2500)(25)} = 320998 m^3.h^{-1}$$

Divide this by the relevant cross-sectional area to obtain the gas velocity:

i. LOWER TRANSFER LINE

$$Velocity = \frac{320998}{2.14} \times \frac{1}{3600} = 41.7 m.s^{-1}$$

ii. CROSS-SECTION OF A BANK OF STEAM COIL TUBES

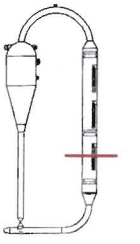

$$Velocity = \frac{320998}{8.32} \times \frac{1}{3600} = 10.7 m.s^{-1}$$

iii. MAXIMUM INTERNAL DIAMETER

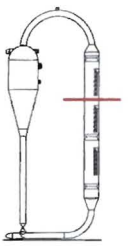

$$Velocity = \frac{320998}{10.52} \times \frac{1}{3600} = 8.5 m.s^{-1}$$

APPENDIX III

RIB BAFFLES FOR REDUCING EROSION OF STEAM COIL TUBES

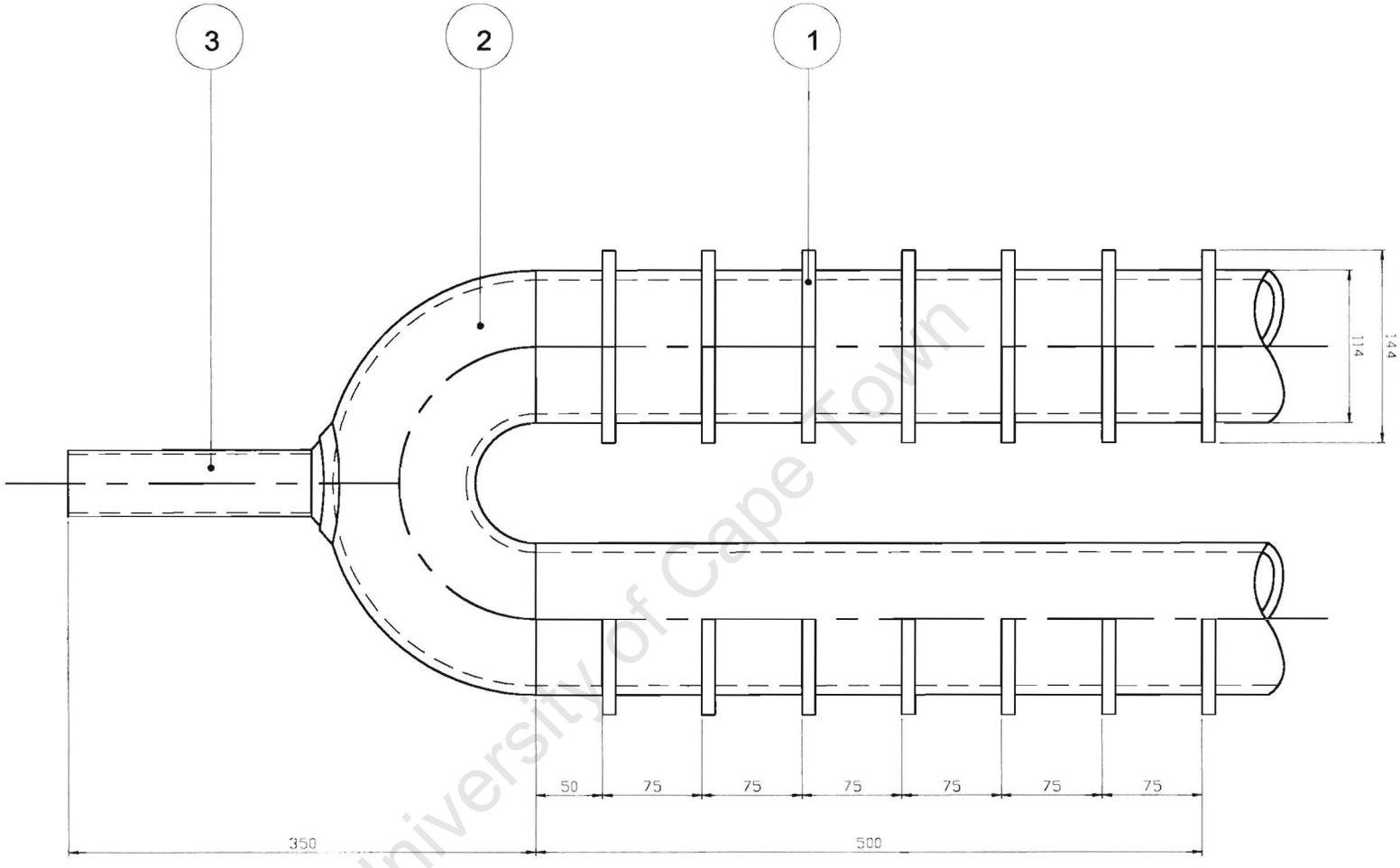

Part No.	Description	Material	No. off
3	Steam Coil Tube	1.6580	1
2	Tube Guide	BS 4360 GR 43A	1
1	Split Ring Baffle	1.6580	1

CENTRE FOR MATERIALS ENGINEERING
UNIVERSITY OF CAPE TOWN

Project: MSc Thesis
Title: Coil Tube Baffles
Scale: 1:5
Date: 20/07/02
Sheet: 1/2
Drawn by: Sean E. Fewell
No.: 0001/02/01

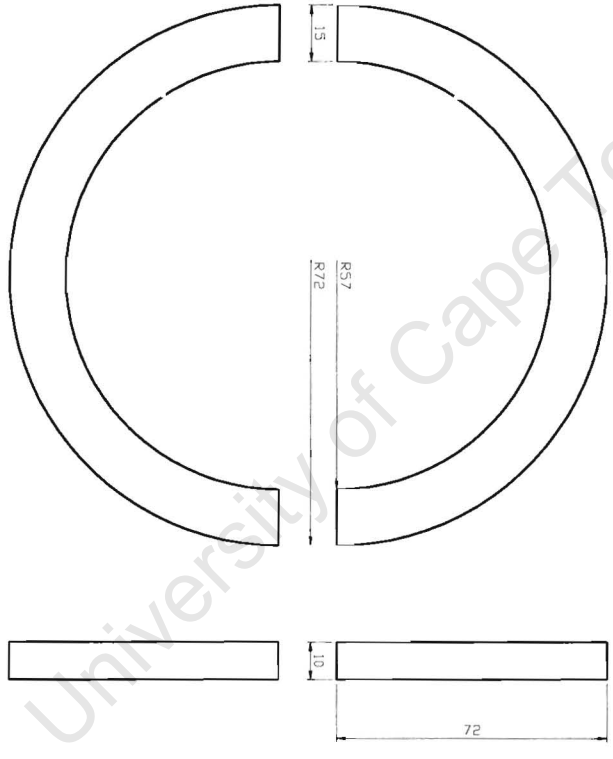

Part No.	Description	Material	No. off
1	Split Ring	1.6580	7

CENTRE FOR MATERIALS ENGINEERING UNIVERSITY OF CAPE TOWN		Project MSc Thesis	Scale 1:2	Date 20/07/02	Sheet 2/2
		Title Coil Tube Baffles	Drawn by Sean E. Fewell		No. 0001/02/02

EFFECT OF PARTICLE SIZE AND IMPACT ANGLE ON EROSIVE WEAR IN A SYNTHOL REACTOR

S.E. Fewell & C. Allen

Centre for Materials Engineering, University of Cape Town

The Synthol process, based on the Fischer-Tropsch process, is used for producing liquid fuels from natural gas feedstock. In the synthol reactor, a catalyst consisting of reduced Fe and a small percentage of Fe oxides is entrained in a gas stream, causing erosive wear damage to the steam coil tubes inside the reactor. The objectives of this work are to determine the influence of operating parameters on this erosive damage.

Erosion testing is being carried out using a gas-blast erosion rig in which erodent particles are fed into a pressurised air stream and impact on specimens. Wear rates are determined from mass (i.e. volume) loss measurements of steel specimens as a function of the amount of erodent passing through the apparatus.

The erodent employed is reduced catalyst which has been identified using X-Ray diffraction as predominantly Fe_3O_4 (magnetite). A laser particle size analyser was used to obtain a size analysis. The average size is 38.9 μm, with a size distribution of 1.4 % finer than 3.9 μm and 97.7 % finer than 124.5 μm. Laboratory test sieves were used to separate the catalyst into the following particle size ranges: <38 μm; 38-63 μm; 63-106 μm and >106 μm. The target material is a low alloy steel similar to that used in the reactors.

Erosion rate is a function of the impact angle[1] and for this system the highest erosion was observed between 30°-40° (see fig. 1). It has also been found that smaller particles are more aggressive than larger particles, based on tests performed using particles from each of the above size ranges.

Scanning electron microscopy was used to characterise the erodent and to determine the process of metal removal and damage sustained by the steel due to the erodent particles. A Leica S440 fully analytical SEM was used for all micrographs. The operating conditions were 10-20 kV with a working distance of 18-25 mm. The erodent particles were Au/Pd sputter coated.

The SEM micrographs of the erodent in fig. 2 show that the finer particles, fig. 2(a), are more angular than the larger particles, fig. 2(b). Finer particles are irregular with sharp edges, while the larger particles are more spheroidal. Damage to steel specimens by individual particles striking the surface is illustrated in fig. 3. In figure 3(a) a small erodent particle, indicated by the arrow, has been embedded in the steel surface, by a ploughing action. The steel has piled up, and peeled back due to plastic deformation around the wear scar at the lower part of the image. Figure 3(b) shows evidence of micro-machining. A sharp corner of a larger particle has removed a vee-shaped steel chip by a cutting action[2].

It is anticipated that on the evidence of the work performed so far, alterations to the present reactor operating conditions will be made, resulting in less wear which translates into reduced costly downtime.

The financial support of Mossgas is gratefully acknowledged.

References

1. Sundararajan, G. & Roy, M. (1997) Tribology International 30, 341.
2. Hutchings, I.M. (1992) Tribology: Friction and Wear of Engineering Materials. London, Edward Arnold, 176.

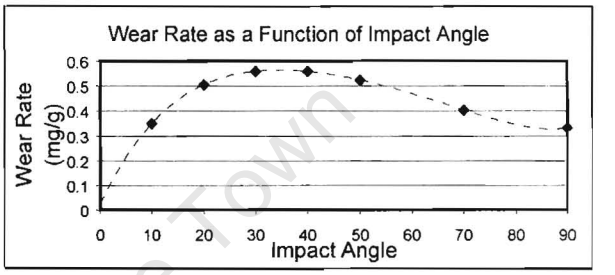

Fig.1 Influence of impact angle on erosion rate for a low alloy steel impacted by SiO_2 particles.

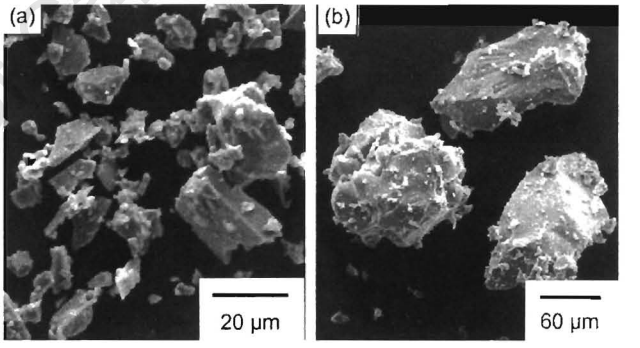

Fig.2 Morphology of Fe_3O_4 particles, (a) <38 μm and (b) 63-106 μm, as revealed by SEM.

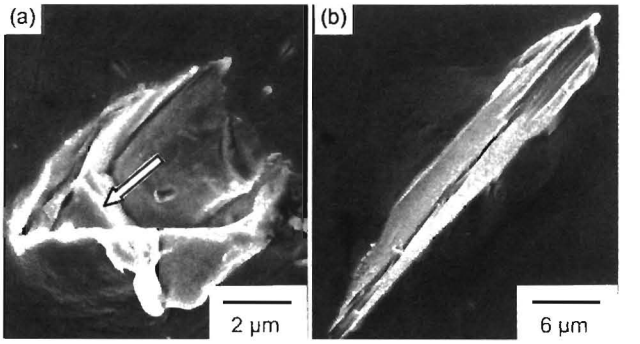

Fig.3 SEM micrograph of single-impact wear damage by Fe_3O_4 particles, (a) <38 μm and (b) 63-106 μm, striking a low alloy steel specimen.

Email: seanfewell@hotmail.com